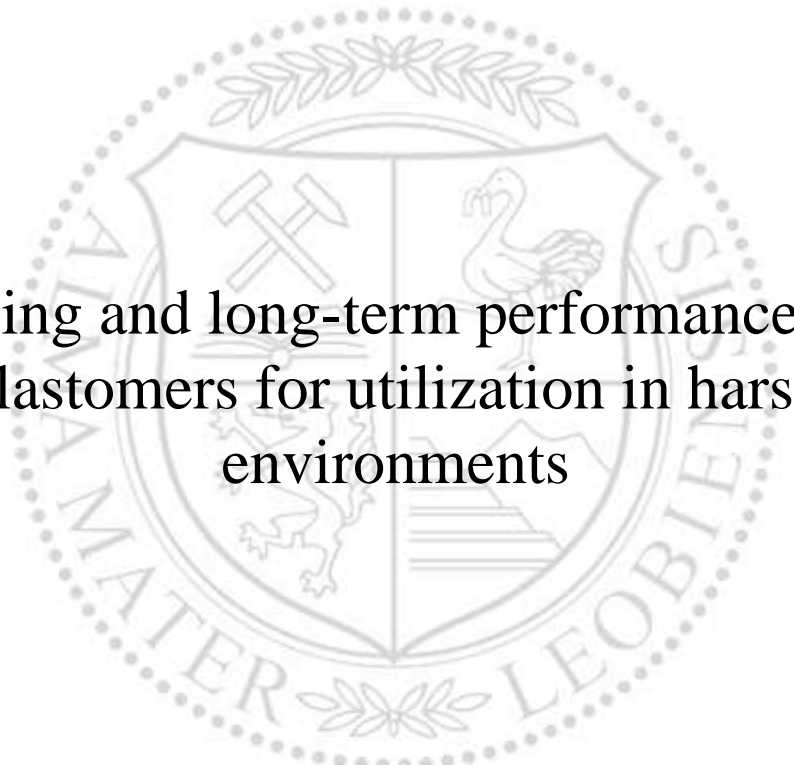




Chair of Materials Science and Testing of Polymers

Doctoral Thesis



Aging and long-term performance of
elastomers for utilization in harsh
environments

Winoj Naveen Balasooriya Arachchige, M.Sc.

April 2019

Dedicated to my parents
Kusum and (late) Tissa.

“What you think, you become” (Siddhartha Gautama, 6th century B.C.)

I declare on oath that I wrote this thesis independently, did not use other than the specified sources and aids, and did not otherwise use any unauthorized aids.

I declare that I have read, understood, and complied with the guidelines of the senate of the Montanuniversität Leoben for "Good Scientific Practice".

Furthermore, I declare that the electronic and printed version of the submitted thesis are identical, both, formally and with regard to content.

April 2019

Winoj Naveen, Balasooriya Arachchige

Matriculation Number: 01156143

ACKNOWLEDGEMENT

I would like to express my sincere gratitude to those who advised, supported and encouraged me during the preparation of this dissertation.

First, I owe deep gratitude to Univ.-Prof. Dipl.-Ing. Dr. mont. Gerald Pinter, Chair of Materials Science and Testing of Polymers, who has been my academic advisor, for his continuous supervision, numerous fruitful discussions and tremendous help throughout this work. I would also like to thank Prof. Francesco Briatico Vangosa for his interest in my work and acceptance to act as the second referee of my doctoral committee.

I am very grateful to Dipl.-Ing. Dr. mont. Bernd Schrittester, first for his patronage and trust in me, then his continual interest in my work, valuable ideas and lengthy scientific discussions. Especially, without his encouragement, personal support and the friendly working atmosphere, this work would have been a much more difficult task.

I am indebted to SKF Sealing Solutions Austria GmbH, for acting as a project partner, and particularly I would like to thank Dipl.-Ing. Dr. mont. Thomas Schwarz and Dipl.-Ing. Mario Mitterhuber for scientific discussions, supplying the materials and allowing me to access the laboratory facilities for conducting the experiments necessary for this scientific work.

Special thanks should go to some of my colleagues, Nicole Zarfl, Gerald Mayer, Raphaela Mühleder, Jürgen Grosser, Dipl.-Ing. Chao Wang, Dipl.-Ing. Dr. mont. Andreas Hausberger and Dr. Santhosh Karunakaran, who supported me with some experiments and their knowledge on constructing specific testing equipment. Furthermore, I would like to express my appreciation to the members of the PCCL, who always created a cozy and amusing atmosphere, on and off working hours.

Finally, I want to sincerely thank the most important people in my life, my family and friends, for their unconditional support and encouragement throughout this journey. Especially, I am deeply indebted to my mom Kusum, and to my siblings, those who set the stage for me to be in this place today. On a final note, I should mention my wife Thanuja, for her great understanding, not complaining about some late working hours and lifting me up when it was most necessary during this work.

The research work was performed at the Polymer Competence Center Leoben GmbH (PCCL, Austria) within the framework of the COMET-program of the Austrian Federal Ministry for Transport, Innovation and Technology (BMVIT), the Austrian Federal Ministry of Digital and Economic Affairs (BMDW) with contributions from the material science and testing of polymers of the Montanuniversität Leoben and SKF Sealing Solutions Austria GmbH. The PCCL is funded by the Austrian Government and the State Governments of Styria, Lower Austria and Upper Austria.

Winoj Balasooriya

Leoben, April 2019

ABSTRACT

Despite remarkable growth in alternative energy sources, the energy requirements in the foreseeable future will still depend on fossil fuels, and the oil and gas industry will have to contend with more and more hostile down-hole conditions to fulfill the future energy demand. Elastomers are an essential class of materials in oil field applications, not only as seals but also in several other crucial components, due to their intrinsic properties. However, the functional properties, the performance and the service life of components are affected by the working conditions, for example, the viscoelastic effects, the surrounding media in high-pressure and high-temperature conditions. Especially, seal damage caused by the rapid gas decompression (RGD) is a well-known failure in high-pressure fluid handling conditions but this is still under discussion and holds financial, safety and environmental implications for the stakeholders.

This study concerns the use of hydrogenated nitrile butadiene rubbers (HNBR) as seals in oil and gas field applications and discusses the results under three main topics; (i) thermo-oxidative aging, (ii) swelling induced aging, and (iii) utilization in harsh environments. Accordingly, the aging behavior (at elevated temperatures in the presence of oxygen and in contact with liquids) of HNBR in different conditions was investigated and the effects of intense aging on bulk and surface properties were evaluated. Further, the environmental influences on component level RGD resistance as well as the relevance of additives, especially carbon black (CB), on the development of RGD-improved material grades was investigated.

Within the evaluation, the classical test set-ups on tensile, tear, and dynamic mechanical analysis, as well as the special test apparatus on RGD and tribological behavior of seals at the component level, were instrumented. Furthermore, the material composition, composite structure, microstructural changes, and possible damage mechanisms were analyzed. The thermo-oxidative aging deteriorated the mechanical properties, for example, the tensile strength, strain at break, tear resistance and damping properties were decreased, and the stiffness was increased. The different aging temperatures and the exposure times revealed the onset and intensity of property degradations. However, the RGD resistance improved in thermally aged conditions. The elastomers absorbed the fluids in

contact and their morphology and subsequently their properties, physically as well as chemically, were changed. Therefore, in the swollen conditions, the bulk, as well as the surface properties, were degraded. However, RGD resistance was enhanced in swollen conditions as both of these phenomena involve fluid absorption and dissolution into the elastomer. The physically altered mechanical properties were regained after fully drying the samples; however, the degree of the swelling irreversibly degraded the surface and deteriorated the tribological properties influencing damage modes and component lifetime. In general, adding CB improves the mechanical properties of elastomer compounds and the surface area of CB is primarily responsible for the size and shape of filler aggregates and agglomerates, which are decisive factors in forming filler-filler and filler-rubber interactions. In the tested higher CB loading conditions, which already deliver a certain level of mechanical properties, the higher surface area CB adversely affected RGD resistance. Apparently, the higher surface area CB created a densified filler network and a lower amount of matrix component around the CB grades, which adversely affected the RGD resistance. Therefore, the environmental factors as well as the material quality and composition influence the RGD resistance. In future work, the information gained in this study will be useful in material modeling and simulation purposes for determining the possible damage and service life in actual working conditions.

KURZFASSUNG

Trotz des bemerkenswerten Wachstums im Bereich der alternativen Energiequellen wird jedoch der weltweite Energiebedarf in naher Zukunft nur mit Hilfe der Unterstützung von fossilen Brennstoffen gedeckt werden können. Dies stellt die Öl- und Gasindustrie vor neue Herausforderungen um tiefere Rohstoffreservoirs zu erschließen und konfrontiert die eingesetzten Materialien mit immer extremeren Einsatzbedingungen. Elastomere sind aufgrund ihrer intrinsischen Eigenschaften eine unverzichtbare Werkstoffklasse im Bereich der Erdöl und Erdgasindustrie, nicht nur im Bereich der Dichtungen, sondern auch in vielen weiteren sicherheitsrelevanten Komponenten (z.B. Blow Out Preventer). Die Funktion und Eigenschaften der eingesetzten Komponenten sowie die Lebensdauer der Bauteile werden durch die vorherrschenden Arbeitsbedingungen stark beeinflusst (z.B. Druck-, Temperatur- und Medienbeanspruchung). Dichtungsschäden, die durch die schnelle Gasdekompression (RGD) verursacht werden, sind ein bekanntes Versagen im Bereich der Hochdruckanwendungen, jedoch sind die Grundlagen dieses Versagens bis heute aufgrund der Komplexität der Belastung wissenschaftlich unter Diskussion was zu signifikanten finanziellen, sicherheitstechnischen und ökologischen Auswirkungen führt.

Diese Arbeit befasst sich mit hydriertem Nitril-Butadien-Kautschuk (HNBR), welcher als Dichtungsmaterial in Öl- und Gasanwendungen eingesetzt wird und betrachtet die Ergebnisse im Rahmen dreier Hauptbereiche: (i) thermo-oxidatives Altern, (ii) quellinduziertes Altern und (iii) Einsatz unter extremen Umgebungsbedingungen. Dementsprechend wurde das Alterungsverhalten (bei erhöhten Temperaturen in oxidativer Atmosphäre und in Kontakt mit Flüssigkeiten) von HNBR unter verschiedenen Bedingungen untersucht und die Auswirkungen der intensiven Alterung auf die Material- und Oberflächeneigenschaften bewertet. Des Weiteren wurde der Einfluss der Alterung auf die RGD-Beständigkeit von Bauteilen sowie die Relevanz von Additiven, insbesondere Ruß (CB), für die Entwicklung von RGD-verbesserten Materialtypen untersucht.

Im Rahmen der experimentellen Untersuchungen wurden klassische Versuchsaufbauten zur Prüfung der Zug- sowie Weiterreißigenschaften und dynamischen Methoden zur Analyse des dynamisch-mechanischen Verhaltens

implementiert. Darüber hinaus erfolgte die Charakterisierung der Materialien im Bereich des Widerstands gegen explosive Dekompression (RGD Verhalten) sowie die Untersuchung des tribologischen Verhaltens von Dichtungen auf Bauteilebene in unterschiedlichen Kontaktsituationen. Des Weiteren wurden basierend auf den unterschiedlichen Materialzusammensetzungen und Füllstoffen der Einfluss mikrostruktureller Veränderungen und mögliche Schadensmechanismen analysiert. Durch die thermo-oxidative Alterung konnte eine deutliche Verschlechterung der mechanischen Eigenschaften (Zugfestigkeit, Bruchdehnung, Reißfestigkeit) und Verringerung der Dämpfungseigenschaften sowie eine Erhöhung der Steifigkeit festgestellt werden. Aufgrund der gewählten Auslagerungstemperaturen und unterschiedlichen Expositionszeiten, konnten der Beginn sowie die Intensität der Veränderung der Materialeigenschaften erfasst werden. Im Kontrast zu den eindeutigen Ergebnissen (Verschlechterung) der mechanischen Eigenschaften wurde der Widerstand gegen die explosive Dekompression mit thermisch gealterten Materialien verbessert. Es erfolgte eine Absorption der im Kontakt befindlichen Flüssigkeiten durch die eingesetzten Materialien und somit eine Veränderung der Morphologie und damit eine Veränderung der Materialeigenschaften. Dieser Einfluss konnte auch durch die Quellversuche mit unterschiedlichen Flüssigkeiten gezeigt werden, wobei es zu einer deutlichen Verschlechterung der Oberflächeneigenschaften gekommen ist. Im Vergleich dazu konnte jedoch der Widerstand gegen explosive Dekompression (RGD) im gequollenen Zustand erhöht werden, da beide Phänomene die Flüssigkeitsaufnahme sowie die Lösung des Gases in den Werkstoff beinhalten. Nach erfolgter vollständiger Rücktrocknung der Proben wurden die mechanischen Eigenschaften erneut gemessen und annähernd die gleiche Materialperformance gemessen. Jedoch konnte eine deutliche Beeinträchtigung der Oberflächeneigenschaften festgestellt werden und somit eine Verschlechterung der tribologischen Performance. Des Weiteren änderte sich der Schadensmodi sowie die Lebensdauer der Komponenten signifikant. Im Allgemeinen verbessert die Zugabe von CB die mechanischen Eigenschaften von Elastomer-Werkstoffen, wobei die Oberfläche, Größe und Form der Füllstoffaggregate und Agglomerate entscheidende Faktoren bei der Bildung von Füllstoff-Füllstoff und Füllstoff-Gummi Wechselwirkungen sind. Während der Charakterisierung konnte jedoch ein negativer Einfluss auf die RGD Beständigkeit

aufgrund einer höheren Füllstoffoberfläche des verwendeten CB festgestellt werden. Die durchgeführten Untersuchungen zeigten, dass die Umgebungsfaktoren sowie die Materialqualität und Zusammensetzung der Werkstoffe einen signifikanten Einfluss auf die RGD-Beständigkeit haben. Des Weiteren werden die in dieser Studie gewonnenen Informationen für zukünftige Materialmodellierungen und Bauteilsimulation zur Bestimmung möglicher Schäden im Einsatz und Standzeiten unter realen Arbeitsbedingungen implementiert werden.

TABLE OF CONTENTS

ACKNOWLEDGEMENT	IV
ABSTRACT	VI
KURZFASSUNG	VIII
TABLE OF CONTENTS	XI
PART I: INTRODUCTION, SCOPE AND BACKGROUND	12
I.1 Introduction, scope, and objectives	12
I.2 Background	14
1.2.1 Elastomers	14
1.2.2 Elastomeric properties and additives	15
1.2.3 Basic properties for oil and gas field applications	22
1.2.4 Rapid gas decompression (RGD)	25
1.2.5 Elastomers for the oil and gas industry sealing applications	31
1.2.6 Component level RGD testing	39
I.3 References	43
I.4 Acronyms and symbols	49
PART II: STRUCTURE, CONTENT AND COLLECTION OF PAPERS	51
II.1 Structure and content	51
II.2 Outline of papers	52
II.3 Outlook	56
II.4 Collection of papers	58
Paper 1: Influence of thermo-oxidative ageing of HNBR in oil field applications	
Paper 2: Induced material degradation of elastomers in harsh environments	
Paper 3: Tribological behavior of HNBR in oil and gas field applications	
Paper 4: The effect of the surface area of carbon black grades on HNBR in harsh environments	

PART I: INTRODUCTION, SCOPE AND BACKGROUND

I.1 Introduction, scope, and objectives

The oil and gas industry is increasing the demand for better performing materials which can withstand more and more hostile operating conditions, as the resources continue to decline and the demand for energy sources increases [1]. Despite the outstanding growth in renewable energy technologies, at least the near future world's energy needs will predominantly depend on fossil fuels [1–3]. The increased price of oil and gas, has spurred the activities on many different fronts world-wide and opened the doors to exploration and development of non-traditional resources: The resources in extreme environments, for example, in arctic and deep-water drillings, heavy and viscous oil deposits, oil and gas shales [2,3]. Some of the exposure conditions for real oil field applications were recorded as follows. In the Indian ocean, where the bottom-hole temperatures reach more than 232 °C and the bottom-hole pressures are greater than 90 MPa at depths of less than 5183 m. In the Gulf of Thailand, where over 450 wells/year are being drilled, temperatures reach 200 °C with moderate down-hole pressures. Applications in the Gulf of Mexico, where the ultra-deep water wells are drilled in a relatively low temperature, 150 °C, but the bottom hole pressures are greater than 130 MPa, while in the UK North Sea, the temperatures reach 210 °C with pressures up to 100 MPa [2]. The future de-carbonization projects rely mostly on hydrogen (H₂) as an alternative; however, the H₂ production from fossil fuels is reckoned the significantly less expensive source than the other methods in large-scale markets [4]. In addition, the research and development work on materials used in the oil and gas industry applications are necessary also for other alternative energy applications, for example, the storage and transportation of hydrogen and complex material behavior in high-pressure applications [4,5].

In the oil and gas industry, elastomeric components are mainly being used as seals, however some other applications, for example, as hoses, flexible joints, valve sleeves, dampening items, electrical insulations, etc., share a small fraction of the applications [6–8]. The functional properties of elastomers, namely, soft,

viscoelastic and incompressible, make them suitable for their applications [6]. Furthermore, the elastomeric materials are supposed to have great toughness properties (under static or dynamic conditions), as well as high abrasion resistance, which is even higher compared with the steel [9]. The elastomeric sealing components face severe environmental conditions, i.e., extremely high and low temperatures, extreme and differential pressures, containment of aggressive fluids and gases, shocks and vibrations, cyclic and complex loading (compressive, shear, and tensile), long working periods, etc. In general, a combination of many of these stresses is apparent in real operating conditions and they are strongly affecting the performance of sealing components [2,3,10]. Exposure to extremely high or low temperatures, chemical degradation or the elastomer's becoming stiff and brittle may be expected, in respective conditions. In containment with fluids, swelling of the elastomer, subsequently weakening the polymer, leaching out soluble constituents, changing component dimensions and density, etc., can be expected. Further deterioration effects may occur based on the toxicity of the fluids [6,10]. In general, gases swell the elastomers in high-temperature high-pressure conditions. Mainly, the changes in pressure gradients and temperatures lead to catastrophic failures of elastomeric components: the so-called rapid gas decompression failure (RGD) also called explosive decompression failure (XDF) [3,10,11]. Moreover, the expected properties of elastomeric components vary with the frequency or time-dependent changes on the working atmosphere due to their viscoelastic nature, and are manifested as creep, relaxation, dampening or stiffness changes [6].

Generally, the elastomeric materials in oil and gas fields, especially sealing solutions, encounter several functional failures due to thermal aging, swelling, RGD, unexpected tribological losses in dynamic conditions and time-dependent loads, which reduce the life expectancy of the components considerably [6,10]. Failures in these applications can be catastrophic, with high financial as well as environmental costs, and possibly can end up in legal or criminal action [8]. Therefore, scientists and engineers push the limits of material science to withstand the technical requirements posted by harsh environments. The mechanical, thermal and chemical properties of elastomers can be improved by correct material selection and intensive research on the material behavior at laboratory scale in accelerated aging studies predicting the performance on real-time applications. This would benefit in

increasing the operating limits and improvement in reliability. Additionally, this could be potentially translated into substantial operational cost savings.

This doctoral thesis is articulated into two parts; the first part explains the importance of studying the topic, background and overall objectives of this scientific work, which comprises the comprehensive material and experimental developments for elastomeric materials. The second part contains a collection of four papers in total, published in reputed journals. The outlines of each paper, which discuss the specific aspects of elastomeric materials in harsh environment utilization and relevant test method development, are also provided.

I.2 Background

1.2.1 Elastomers

The word “elastomer” refer to rubber and the polymers which behave similarly to rubbers [12]. Rubber is often loosely used to refer to a material, which returns quickly to its original shape after releasing the stretched body. However, the term rubber came to the English language after the use of “caoutchouc” (weeping wood) erasers to rub off pencil writing [13,14]. Nowadays in industry, the term “rubber” is used differently. For example, for the primary raw polymer of a rubber product, it is a compound that has many ingredients before vulcanizing, as well as for the vulcanized product. Some use the word rubber to mean only natural rubber (NR) [14]. However, in this scientific work, the words “rubber” and “elastomer” are used to introduce the cured polymer with typical viscoelastic properties unless stated otherwise.

The natural rubber, which primarily consists of polyisoprene, is the sap of the *Hevea brasiliensis* tree which was originally found from the jungles of Brazil [13,14]. However, the industrial use of NR increased after the accidental discovery of Sulphur vulcanization by an American scientist, Charles Goodyear, in 1839. Vulcanization eliminated the sticky nature of NR products and increased the strength of the final product and this breakthrough drove the industry to a different dimension and claimed the vast majority of products available today [14].

Synthetically polymerized rubber was introduced due to the shortage of NR during the Second World War. Initially, the styrene-butadiene copolymer (SBR) was invented and then with time, polychloroprene (CR), acrylonitrile butadiene rubber (NBR), butyl rubber (IIR), fluoroelastomer (FKM), and ethylene propylene diene rubber (EPDM) were produced. In the meantime, the thermoplastic elastomers (TPE) were introduced which showed rubbery features at room temperature but softened like plastics when heated and return back to the rubbery state again after cooling down. Therefore, they have the combined properties of semi-crystalline/glassy thermoplastics and elastomers, which enable the rubbery materials to be processed similarly to thermoplastics [14–16]. Additionally, the TPE's ability to be recycled and the lower energy cost for processing along with the availability of uniform and standard grades encourages use in more applications [16].

1.2.2 Elastomeric properties and additives

Today, the elastomeric materials are widely used as key components in almost every main industry, and they are expected to remain a long and trouble-free life providing their anticipated functions [9,17]. However, the primary raw rubber is mechanically weak, subject to intensive swelling in contact with fluids and unable to hold the required shape after molding. But, compounding with specific ingredients converts it to a useful material grade for applications with certain properties [14]. A basic compound mixture contains raw rubber, a vulcanizing agent, fillers, accelerators, plasticizers, antioxidants, etc. [14,18]. These additives generally enhance the mechanical properties, aging resistance, and processability [18].

Vulcanizing

Historically, the word “vulcanization” was used to imply the cross-linking process of rubber with sulfur (S) or S-based compounds. The cross-linking, which is also called curing or hardening of the raw rubber, is the forming of a three-dimensional network structure by linking the bonds (bridges) between the individual long polymer chains [19]. This process strengthens the material and provides the load-bearing property and reversibility. The theory of rubber elasticity (Flory) explains that the retractive force against deformation is proportional to the number of cross-links per unit volume of elastomer. However, increasing the number of cross-links enhances the

load bearing capabilities of the rubber material to an optimum level [20,21]. Fig. 1 summarizes the influences on the mechanical properties of elastomers with increasing the cross-link density [22]. The elastomeric materials contain chemical cross-linking, which is irreversible, while the thermoplastic-elastomers contain the physical cross-links, which are reversible [19]. The physical cross-links are found in different forms, for example, hydrogen bonds, intermolecular/intramolecular entanglements, polar, London dispersion forces between polymer chains [21].

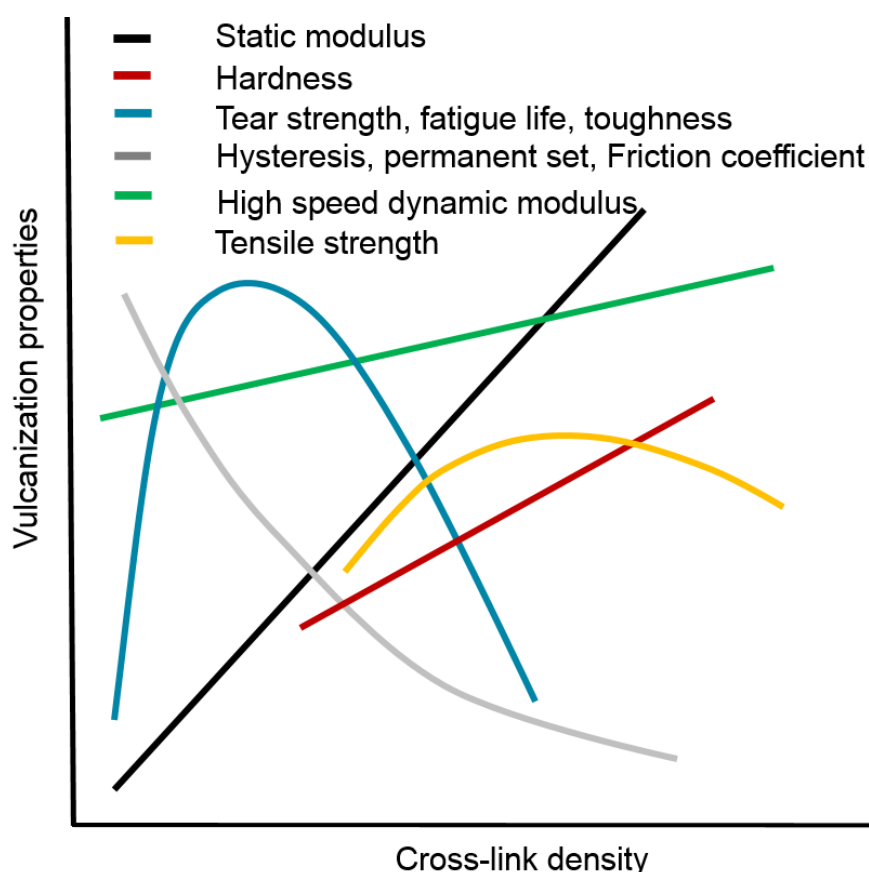


Fig. 1. Cross-link density influence on vulcanization properties [22].

Currently, many chemical cross-linking techniques have been developed besides the S-based vulcanization; for example, peroxides, metal oxides, phenolic resins, quinones, amino acids, silane etc., and they determine the quality and structure of the cross-links, and subsequently the properties of the rubber [19,21]. The S-vulcanization can be utilized only for unsaturated elastomer macromolecules, which contain reactive functional groups, i.e. reactive hydrogen, double bonds, etc., in the presence of relevant accelerators and activators. Otherwise, the S reaction with the rubber is slow and forms only cyclic structures, not cross-links and additionally, the

long temperature and oxygen exposure leads to oxidative degradation [19,21,23]. The **accelerator** type and the amount in the composition of reagents decide the reaction time, cross-link density and the length of cross-links, which in turn determine the thermal and mechanical dynamic properties of the rubber [21]. Mostly, the accelerators are organic compounds, which contain nitrogen (N) or S, for example, *N*-cyclohexyl-2-benzothiazole sulphenamide (CBS), 2-mercaptobenzothiazole (MBT), etc. The **activators**, which are generally a metal oxide, fatty acid or a nitrogen-included base, are essential ingredients to activate the curing process and to improve the curing efficiency along with the accelerators. Zinc oxide is a well-known metal oxide, while stearic acid is the most often used fatty acid and additionally lauric, palmitic, oleic and naphthenic acids also used in industry [19,23]. Additionally, the S-vulcanization reagents generally contain retardants and pre-vulcanization inhibitors, which retard the premature vulcanization during processing. These compounds increase the induction time by reacting with the active accelerators and slowing down the process [19,24].

Peroxide cross-linking is a widely used vulcanization technique in the industry thanks to the ability to vulcanize the unsaturated as well as saturated elastomer chains, which are hard to be cross-linked with other vulcanizing agents. Further, this is a rather simple process compared with the sulfur vulcanization [19]. The use of peroxide leads to a more uniform distribution of cross-linking throughout the bulk material compared with the other methods [25]. Most importantly, this method forms C-C bonds as the cross-links, but not the parts of peroxide or its by-product as a part of cross-link. Therefore, it provides better thermal properties to the material and lower compression set. Additionally, the peroxide cross-linking has a comparatively shorter curing time as well as the ability to form transparent elastomers [19,26]. Fig. 2 shows the peroxide cross-link mechanism, where Fig. 2a indicates the homolytic decomposition of a peroxide forming primary alkoxy radicals, while Fig. 2b shows a hydrogen-atom abstraction from a hydrocarbon to the radical forming a polymer radical, and Fig. 2c shows the recombination of hydrocarbon radicals forming a cross-link through C-C bonds [19,27].

The possible reactions in Fig. 2c can be through coupling with another polymer radical or through additional reactions in-chain or pendant double bonds in

unsaturated polymer conditions. In the unsaturated elastomer chains, the primary radicals can be formed by a peroxide decomposition, abstracting a hydrogen atom from an alpha carbon to the double bond [19,27]. The antioxidants as hydrogen donors in the composition, for example, acidic fillers, aromatic oils, etc., or dissolved oxygen can reduce the cross-linking efficiency [19,26,27]. These non-productive reactions could include polymer scissions, other forms of degradative reactions and delayed scorch time. However, the coagents are added to the composition increasing both the rate and quality of curing [27]. Mainly, there are two forms of coagents, (i) polar monomers (acrylate, methacrylate esters, etc.), which form reactive radicals by addition reactions, (ii) monomers (isocyanurates, phthalates, homopolymers or copolymers of dienes, etc.), which form radicals by hydrogen abstraction [27].

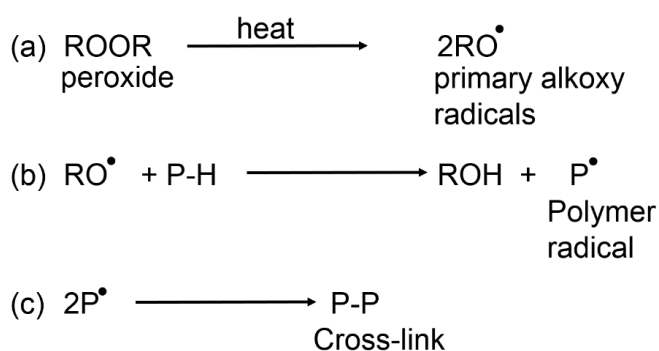


Fig. 2. Peroxide vulcanization mechanism; (a) hemolytic decomposition of peroxide, (b) hydrogen atom abstraction and hydrocarbon radical formation, (c) radical coupling with another radical and forming cross-links.

Fillers

Generally, the raw elastomers are weak, even after the cross-linking process, therefore reinforcing by fillers is widely applied in almost every modern rubber related product [14,17,18]. Reinforcing fillers, also called active fillers, are responsible for enhancing properties, for example, strength (tensile and tearing), stiffness, hardness, fatigue resistance, cracking resistance, abrasion resistance, etc. Consequently, they improve the lifespan of the rubber component in service [14,18]. The inactive fillers are utilized for reducing the price, better processing abilities, good compression set, and enhancing the heat conductivity, etc., of the product. Carbon black (CB), silica and resins generally serve as reinforcing fillers and clay, whiting and, talc are often used as inactive fillers. Even active fillers

become inactive in use with higher primary particles, for example, CB up to 100 nm diameter particles act as reinforcement, however particles larger than 1 μm are hardly responsible for the reinforcing effect [14,18,28]. The reinforcing effect of a filler mainly depends on the primary particle size, which decides the filler-filler and filler-rubber interactions, and the structure of the filler, which is the irregular nature of the filler unit and this decides the degree of restrictive motion of the elastomeric chains under external load [29,30]. Proper dispersion of the filler also plays a role in reinforcement properties and it can be achieved by mixing in a two-roll mill or an internal mixer [31]. Therefore, the active fillers in a rubber compound considerably influence the static and dynamic loading properties of rubber components. Fig. 3 illustrates the typical behavior of shear modulus as a result of the dynamic shear deformation in filled rubber conditions [29–31].

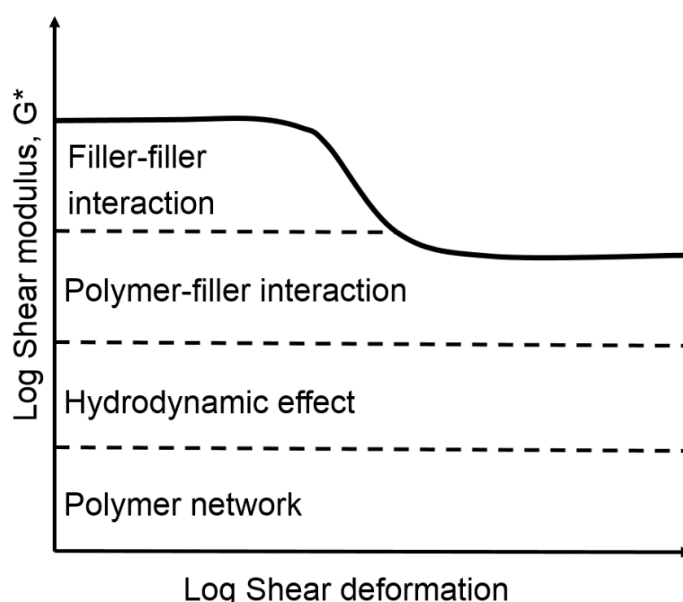


Fig. 3. A typical modulus curve of dynamic shear deformation in filled rubber [29–31].

As illustrated in Fig. 3, the mechanical properties are contributed by the polymer network, hydrodynamic effect, polymer-filler, and filler-filler interactions. The polymer network represents the properties of an elastomer and the cross-link density of the matrix and that is the effect of unfilled rubber. The hydrodynamic effect is the contribution to the modulus by the rigid particles, as they are inextensible particles, which cannot deform. Therefore, the elastomer chain movements are

restricted. The filler-rubber interactions, which are chemically or physically formed bonds, contribute to the mechanical property reinforcement. Depending on the surface area, the rubber chains, which are bonded to the particles, resist the deformation and this strong rubber layer is called “bound rubber”. In higher filler structures, the inner voids between the irregular contours are filled with rubber, they are restricted from free movements, and this is called “occluded rubber”. Immobilized rubber increases with the effective filler amount. Further, the mechanical properties are influenced by the filler-filler networks in the material, which are bonds between filler aggregates forming filler agglomerates. However, this requires a certain level of filler loading [29,30,32,33]. As Fig. 3 suggests, the contribution to the mechanical properties from filler-filler interaction and partly from the filler-rubber interaction (the physical rubber-filler interactions, for example, Van der Waals bonds, entanglements, etc.) are strain-dependent [29,32]. The stress softening at low strains is widely discussed in the rubber world as “Payne’s effect” and explained as a result of partially reversible breakdowns of the filler-filler bonds and physical filler-rubber interactions [29,30,34]. Similarly, with larger cyclic strain conditions, filled rubber experiences stress softening in the subsequent uploading cycle up to the maximum previously encountered strain. This phenomenon is referred as “Mullin’s effect” and it is generally accepted as an effect of breaking down filler-filler interactions and physical filler-rubber interactions [18,35,36].

Plasticizers

Plasticizers, which are loosely called softeners, are mainly used in the rubber compound to enhance the deformability of elastomeric material, improve filler distribution within the material, adjust the mechanical properties required in the applications as well as reduce the compound cost, etc. [14]. Processing aid oils, fatty acids, waxes, esters, low molecular weight polyethylene, pine tars, etc. are widely used in certain applications based on the requirements and conditions. Improving processing by adding the petroleum oils is well-known and they are categorized into paraffinic, naphthenic, and aromatic oils based on their chemical nature [17,37]. The compatibility of the oil and the polymer system is important; if the oil migrates out from the material, the expected physical and surface properties are deteriorated [37]. The elastomer-oil affinity is mainly based on polarity, viscosity, molecular weight, etc. Therefore, petroleum oils are mostly suited for elastomers,

which possess slight, or no polarity from the structure. For example, Nitrile butyl rubber (NBR) contains polar –CN groups, therefore polar liquid plasticizers (esters) are widely used [14,37]. Naphthenic oils are mainly used with ethylene propylene diene monomers (EPDM), styrene-butadiene rubber (SBR), polychloroprene (PC), etc. [37]. Pine tar is added to improve tack, fatigue resistance, filler dispersion, and component-to-component adhesion, while fatty acids are added to improve the filler dispersion [14,37]. The low molecular weight polyethylene, even in small amounts, reduces the stickiness of rubber in the processing in the mill or in the calendar rolls [14].

Stabilizers

Rubber grades before and even after vulcanization are susceptible to degrade in chemical, environmental, and service-related aging with the exposure to ozone, oxygen, heat, ultraviolet (UV) light, heavy metal contamination, and in contact with the oil and solvents, etc., due to possible unsaturation in the rubber chains [14,17,38]. This mainly steers to radical formations and to the chain reactions up to either cross-links or chain-scissions [17]. Therefore, the compound formulation includes stabilizers considering the used polymer type and the curing agents [38]. These reactions are accelerated at elevated temperatures. UV light helps to initiate the free radicals and generate an oxidized layer on the surface and the presence of heat, humidity, moisture, or exposure to ozone could produce fine cracks on the surface, which leads to easy abrading [17,38]. The cracked surfaces in applied service conditions, especially in cyclic loading, can become stress raisers and create easy paths to crack propagation wider into the material [17]. The presence of heavy metal ions catalyze the oxidation reactions and lead to quick aging processes [38]. Mainly, anti-oxidants and anti-ozonants are used in the compound formula as stabilizers. The use of anti-oxidants significantly retards the propagation of chain reactions, which are initiated by radical formation. Two general classifications can be found based on the method of reaction inhibition, (i) primary anti-oxidants, which terminate the chain reaction by trapping the oxy-radicals by donating H atoms, (ii) secondary or preventive anti-oxidants, which decompose the peroxides for eliminating possible alkoxy and hydroxyl radicals [17]. Anti-ozonants as chemicals or wax in the compound can migrate to the surface from the bulk and act as a protective layer against the ozone attacks [39].

Processing

The steps of processing include the mixing of elastomers and additives, shaping the product and curing. A proper mixing process utilizing mills and/or internal mixers achieves the fine blending and homogeneous distribution of additives. The processing technique, for example, a calendaring, extrusion, molding or dipping method, shapes the required component from the mixed compound. Molding has subcategories, compression molding, transfer molding or injection molding, depending on the application and the material. The shaped component is directly cured or it can be cured later in a mold, autoclave or in an oven. The supplied heat provides the vulcanizing state of the final product and gives a dimensionally stable, elastic component [14,40].

1.2.3 Basic properties for oil and gas field applications

The oil and gas industry is a major field, where elastomeric materials are applied due to their unique properties (for example, soft, highly elastic, damping, high abrasion resistance, incompressibility, etc.) as different components [6,8,9,41]. However, the demanded properties of elastomers differ from other industries due to the extreme exposure to elevated pressure and temperature conditions in a hostile chemical environment [10,11]. Among many elastomeric applications, sealing (dynamic or static) components are the primary usage in oil and gas industry [6–8,17]. The dynamic or static sealing applications are subcategorized as compliant and energized seals based on the application. O-rings, swab cups and V - packing, which are in the compliant seals category, are fitted to a predetermined shape and its interaction with the surroundings completes the sealing function. Packers are a prime application of energized sealing, which expects an outside force to distort the sealing component and interfere with surroundings [17,42]. Downhole packers and annular packers as blowout preventers, and inflatable packers are widely used as energized sealing [17]. The compliant seals are more sensitive to seal loss due to chemical and physical changes from environmental factors. However, the energized sealing applications are rather sensitive to initial elastomer properties, which is a balance of various properties, i.e., resilience, extrusion resistance, tear resistance, etc. [6,17]. The resistance to fluid absorption of elastomers is the primary concern of material selection for a sealing application, and the resistance to exposure of high/low temperatures is also considered important. Further, the material properties,

for example, resilience, compression set, stress relaxation, permeation and other mechanical properties (strength, strain at break and modulus) are expected depending on the application [42].

1.2.3.1 Fluid absorption

The swelling behavior as a result of liquid absorption is mainly a matter of the chemical structure of the elastomer. It is generally accepted that the polar media are compatible with polar elastomers and, similarly, the non-polar media are compatible with non-polar elastomers. Therefore, the polar monomers in elastomers are incompatible with non-polar fluids and vice versa [43–45]. The dipole-dipole interactions work as inter-molecular forces for compatibility [44]. The chemical resistance can vary from excellent, where there is no or little interaction, to poor, where the solvent dissolves the elastomer [45]. However, between these two extremes, the elastomer swells in contact with a fluid. The fluid molecules are transported into the network structure of vulcanized rubber by a diffusion process, where the fluid molecules transfer from a high-concentration to a lower-concentration due to random thermal motions. Therefore, the effect of the liquid depends on the time of contact and dimensions of the rubber component [46,47]. Typical polar and non-polar media are summarized in Table 1.

Table 1. Typical classification of polar and non-polar fluids [43]

Polar media	Non-polar media
water, alcohols, acids and bases, detergents, ketones, esters, etc.	mineral oils, petrol, vegetable and animal fats, grease and hydrocarbons, silicone oils, etc.

The degree of swelling of elastomers is usually a measure of resistance to a certain liquid; the polar elastomers do not swell significantly in oil or other non-polar media, however, they may swell substantially in certain polar liquids [47]. Other than the chemical nature of the monomer, the free volume between chains, cross-link density and filler mainly control the liquid uptake. Increasing the glass transition temperature (T_g) decreases the free volume, which could accommodate absorbed liquid, and subsequently, reduce the degree of swelling. Cross-links work against the movement of molecules and thus inhibit the swelling ability. Fillers improve the

mechanical properties and, simultaneously, reduce the amount of matrix material available for liquid absorption [6]. Similar to liquids, gases in high-pressure conditions dissolve into the surface of elastomers and diffuse to the interior. The polarity of elastomer functional groups increases the solubility of polar gases into the material [48]. The sour gaseous environments, for example, carbon dioxide (CO₂) or hydrogen sulfide (H₂S), which occur naturally as well as in conditions in which they are purposely injected to reduce the viscosity of the oil to improve the yield, are more complex as they form aqueous and non-aqueous electrolytes and interact with elastomers [10]. HNBR is stiffened by increasing cross-link density at the exposure of H₂S, which can dehydrogenate the HNBR molecules and lead to more C–C linkages at elevated temperatures [49]. H₂S ages FKM by removing hydrogen and fluorine from the backbone (dehydrofluorination), that increases the unsaturation and later it also increases the chain reactions up to the chain-scissions at elevated temperatures [49]. Similar to the liquids, the gas sorption decreases with increasing cross-links, T_g and amount of filler with good filler-rubber interactions [48].

1.2.3.2 Thermal resistance

The elastomeric materials used in oil and gas field applications are expected to face a broad range of temperatures, for example, in arctic conditions, subzero temperatures during off periods, extremely high-temperatures during production, etc. [17]. Therefore, it degrades chemically in higher temperatures and loses its flexibility in lower temperatures [6]. In the presence of oxygen, the heat accelerates the polymer oxidation through possible free radical chain reactions which leads to cross-linking or polymer chain-scission [50,51]. This oxidative degradation is identified as a serious problem, which the rubber encounters at elevated temperatures [51]. During thermo-oxidative aging, if the chain-scission dominates, the material softens and subsequently hardness and stress at certain strain decreases; further, depending on the degree of aging, the strain at break either decreases or increases. If the cross-linking dominates, the material stiffens and subsequently the hardness and stress at certain strain increases, while the strain at break decreases [52]. The ratio and the extent of these two phenomena are based on elastomer type, compounding as well as the temperature and oxygen

concentration [53]. Several factors can improve the resistance to thermo-oxidative degradation, for example, chemical composition, chain length, type and density of cross-links, etc. Unsaturated elastomers, which contain electron-donating groups, are easily attacked by oxygen at elevated temperatures and subsequently the properties are degraded. Therefore, elastomers with the least unsaturation show good or excellent heat resistance [54]. In addition, anti-oxidants, which retard possible chain reactions initiated in the presence of oxygen at a higher temperature, are used to increase the heat resistance, as described in the chapter of stabilizers.

At lower temperatures, near or below the T_g , the elastomeric material changes from an entropy elastic state to a stiff energy elastic state, which reduces the resilience of the material, and it loses the rubbery nature and consequently the sealing properties [55]. However, the flexibility of most elastomers remains only above 10 °C from the T_g ; below that they stiffen exponentially [17,42]. The chemical structure of an elastomer mainly determines the glass transition temperature. For example, introducing 'irregular' monomers to the backbone can reduce the tendency to crystallize and as a result, decreases the T_g and improves the low-temperature flexibility, depending on the main chain features [56]. Furthermore, additives, for example, plasticizers, are commonly added to the compound increasing the low-temperature properties; however, this reduces the modulus and some other mechanical properties [17,56].

1.2.4 Rapid gas decompression (RGD)

The RGD damage is a structural failure expected in elastomers, especially in seals, when they are exposed to high-pressure gas and fail upon the sudden release of the pressure. This process leads to a great volume increase (even up to 20%), depending on the gas/elastomer composition and ambient conditions. Consequently, void formation, blistering and internal cracking up to component failure can be expected [48,55,57–64]. This particularly concerns the applications in oil and gas field facilities subjected to a "dry" environment (typically less than 5% liquid content) in high-pressure, high-temperature exposures [61]. The complete RGD process can be divided into two steps; (i) compression phase, where the elastomer is exposed to a high-pressure gas and subsequent gas sorption into the material, (ii) decompression phase, where the elastomeric component experiences

the sudden release of ambient pressure and subsequent gas desorption from the material.

Compression phase

When elastomers are exposed to high-pressure conditions, the gas on the elastomer engages in two separate and distinct phenomena, namely, the material compression from applied hydrostatic pressure and the gas sorption into the elastomer [48,55,58,59]. The gases diffuse into the elastomeric material and mobilize the elastomer chains, increasing the free volume and even ending up at plasticization depending on the amount of gas. However, the compression from the ambient pressure on the material works against these effects [48,65]. Therefore, the volume change of elastomeric materials exposed to gases can be contractive or dilating, based on the mentioned predominant factors and can be varied with, for example, type of gas, temperature, pressure, elastomer grade, etc. [48,59].

The gas saturates the elastomer with time, and the amount of gas in the material primarily decides the plasticization and the degradation of mechanical properties. Further, the dissolved amount of gas is adversely affected in the decompression phase, which nucleates and expands the elastomer during the release of ambient pressure conditions [48,55,65]. The increased solubility and decreased permeability properties of a gas/elastomer combination increase the degree of gas within the elastomer [55]. Generally, the gas enters to the elastomer surface by gas adsorption and it is governed by Henry's law, as shown in Equation 1 [48,63–65]. Where C , S and P are the gas concentration, solubility coefficient and the applied gas pressure, respectively. This theorem has been applied and proved up to 10 MPa conditions [64], however for the higher pressure applications, the equation needs to be adjusted or other models are applied [48].

$$C = S \cdot P \quad \text{Eq. 1}$$

Adsorbed gas on the surface diffuses to the bulk of the elastomer and later it dissolves into the matrix or permeates through the body [63,65]. The permeability of an elastomeric membrane, which is a combination of adsorption and diffusion, can be expressed by applying the Fick's law of diffusion to Equation 1, as shown in Equation 2. Where q/t , D , Q , ΔP , h and A are the gas permeation rate, diffusion coefficient, permeation coefficient, pressure difference, thickness of the membrane

and the membrane surface area, which is perpendicular to the thickness, respectively [63]. Once these values are determined experimentally, the gas concentration in a pressurized elastomer component can be calculated after an exposure.

$$\frac{q}{t} = \frac{D \cdot S \cdot A \cdot \Delta P}{h} = \frac{Q \cdot A \cdot \Delta P}{h} \quad \text{Eq. 2}$$

Decompression phase

The general phenomenology of this gas-induced failure during decompression after exposure to a high-pressure ambient is shown in Fig. 4. As illustrated, the sudden pressure release may induce a hydrostatic pressure difference between the elastomer and the surrounding and a thermal field as a result of adiabatic cooling [48]. The ambient pressure release creates a negative hydrostatic tension state internally in the material and simultaneously the material becomes supersaturated with the gas and the surplus gas diffuses out of the component producing a gas concentration gradient. This creates effective hydrostatic stress gradients in the material and, consequently, the local volume changes. Simultaneously, the dissolved gas expands and creates additional stresses inside the material [48,59]. The matrix material transfers the stresses to fillers in the composites or to possible hard inclusions and these may become stress raisers [59,63]. If the stress concentration exceeds the critical stresses, a crack is initiated. The magnitude of the stresses is based on the dissolved gas amount, induced damage of the sample, the decompression rate, etc., and the cracks can propagate even up to the surface of the component, which appear as surface blisters or cleavage cracks on the surface [59,63,64]. However, the failure initiates within the matrix as cavitation at a void, pre-existing flaws, or softer matrix area [48,59]. Further, the weakly bonded filler/hard inclusion interfaces can be detached as a result of stress raising and form vacuoles. However, the vacuoles propagate into the matrix and lead to failure [59]. Within the homogeneous elastomers, which contain no filler or dirt, the free volume gaps in the network may interconnect during the gas bubble growth and act as a surface of weakness or softer matrix area, which can act as crack nucleation point [63].

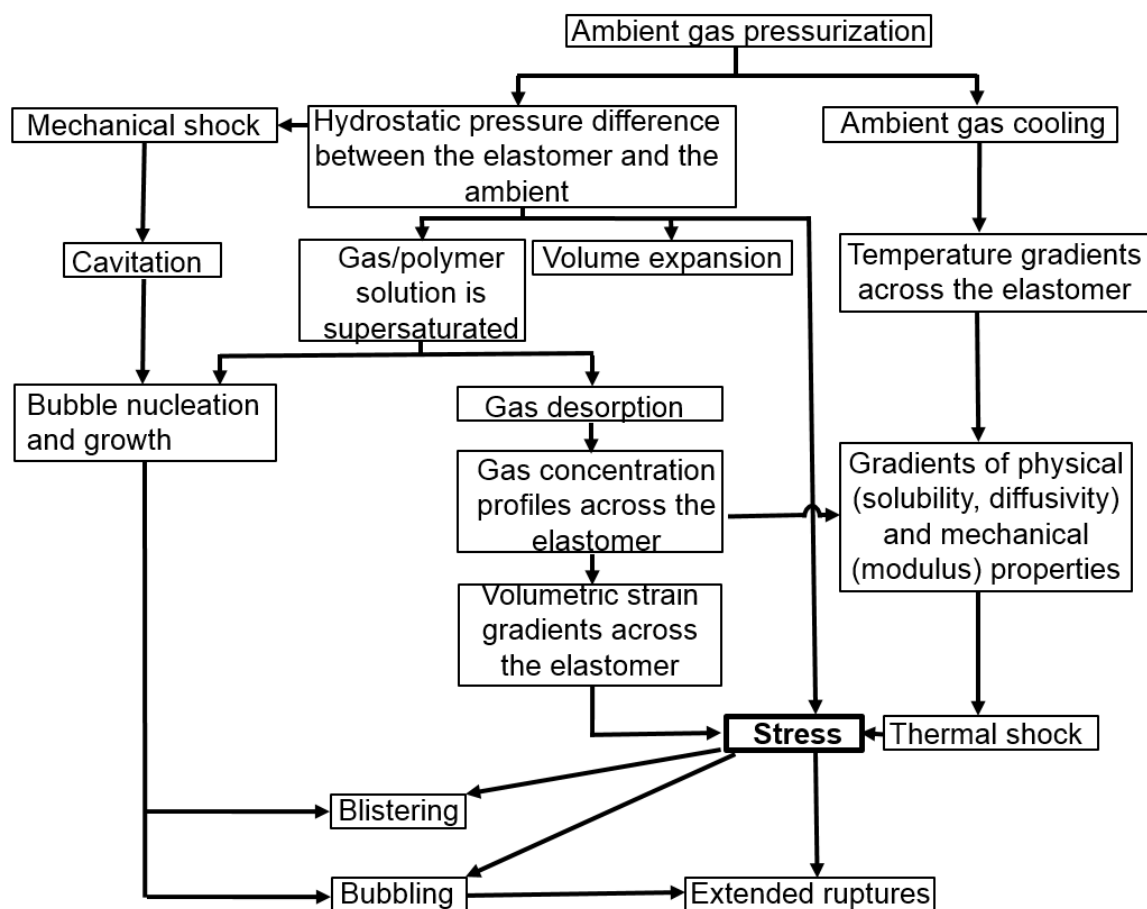


Fig. 4. Schematic illustration of possible phenomenology during the decompression phase [48,65].

Bubbling and blistering

As mentioned above, at the exposure of an elastomeric material to a gas, the supersaturated gas molecules cluster at cavities (initial defect). During the decompression, they experience a tri-axial tension state and form micro-meter sized bubbles within the material [48,59,64]. If no cracks are initiated after the decompression, the formed bubbles are exterminated with desorbing solute gas molecules [64]. However, the blistering or crack initiation would take place by formed bubbles, which are spherical cavities containing an inner pressure. Criteria explaining the inner pressure, which is needed for a blister initiation, can be mainly explained in two classes, for example, the energy approach, and the stress state and finite strains approach [64,66].

A model based on the stress field and the elastic instability inside a bubble reveals that the pressure inside of a stable bubble cannot exceed a critical value for a neo-

Hookean material (incompressible). Therefore, the maximum pressure (P_c) to be withstood before an unstable crack initiates is shown in Equation 3 and 4 as a function of Young's modulus (E) and shear modulus (μ), respectively, considering the isotropic traction [59,63–66]. The detailed derivations of these simplified equations can be found in the literature [64,66].

$$P_c = \frac{5E}{6} \quad \text{Eq. 3}$$

$$P_c = \frac{5\mu}{2} \quad \text{Eq. 4}$$

Utilizing the fracture mechanics tools, especially the energy approach, a criterion (the energy release rate (G)), has been derived for bubble growth in neo-Hookean material under the imposed hydrostatic stress as expressed in equation 5 [64,67]. Where, a_0 is the radius of an un-deformed bubble, λ_1 is the stretch ratio of the inner surface of the bubble (if a = deformed bubble radius, $\lambda_1 = a/a_0$). This equation is simplified assuming a spherical shape cavity in an infinite body. When the energy release rate exceeds the fracture energy for a micro crack (G_c), $G \geq G_c$, the bubble growth engages in blister initiation (irreversible growth) [64,65,67]. The detailed derivation of this equation can be found in Diani, 2001 [67].

$$G = \frac{E a_0 (1 - \frac{2}{\lambda_1} + \lambda_1^2)}{3} \quad \text{Eq. 5}$$

Material requirements for RGD resistance

The degree of RGD failure depends on several factors, for example, the elastomer, additives, ambient conditions (contacting gas, temperature, pressure), number of pressurization and depressurization cycles, depressurization rate, etc. [7,48,58,59,64,65,68]. The elastomers used in the oil and gas industry, especially considering the RGD resistance, require certain mechanical properties and some important features, for example, the tear and tensile strength must be as high as possible, higher hardness (85 IRHD or above), higher elongation at break (above 100% at ambient temperature). An elastomeric compound with no or reduced surface imperfections, better filler-rubber mixing, which can possibly reduce the

stress raisers (filler agglomerates), and a controlled curing process, which avoids the low strength sights and imperfections, are in favor of RGD resistance [7,55,61]. High solubility and a low permeation coefficient in elastomer/gas combination are highly adversely effective in RGD resistance. Under such conditions, high amounts of gas stay in the material and a greater volume expansion during decompression can be expected [55]. A lower solubility of gases in the polymer is expected with higher ACN content, for example, in nitrile-based elastomers [7]. A higher permeation coefficient, which is particularly obtained with higher chain flexibility of the elastomer, can be achieved with the selection of polymer and the amount of filler [65]. Generally, higher filler loading with an inactive filler improves permeability. Therefore, the solubility and permeability can be adjusted during the compounding with additives [7].

Effect of CO₂ in RGD

Carbon dioxide (CO₂), which is a common gas in oil and gas wells, is in a supercritical state at high-pressure (> 74 bar) and high-temperature (> 32 °C) conditions, as shown in Fig. 5 [10,69].

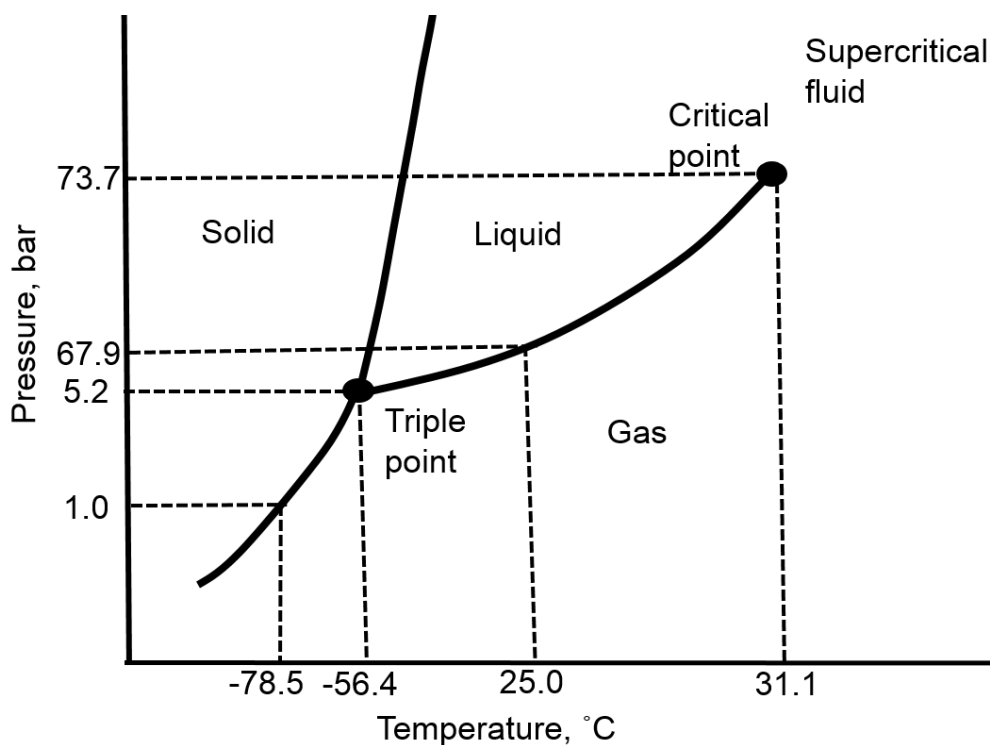


Fig. 5. Schematic of the phase diagram of CO₂ [69–71].

Super-critical CO₂ is far denser than the gaseous state; consequently, it takes up a small volume compared with its gaseous phase [70,71]. Therefore, in the RGD phenomenon, being a “small” molecule, critical CO₂ can increase the sorption into an elastomer and during the sudden ambient pressure release, losing the critical state can increase the volume significantly. This process greatly affects the RGD resistance [69]. Furthermore, CO₂, which has a small and permanent dipole that is not canceled in the critical state by rotation, is capable of multiple types of associations with polar elastomers [69,71]. Therefore, a greater amount of swelling is expected in the polar elastomers in contact with CO₂ compared with non-polar elastomers [48,69].

1.2.5 Elastomers for the oil and gas industry sealing applications

Widely used elastomers in oil and gas field applications

To meet the requirements in specific operating conditions of sealing applications, a wide range of polymeric materials are being developed. However, depending on the application, elastomers, for example, nitrile and hydrogenated nitrile rubbers (NBR and HNBR grades), a high number of different fluororubber grades (Fluorocarbon (FKM), Tetrafluoroethylene propylene copolymer (FEPM), Perfluoroelastomer (FFKM), etc.) are conventionally used [11,72,73]. In addition, some thermoplastic elastomers, for example, Polytetrafluoroethylene (PTFE) and PTFE compounds, polyurethane (PU) compounds, and high-performance thermoplastic grades like polyether ether ketone (PEEK) or fiber reinforced PEEK compounds are added to the sealing component [11].

Due to the excellent balance in oil-resistance, mechanical properties and durability, NBR is one of the oldest and most widely used classes of elastomers [17]. This is a product of butadiene (BD) and acrylonitrile (ACN) and depending on the application, the ACN content varies from 18 - 51% [9,17,74]. The polar nature of ACN content increases the chemical resistance and in particular resistance to non-polar solvents [72]. It is difficult to maintain both good resistance to fuels as well as low-temperature flexibility. Therefore, a compromise in properties is expected [42]. The high level of unsaturation is subjected to oxidation and sulphur attack [17]. Therefore, it can be used only up to 100 °C in general circumstances [42]. However, NBR grades can

be used at elevated temperatures up to 200 °C in downhole environments, where usually an oxygen-free atmosphere is expected [72]. The hydrogenated nitrile butadiene rubber (HNBR), which is formed by hydrogenating the double bonds in the backbone of NBR, is expected to perform better in higher temperature applications [17]. HNBR shows excellent heat and oil resistance, further, the ability to control the residual double bonds (RDB), ACN content, molecular weight, and certain other properties according to the application is particularly convenient [72,75]. Fluoroelastomers have incorporated the fluorine into the polymer backbone, which increases the polarity of the structure and bond strength. Therefore, it increases the resistance to hydrocarbon fluids and at the same time decreases the low-temperature flexibility and processability. The saturated chemical structure is prone to provide thermal resistance [42]. Therefore, fluororubber grades, for example, FKM and FFKM, provide higher resistance to thermal and chemical-induced aging, compared with nitrile-based rubber grades [72]. FEPM, on the other hand, which contains an ethylene part, decreases resistance to non-polar fluids but increases the resistance to water and other polar fluids, compared with FKM or FFKM [42].

As a thermoplastic elastomer, PU cannot withstand high-temperature or load conditions, which deform plastically and is not be recoverable [42]. However, PU brings excellent leakage, wear and pressure resistance, and reasonable fluid compatibility to the sealing components [11]. PTFE is preferred for harsh environments depending on the application due to its high chemical and temperature resistance (up to 300 °C), friction and wear resistance, low swelling from liquid or gas [11,76].

Selecting an elastomeric class for a sealing application operating in harsh service conditions needs to consider certain performance factors depending on the working atmosphere. The ability to work in high-temperature conditions as well as the possibility to operate at low-temperatures without becoming stiff and brittle is vital, as is excellent swell resistance or controlled swelling based on the application in contact with aggressive fluids. The resistance to failure, for example, by RGD, requires high mechanical properties, and other sealing functions would require low compression set, resilience and high abrasion resistance. However, an elastomer

grade, which can equally offer the oil resistance, thermal resistance, and low-temperature flexibility, does not yet exist. Therefore, both the temperature and the surrounding medium should be taken into consideration when selecting basic elastomer grades for oil and gas field sealing applications [8,22,41]. Fig. 6 shows the ASTM D2000 Chart, which plots some common rubber elastomers and their resistance to chemical and thermal conditions. This chart even rates some other well-known elastomer grades, for example, silicon rubber (VMQ), EPDM, NR, SBR, and it reveals their inapplicability to oil and gas field applications compared with the fluoro or nitrile-based rubber grades [8,41]. EPDM is a well-known sealing material containing ethylene, propylene monomers and a third monomer, diene, in the backbone. This provides the best resistance to hot water, steam and some polar solvents. However, the diene reduces the resistance to thermal aging and its non-polar nature allows swelling in hydrocarbon oils, greases, and fuels. Therefore, it ousts to be selected for oil and gas field applications [42].

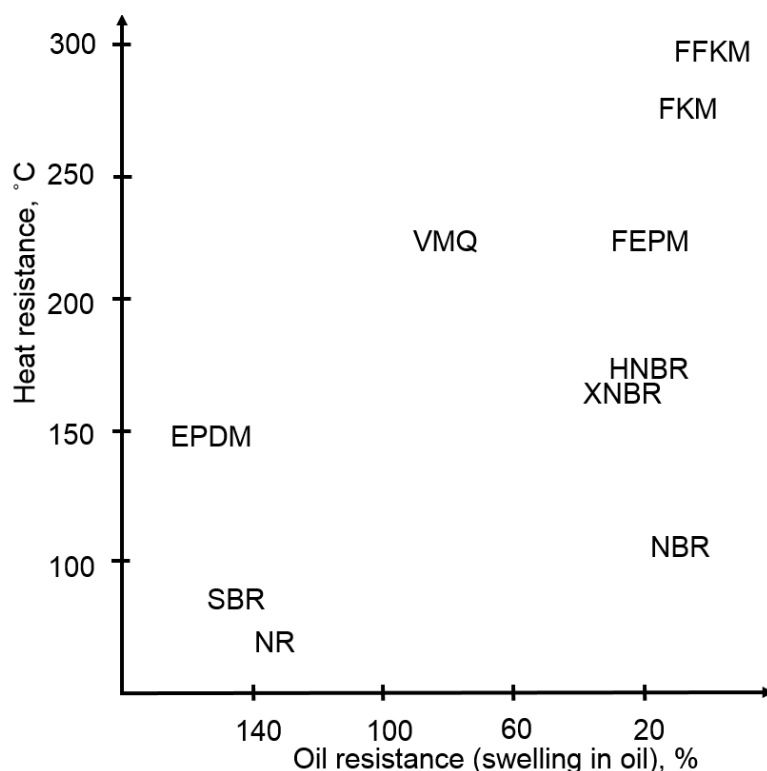


Fig. 6. Comparison of some elastomeric grades with their oil resistance and thermal resistance [8,41].

Furthermore, the processing and performance properties in some widely used elastomeric grades in oil and gas field are summarized in Table 2 [8,17].

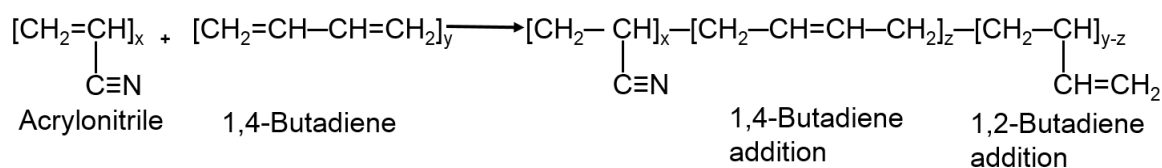
Table 2. Comparison of some basic processing and performance properties of widely used elastomers in the oil & gas industry [8,17].

Basic property	NBR	HNBR	XNBR	FKM
Compression resistance	1	1	2	1
Resilience	2	2	3	2
Tear strength	2	2	1	2
Abrasion resistance	2	2	1	3
Low temperature (°C)	-40	-35	-35	-18

Very good = 1; good = 2; average = 3; poor = 4

Hydrogenated nitrile butadiene rubber (HNBR)

As the name suggests, the HNBR is the hydrogenated NBR, (also known as highly saturated nitrile (HSN) in former times) [17]; it provides major improvements in chemical and heat resistance as well as in physical properties compared with the NBR [7]. The NBR material grade is synthesized by polymerizing the acrylonitrile (ACN) and butadiene (BD) monomers. As depicted in Fig. 7, BD can be placed in two different ways in the free radical polymerization, for example, addition to 1,4 position or 1,2 position, which form the bulk of the BD fraction and a pendant carbon-carbon double bond, respectively [17].

**Fig. 7.** NBR Polymer structure [17].

The saturation process of NBR to hydrogenated nitrile butyl rubber (HNBR) reduces the number of double bonds in the backbone considerably as shown in Fig. 8, which greatly improves the heat resistance by eliminating the typical sites that get attacked by oxygen [9,17]. Further, transforming the irregularly placed double bonds into regular ethylene units improves mechanical properties [7].

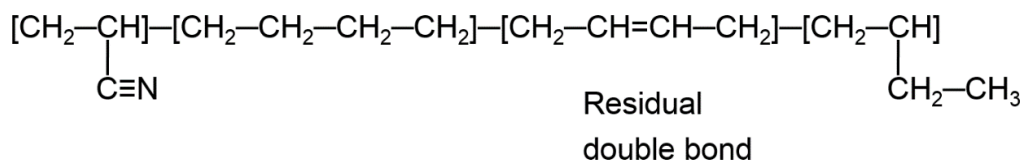


Fig. 8. HNBR Polymer structure [17].

Similarly to the NBR, the ACN/BD ratio decides the properties of the resulting HNBR elastomer. A better resistance to oil, gasoline and solvents, as well as a lower gas solubility into material are expected with the higher degree of ACN content. Further, increasing ACN content improves the thermal stability, however the polarity of an ACN group creates strong attractive forces, which restrain the molecular mobility and subsequently reduce the flexibility of the material and increase the hardness [9,17,68,74,77,78].

The combination of nearly saturated backbone, polar and inert ACN groups of HNBR creates a nearly ideal elastomer to deliver the performance criteria in oil and gas field applications [7], and further, it is widely used in many other engineering applications in the automotive and heavy-duty markets [75] due to its unique combination of excellent properties. For example, HNBR has good mechanical, dynamic, and sealing characteristics even at elevated temperatures including resistance to tearing, abrasion and extrusion. At the same time, it shows considerable chemical resistance to fuels, oils and sour gas exposure, which are essential properties expected in oil and gas industry and further in the resistance to RGD [7,8,75].

The residual double bonds (RDB) in the backbone are favorably effective in the vulcanization process, however, the resulting elastomer is susceptible to ozone, oxygen, or active sulfur in the environment, especially at elevated temperatures [17,79] (A detailed explanation of thermo-oxidative aging is given in the next chapter). Nevertheless, HNBR contains a relatively low RDB content; therefore the vulcanization with active-sulfur and sulfur donors is almost impossible (if the RDB level is below 4%). Therefore, organic peroxides are widely used for HNBR vulcanization. Sulfur or peroxide vulcanization has its own properties, where a sulfur vulcanized elastomer demonstrates a fair balance of high ultimate elongation and compression set resistance, while peroxide cross-linked HNBR has better

compression set resistance and heat resistance [17,79]. For effective vulcanization, generally, HNBR requires 5-8 phr of peroxide levels. The vulcanization process and temperature decide the specific peroxide to be used, as there are many different possible varieties available. However, dicumyl-peroxide at conditions under 177 °C or α , α -bis (t-butylperoxy) diisopropylbenzene at conditions above 150 °C on an inert carrier for vulcanization are widely applied organic peroxides in the synthesizing of HNBR [17,80]. Coagents are used to enhance the effectiveness of peroxide vulcanization, which stabilize the free radical source formed by peroxide decomposition and reacts with HNBR to create possible cross-links within the chains [17].

Among extensively used elastomeric material grades, HNBR plays a vital role in the history of seals in aggressive oil and gas applications, having a high number of HNBR sealing parts, due to high chemical and thermal resistance [9,81]. Additionally, they can be easily removed and replaced during routine maintenance as the HNBR is a relatively cost-effective material [81].

Thermo-oxidative aging of HNBR

According to the literature, the increase in cross-links, as well as chain-scissions, are the main possible aging mechanisms at elevated temperatures for HNBR [77,79,82]. Despite hydrogenation, RDBs do exist on the main chain of HNBR and they have been identified as the strongest factor for cross-linking and chain-scission mechanisms of HNBR [74,77,79,83–85]. Stable delocalized radicals are generated by the abstraction of the allylic hydrogen (a hydrogen atom, which is attached to a carbon atom next to the RDB) or reaction with the O₂, compared with the other possible alkyl radicals [74,79]. The possible chain reactions in thermo-oxidative aging can be divided into two main steps, (i) the formation of hydro-peroxides and (ii) reactions of formed hydro-peroxide with the main polymer. Fig. 9 shows a possible reaction of allylic hydrogens with the oxygen molecules, and subsequently forming stable radicals. Oxygen molecules as di-radicals easily react with the polymer radical, which creates a more stable peroxy-radical. In the presence of oxygen, the peroxy-radical abstracts hydrogen from another polymer chain to form a hydro-peroxide and finally a new polymer radical and continue the chain reactions. At elevated temperatures, these autocatalytic reactions lead to a high-concentration

of hydro-peroxide within the polymer and it could lead to a number of other reactions resulting in highly oxidized moieties, as shown in Fig. 10. In the presence of metal ions, the oxidation process is accelerated [77,79,86]. As depicted in Fig. 9 and Fig. 10, autocatalytic reactions generate main chain polymer radicals, however by their recombination, stable compounds are created increasing the cross-linking density [79,84].

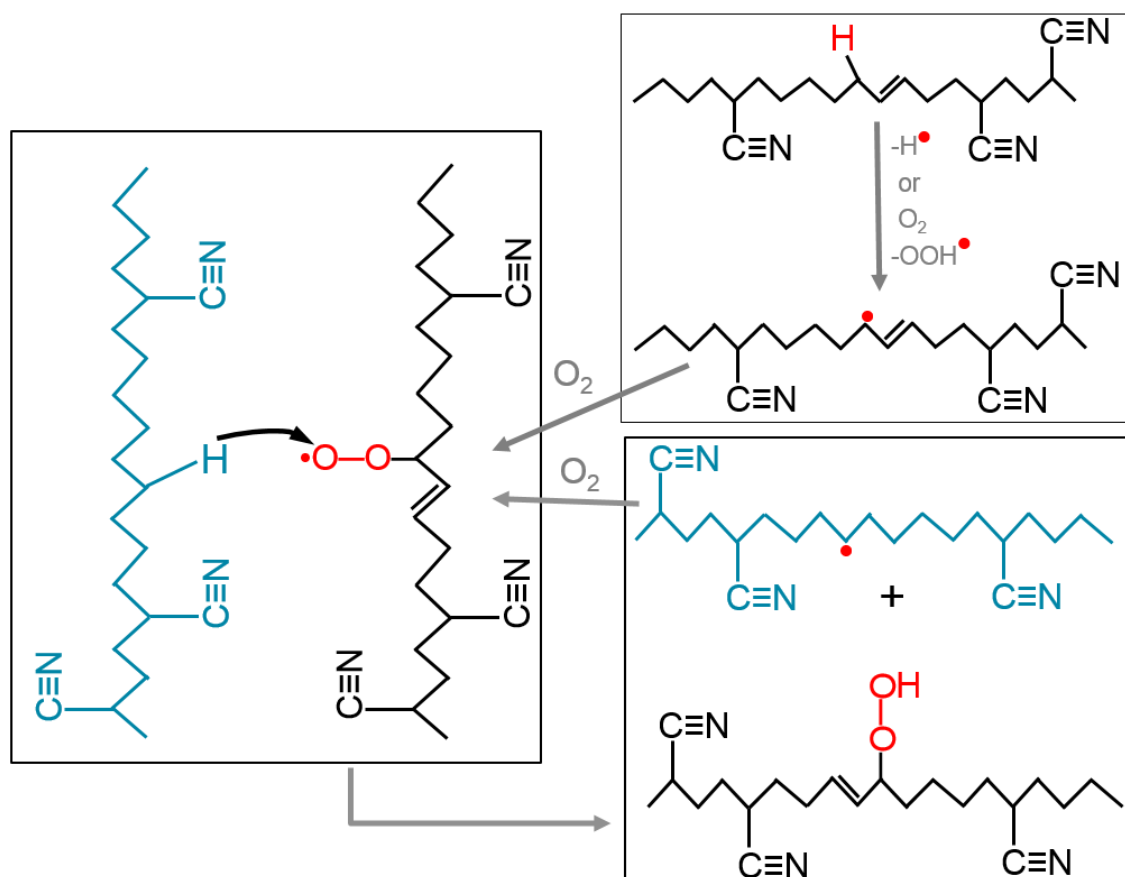


Fig. 9. Formation of hydro-peroxide as a result of thermo-oxidative aging [79,86]

As depicted in Fig. 9 and Fig. 10, several chemical reactions of HNBR in the presence of oxygen form hydro-peroxide and more other radicals (alkoxy, peroxy, hydroxyl, and etc.) and they can lead to the breaking of the main chains, as summarized in Fig. 11 [74,77,79]. The possible further chain-scission reactions are shown in Fig. 11, while Fig. 11a indicates the possibility of oxidizing the hydro-peroxides, and b and c show the influence from nitrile group on the hydrogen of α carbon and possible β scissions providing more polymer radicals. Newly formed

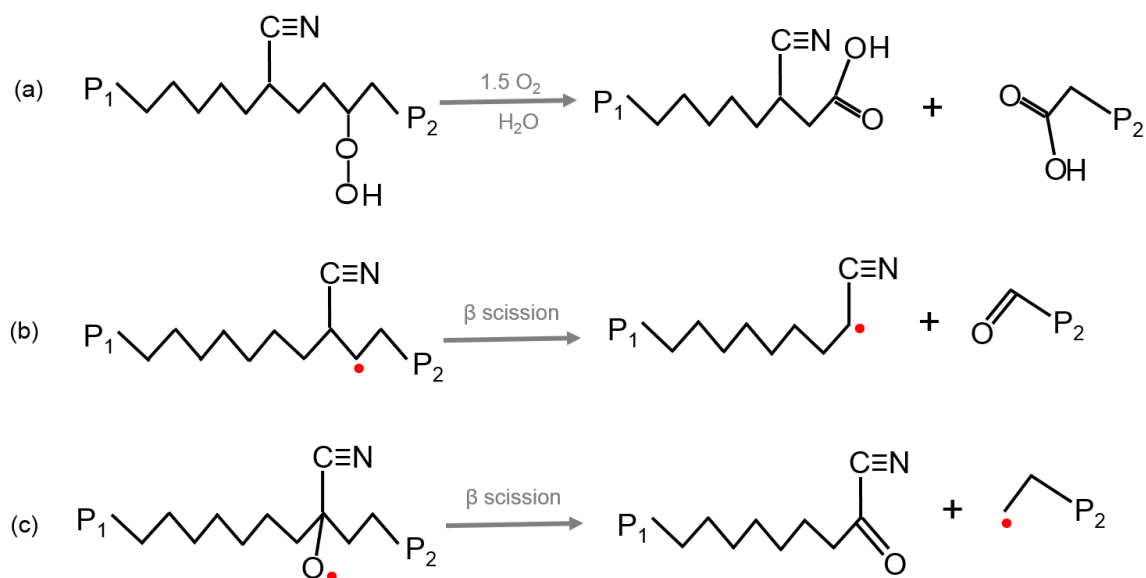


Fig. 11. Possible chain-scission reactions for HNBR (P1, P2 = polymer segments)

1.2.6 Component level RGD testing

Testing standards

As previously explained, the RGD phenomenon occurs when elastomeric components are exposed to high-pressure gas and fail when the pressure suddenly drops [48,58,62,68]. This process depends on several service factors, for example, temperature, exposed media, pressure, housing geometry, seal geometry, cyclic conditions, etc. [87]. To identify possible damage during service conditions, several industrial and customer specific testing standards are available, which differ from each other in certain aspects to guarantee the material applicability in different conditions [61,87]. However, NACE TM0192-2012-SG [88] and Norsok M-710 [89] testing standards are widely accepted for the appraisal of elastomers in the oil and gas industry. Table 3 summarizes NACE and Norsok standards and their different testing conditions.

The NACE standard is applicable only with the extreme conditions similar to the high-concentration of CO₂. However, Norsok is widely used in industry, as it is more comparable with actual service conditions (high/low or pure CO₂, or CH₄: CO₂ mixture) [61]. Further, the Norsok standard contains a ranking procedure to define seal failure considering crack lengths, crack position and quantity of cracks within the cross-section. For the ranking, the RGD tested O-rings are sectioned into four

similar size pieces and the cross-sections are then analyzed microscopically. The ranking system rates the materials from 0-5 for each section where 0 = no cracks or blisters, and 5 = cracks throughout the cross-section or seal fragment. A failure criterion for a NORSOK test is defined by a rating of 4 or 5 in any section quadrant [89].

Table 3. NACE and NORSOK standard test procedures [88,89].

Parameter	Standard	
	NACE	NORSOK
Media	CO ₂	CO ₂ , CH ₄
Temperature [°C]	RT, 50, 100, 120, 150, 175, 230	100, 150, 200
Pressure [bar]	70, 170, 280, 380	150, 200, 300
Cross-section [mm]	5.33	5.33
Internal diameter [mm]	37.47	37.47
Exposure period [hours]	24	72
Decompression rate [bar/min]	70	20-40
Constraints	Free or constrained	Constrained
Cycles	1	1, 5, 10, 30
Inspection	internal & external, hardness, tensile strength, diameter, modulus & elongation	internal and external, 10 times magnification

Component level RGD test set up

The characterization of RGD failure resistance of elastomeric seals in this research work was conducted using an autoclave test set up. A specially designed autoclave by SITEC (Sieber Engineering AG, Zürich, CH), which is located in the facility of SKF Sealing Solutions Austria GmbH, provides the possibility to carry out the tests on a component scale varying the gas type, test temperature, maximum pressure, and decompression rate. The system consists of a high-pressure autoclave, CCD camera system, a control-heating unit, and a data acquisition system as shown in Fig. 12.

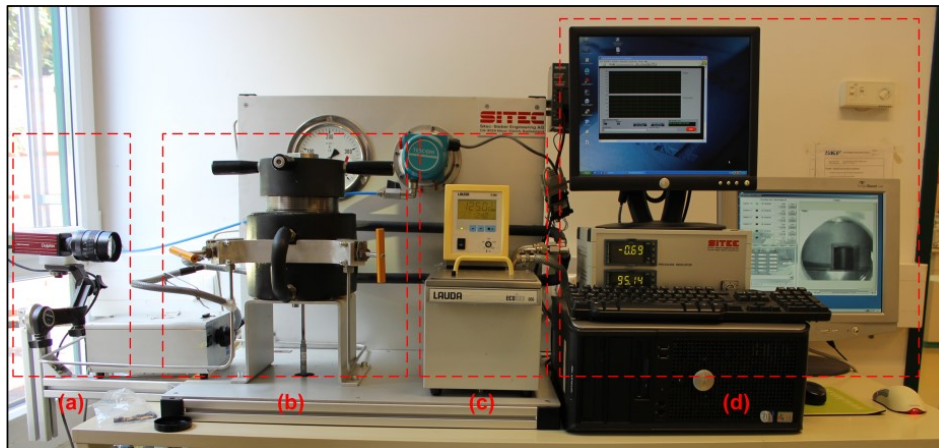


Fig. 12. The autoclave test set up for component level RGD tests; (a) Camera system, (b) autoclave, (c) heating unit, (d) monitoring and data acquisition [65].

The autoclave, which is 500 cm^3 in volume, allows pressure up to 300 bar, temperature up to $145 \text{ }^\circ\text{C}$, and the fastest decompression rate up to 25 bar/second. The system is equipped with the possibility to work with CO_2 and CH_4 in pure and mixed combinations. Further, the test set up is equipped with built-in pressure and temperature sensors, which provide the actual measurements in the autoclave chamber. The transparent glass window of the autoclave allows the camera to capture in-situ pictures, which can be used later to calculate the volume increase during the compression and decompression phases. Complete O-rings or cross-sections of O-rings (cylindrical specimens) can be tested in constrained or unconstrained conditions utilizing the test set-up. Fig. 13 shows certain stages of volume change of unconstrained cylindrical specimens during a typical test procedure. The tracker software package (Tracker 4.95, Douglas Brown physlets.org/tracker) was employed for measuring the height and diameter of the cylindrical specimen, which can be utilized for calculating the volume change during the test. Therefore, the saturation time and the volume expansion in the pressurization phase, the reduction of chamber temperature in the decompression phase, and the volume expansion in the decompression phase can be observed in different testing conditions.

During the RGD tests, generally, the chamber experiences a snap, however a slight, temperature increase in the pressurization phase and this disappears at the stabilized pressure. During the decompression, the previous testing experiences

also revealed a whit phase shift in temperature reduction in the chamber with the pressure release, as a result of an extremely high release rate or uneven pressure release rate, where the elastomeric component may encounter adiabatic heating in the bulk [58,65]. Therefore, the typical temperature and volume change in elastomeric specimens in pressure increase and sudden release during pressurisation and depressurisation phases, respectively, are as shown in Fig. 14. The volume increase during the compression phase and the decompression phase are indicated in the graphs as ΔV_{comp} and ΔV_{decomp} , respectively. The time taken to initiate (t_{ini}) and to achieve the maximum of volume increase (t_{max}) during the decompression phase as well as the gradient of the volume change (k_{decomp}) are indicated in Fig. 14b. However, an even and moderate pressure release rates can assume no or slight temperature reduction in the autoclave during the decompression phase.

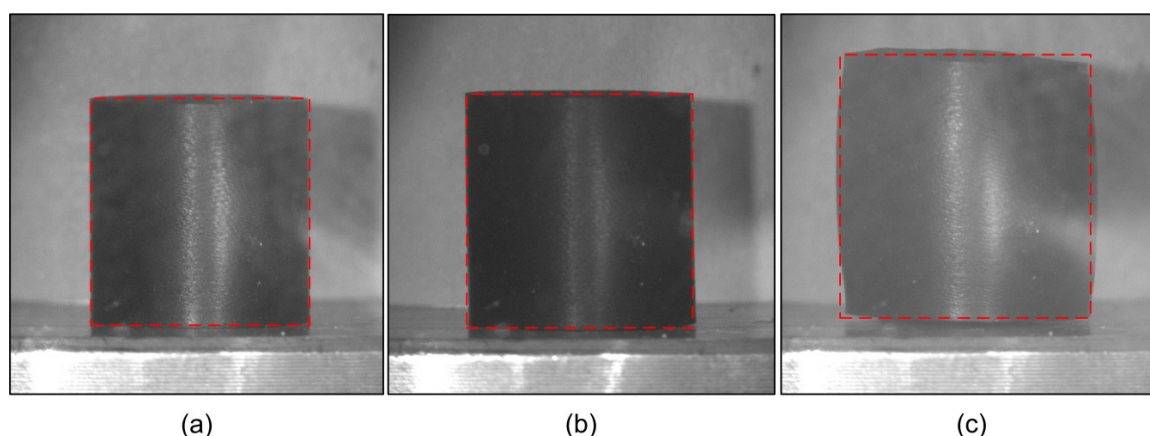


Fig. 13. Sample picture analysis for volume change calculations during component level RGD tests in autoclave test system; (a) Start of pressurization, (b) During compression phase, (c) during decompression phase [65].

Testing for rapid gas decompression as a complex phenomenon, which encounters several factors, needs to avoid the inherent inhomogeneity and imperfections of the materials and components for achieving reproducible results. Further, test parameters, boundary conditions and maintaining a constant pressure release rate are needed for obtaining better results.

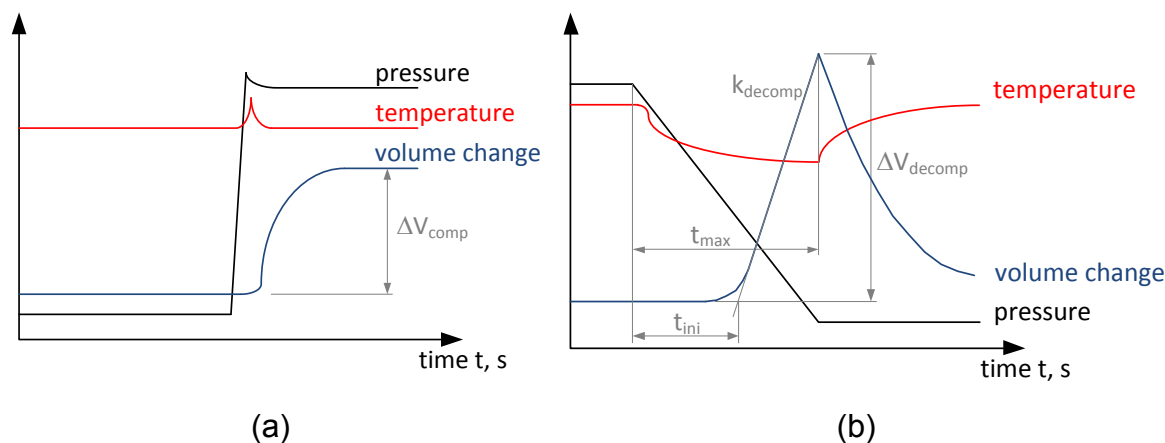


Fig. 14. Typical trend of changing the temperature and volume of the elastomeric specimens during pressure deviation; (a) pressurization, (b) de-pressurization [65].

I.3 References

- [1] World economic forum, Future of oil & gas: Global agenda council on the future of oil & gas, Geneva, Switzerland, 2016.
- [2] A. Belani, S. Orr, A systematic approach to hostile environments, *Journal of Petroleum Technology* 60 (07) (2015) 34–39. <https://doi.org/10.2118/0708-0034-JPT>.
- [3] G. Debruijn, C. Skeates, R. Greenway, D. Harrison, M. Parris, S. James, F. Mueller, S. Ray, M. Riding, L. Temple, K. Wutherich, High-pressure, high-temperature technologies, *Oilfield review* 20 (3) (2008) 46–61.
- [4] S. Sharma, S.K. Ghoshal, Hydrogen the future transportation fuel: From production to applications, *Renewable and Sustainable Energy Reviews* 43 (2015) 1151–1158. <https://doi.org/10.1016/j.rser.2014.11.093>.
- [5] P. Agrinier, D. Roizard, M.F. Ruiz-lopez, E. Favre, Permeation selectivity of gaseous isotopes through dense polymers: Peculiar behavior of the hydrogen isotopes, *Journal of Membrane Science* 318 (1-2) (2008) 373–378. <https://doi.org/10.1016/j.memsci.2008.03.011>.
- [6] R.P. Campion, B. Thomson, J.A. Lewis, *Elastomers for fluid containment in offshore oil and gas production: Guidelines and review*, HSE Books, Sudbury, 2005.
- [7] D. Achten, Next generation HNBR grades-new materials for oilfield applications, in: *Oilfield engineering with polymers conference 2006*, pp. 187–199.
- [8] B. Stuck, N. Hershberger, Effect of different nitrile elastomers in down hole drilling applications with a review of testing and failure analysis, in: *Fall 184th technical meeting of the rubber division of the American chemical society*, Ohio, USA, 2013.
- [9] W. Hofmann, *Rubber technology handbook*, Hanser Publishers; New York Distributed in the U.S.A. by Oxford University Press, Munich, New York, 1989.
- [10] D.L. Jr Hertz, Oil and gas industry seals and sealing - success and failure, in: *ERG Fall technical meeting*.

- [11] T. Schwarz, High performance polyurethanes in the oil and gas industry, in: High performance elastomers & polymers for oil & gas applications: Conference proceedings, Claphorne Hotel, Aberdeen, UK, Smithers Information, Ltd, Shrewsbury, Shropshire, UK, 2012, pp. 153–165.
- [12] D11 Committee, Terminology relating to rubber, ASTM International, West Conshohocken, PA, 2015.
- [13] W. Fidi, Vorlesung Gummiphisik-Materialmodelle, Leoben, Austria, 2017.
- [14] A. Ciesielski, An introduction to rubber technology, Rapra Technology, Shawbury, 1999.
- [15] R.J. Spontak, N.P. Patel, Thermoplastic elastomers: Fundamentals and applications, *Current Opinion in Colloid & Interface Science* 5 (5-6) (2000) 333–340. [https://doi.org/10.1016/S1359-0294\(00\)00070-4](https://doi.org/10.1016/S1359-0294(00)00070-4).
- [16] L.W. McKeen, Fatigue and tribological properties of plastics and elastomers, 2nd ed., William Andrew, Amsterdam, Oxford, 2010.
- [17] R.C. Klingender, Handbook of specialty elastomers, CRC Press/Taylor & Francis, Boca Raton, 2008.
- [18] G. Heinrich, M. Klüppel, T.A. Vilgis, Reinforcement of elastomers, *Current Opinion in Solid State and Materials Science* 6 (3) (2002) 195–203. [https://doi.org/10.1016/S1359-0286\(02\)00030-X](https://doi.org/10.1016/S1359-0286(02)00030-X).
- [19] M. Akiba, A.S. Hashim, Vulcanization and cross-linking in elastomers, *Progress in Polymer Science* 22 (3) (1997) 475–521. [https://doi.org/10.1016/S0079-6700\(96\)00015-9](https://doi.org/10.1016/S0079-6700(96)00015-9).
- [20] D.L. Jr Hertz, Theory & practice of vulcanization, *Elastomerics* (1984) 1–7.
- [21] J. Kruželák, R. Sýkora, I. Hudec, Sulphur and peroxide vulcanisation of rubber compounds – overview, *Chemical Papers* 70 (12) (2016) 347. <https://doi.org/10.1515/chempap-2016-0093>.
- [22] M. Rinnbauer (Ed.), Technical elastomers: The basis of high-tech sealing and, sv corporate media GmbH, D-80992 Munich, Germany, 2007.
- [23] G. Heideman, J.W. Noordermeer, R.N. Datta, B. van Baarle, Effect of Zinc complexes as activator for sulfur vulcanization in various rubbers, *Rubber Chemistry and Technology* 78 (2) (2005) 245–257. <https://doi.org/10.5254/1.3547881>.
- [24] CROW's Polymer Chemistry, Pre-vulcanization inhibitors for sulfur vulcanization. Polymer properties database, 2015. <https://polymerdatabase.com/polymer%20chemistry/Vulcanization%20Retard%20ers.html> (accessed 13 November 2018).
- [25] S.Q. Liu, W.G. Gong, B.C. Zheng, The effect of peroxide cross-linking on the properties of low-density polyethylene, *Journal of Macromolecular Science, Part B* 53 (1) (2013) 67–77. <https://doi.org/10.1080/00222348.2013.789360>.
- [26] J.B. Class, Fundamentals of crosslinking with peroxides, 1995. <http://www.rubbernews.com/article/19951009/ISSUE/310099882/fundamentals-of-crosslinking-with-peroxides> (accessed 13 November 2018).
- [27] S.K. Henning, R. Costin (Eds.), Fundamentals of curing elastomers with peroxides and coagents I: coagent structure-property Relationships, 2005.
- [28] Z.H. Li, J. Zhang, S.J. Chen, Effects of carbon blacks with various structures on vulcanization and reinforcement of filled ethylene-propylene-diene rubber, *Express Polym. Lett.* 2 (10) (2008) 695–704. <https://doi.org/10.3144/expresspolymlett.2008.83>.

- [29] J. Fröhlich, W. Niedermeier, H.D. Luginsland, The effect of filler–filler and filler–elastomer interaction on rubber reinforcement, *Composites Part A: Applied Science and Manufacturing* 36 (4) (2005) 449–460. <https://doi.org/10.1016/j.compositesa.2004.10.004>.
- [30] D.J. Kohls, G. Beaucage, Rational design of reinforced rubber, *Current Opinion in Solid State and Materials Science* 6 (3) (2002) 183–194. [https://doi.org/10.1016/S1359-0286\(02\)00073-6](https://doi.org/10.1016/S1359-0286(02)00073-6).
- [31] C.M. Roland (Ed.), *Reference module in materials science and materials engineering*, Elsevier, New York, NY, USA, 2016.
- [32] C.M. Roland, Reinforcement of elastomers, in: C.M. Roland (Ed.), *Reference module in materials science and materials engineering*, Elsevier, New York, NY, USA, 2016.
- [33] J.B. Donnet, R.C. Bansal, M.J. Wang, *Carbon black: Science and technology*, 2nd ed., Dekker, New York, N.Y., 1993.
- [34] J.A. Harwood, L. Mullins, A.R. Payne, Stress softening in natural rubber vulcanizates. Part II. Stress softening effects in pure gum and filler loaded rubbers, *Rubber Chemistry and Technology* 39 (4) (1966) 814–822. <https://doi.org/10.5254/1.3547145>.
- [35] L. Mullins, Effect of stretching on the properties of rubber, *Rubber Chemistry and Technology* 21 (2) (1948) 281–300. <https://doi.org/10.5254/1.3546914>.
- [36] J. Diani, B. Fayolle, P. Gilormini, A review on the Mullins effect, *European Polymer Journal* 45 (3) (2009) 601–612. <https://doi.org/10.1016/j.eurpolymj.2008.11.017>.
- [37] B. Rodgers, W. Waddell, The science of rubber compounding, in: J.E. Mark, B. Erman, M. Roland (Eds.), *The science and technology of rubber*, Academic, Oxford, 2013, pp. 417–471.
- [38] J.E. Mark, B. Erman, M. Roland (Eds.), *The science and technology of rubber*, Academic, Oxford, 2013.
- [39] Akrochem corporation, Antioxidants and antiozonants: Part I – oxidation/ozonation of rubber. http://www.akrochem.com/pdf/technical_papers/antiox_antioz_part1.pdf (accessed 21 November 2018).
- [40] K. Hanhi, M. Poikelispää, H. Tirilä, *Elastomeric materials*, 2007. http://laroverket.com/wp-content/uploads/2015/03/Elastomeric_materials.pdf (accessed 21 November 2018).
- [41] A.O. Patil, T.S. Coolbaugh, Elastomers: A literature review with emphasis on oil resistance, *Rubber Chemistry and Technology* 78 (3) (2005) 516–535. <https://doi.org/10.5254/1.3547894>.
- [42] R.K. Flitney, M.W. Brown, *Seals and sealing handbook*, 5th ed., Elsevier, Oxford, 2007.
- [43] T. Schwarz. Material data sheet, 2001. <http://files8.webydo.com/92/9259947/UploadedFiles/E6F89B2F-8E5C-81A7-1842-14500807AAEA.pdf>.
- [44] H. Zhang, A. Cloud, Research progress in calenderable fluorosilicone with excellent fuel resistance, Arlon Silicone Technologies Division, 2007.
- [45] J.A. Hiltz, R.M. Morchat, I.A. Keough, A DMTA study of the fuel resistance of elastomers, *Thermochimica Acta* 226 (1993) 143–154. [https://doi.org/10.1016/0040-6031\(93\)80215-V](https://doi.org/10.1016/0040-6031(93)80215-V).

- [46] N. Sombatsompop, Investigation of swelling behavior of NR vulcanisates, *Polymer-Plastics Technology and Engineering* 37 (1) (1998) 19–39. <https://doi.org/10.1080/03602559808006910>.
- [47] A.N. Gent, R.P. Campion, *Engineering with rubber: How to design rubber components*, 2nd ed., Hanser, Munich, 2001.
- [48] B.J. Briscoe, T. Savvas, C.T. Kelly, Explosive decompression failure of rubbers: A review of the origins of pneumatic stress induced rupture in elastomers, *Rubber Chemistry and Technology* 67 (3) (1994) 384–416. <https://doi.org/10.5254/1.3538683>.
- [49] C.J. Norris, M. Hale, M. Bennett, Composition and property changes of HNBR and FKM elastomers after sour gas aging, *Plastics, Rubber and Composites* 45 (6) (2016) 239–246. <https://doi.org/10.1080/14658011.2016.1177271>.
- [50] X. Zuo, K. Zhang, Y. Lei, S. Qin, Z. Hao, J. Guo, Influence of thermo-oxidative aging on the static and dynamic mechanical properties of long glass fiber reinforced polyamide 6 composites, *J. Appl. Polym. Sci.* 131 (3) (2014) n/a-n/a. <https://doi.org/10.1002/APP.39594>.
- [51] A. Mostafa, A. Abouel-Kasem, M.R. Bayoumi, M.G. El-Sebaie, The influence of CB loading on thermal aging resistance of SBR and NBR rubber compounds under different aging temperature, *Materials & Design* 30 (3) (2009) 791–795. <https://doi.org/10.1016/j.matdes.2008.05.065>.
- [52] T.H. Anh, T. Vu-Khanh, Thermo-oxidative aging effects on mechanical performances of polychloroprene, *Journal of the Chinese Institute of Engineers* 27 (6) (2011) 753–761. <https://doi.org/10.1080/02533839.2004.9670926>.
- [53] G.R. Hamed, J. Zhao, Tensile behavior after oxidative aging of gum and black-filled vulcanizates of SBR and NR, *Rubber Chemistry and Technology* 72 (4) (1999) 721–730. <https://doi.org/10.5254/1.3538829>.
- [54] CROW's Polymer Chemistry, Thermal-oxidative degradation of rubber. Polymer database, 2015. <http://polymerdatabase.com/polymer%20chemistry/Thermal%20Degradation%20Elastomers.html> (accessed 25 December 2018).
- [55] E. Ho, Elastomeric seals for rapid gas decompression applications in high-pressure services, *Health & Safety executive*, 2006.
- [56] James Walker & Co Ltd, Low temperature sealing capability of O-rings: the relationship between laboratory tests and service performance: Low temperature sealing, 2012. https://www.jameswalker.biz/cn/pdf_docs/129-low-temperature-sealing-capability-of-o-rings-the-relationship-between-laboratory-tests-and-service-performance.
- [57] P. Embury, High-pressure gas testing of elastomer seals and a practical approach to designing for explosive decompression service, *Sealing Technology* 2004 (6) (2004) 6–11. [https://doi.org/10.1016/S1350-4789\(04\)00231-4](https://doi.org/10.1016/S1350-4789(04)00231-4).
- [58] Z. Major, K. Lederer, M. Moitzi, M. Mitterhuber, T. Schwarz, R.W. Lang, Development of a test and failure analysis methodology for elastomeric seals exposed to explosive decompression, in: *Oilfield engineering with polymers conference proceedings*, London, UK, Rapra, Shrewsbury, 2006, pp. 135–152.
- [59] B.J. Briscoe, S. Zakaria, Gas-induced damage in elastomeric composites, *J Mater Sci* 25 (6) (1990) 3017–3023. <https://doi.org/10.1007/BF00584920>.

- [60] O. Lorge, B.J. Briscoe, P. Dang, Gas induced damage in poly(vinylidene fluoride) exposed to decompression, *Polymer* 40 (11) (1999) 2981–2991. [https://doi.org/10.1016/S0032-3861\(98\)00527-8](https://doi.org/10.1016/S0032-3861(98)00527-8).
- [61] K.J. Monaghan, C. Newlands, E. Ho, Specification of elastomeric materials for rapid gas decompression applications, in: *Oilfield engineering with polymers conference proceedings*, London, UK, Rapra, Shrewsbury, 2006, pp. 119–135.
- [62] B. Schrittester, G. Pinter, T. Schwarz, Z. Kadar, T. Nagy, Rapid gas decompression performance of elastomers – A study of influencing testing parameters, *Procedia Structural Integrity* 2 (2016) 1746–1754. <https://doi.org/10.1016/j.prostr.2016.06.220>.
- [63] A. Stevenson, G. Morgan, Fracture of elastomers by gas decompression, *Rubber Chemistry and Technology* 68 (2) (1995) 197–211. <https://doi.org/10.5254/1.3538735>.
- [64] J. Yamabe, S. Nishimura, Influence of fillers on hydrogen penetration properties and blister fracture of rubber composites for O-ring exposed to high-pressure hydrogen gas, *International Journal of Hydrogen Energy* 34 (4) (2009) 1977–1989. <https://doi.org/10.1016/j.ijhydene.2008.11.105>.
- [65] B. Schrittester, Performance of elastomers for high-pressure applications. Doctoral thesis, Leoben, Austria, August/2014.
- [66] C. Fond, Cavitation criterion for rubber materials: A review of void-growth models, *J. Polym. Sci. B Polym. Phys.* 39 (17) (2001) 2081–2096. <https://doi.org/10.1002/polb.1183>.
- [67] J. Diani, Irreversible growth of a spherical cavity in rubber-like material: A fracture mechanics description, *International Journal of Fracture* 112 (2) (2001) 151–161. <https://doi.org/10.1023/A:1013311526076>.
- [68] B. Schrittester, G. Pinter, T. Schwarz, Z. Kadar, T. Nagy, Impact of the acrylonitrile content on the mechanical performance of elastomeric materials, *Rubber Fiber Plastics International* (11) (2016) 40-.
- [69] F. Daou, C.R. de Miranda, J.L. de Oliveira, B. Engelke, C. Borman, S. Le Roy-Delage, B. Lungwitz, Swelling of elastomers in CO₂ environment: Testing methodology and experimental data, in: *SPE Latin America and Caribbean petroleum engineering conference*, Maracaibo, Venezuela, Society of Petroleum Engineers, 2014.
- [70] C.A. Rochelle, A.P. Camps, D. Long, A. Milodowski, K. Bateman, D. Gunn, P. Jackson, M.A. Lovell, J. Rees, Can CO₂ hydrate assist in the underground storage of carbon dioxide? *Geological Society, London, Special Publications* 319 (1) (2009) 171–183. <https://doi.org/10.1144/SP319.14>.
- [71] D.L. Jr Hertz, *Elastomers in the hot sour gas environment*, New Jersey, USA, 2007. <http://www.sealseastern.com/PDF/HotSourGas.pdf> (accessed 2 January 2019).
- [72] B. Slay, S. Streich, W. Webber, Extreme oil field seal applications, in: *High performance elastomers & polymers for oil & gas applications: Conference proceedings*, Claphorne Hotel, Aberdeen, UK, Smithers Information, Ltd, Shrewsbury, Shropshire, UK, 2012, pp. 129–141.
- [73] ERG Fall technical meeting.
- [74] A. Choudhury, A.K. Bhowmick, C. Ong, M. Soddemann, Influence of molecular parameters on thermal, mechanical, and dynamic mechanical

- properties of hydrogenated nitrile rubber and its nanocomposites, *Polym Eng Sci* 50 (7) (2010) 1389–1399. <https://doi.org/10.1002/pen.21680>.
- [75] V. Nasreddine, K. Kulbaba, C. Mueller, A. Bischoff, B. James, L. Chen, D. Gerrard, J. Goodson, Fluid ageing and explosive decompression resistance of Therban/HNBR, in: *High performance elastomers & polymers for oil & gas applications: Conference proceedings*, Claphorne Hotel, Aberdeen, UK, Smithers Information, Ltd, Shrewsbury, Shropshire, UK, 2012, pp. 67–81.
- [76] Parker Hannifin Corporation, Packing Division Europe, PTFE seal design guide, Boom Belgium, 2011. http://pstsr.eu/wp-content/uploads/2016/05/PTE-3354-GB_CatalogoGuarnizioni.pdf.
- [77] D.J. Carlsson, S. Chela, D.M. Wiles, Chemical and spectroscopic methods for investigating polymer degradation and stabilization: Oxidative degradation of a hydrogenated nitrile rubber, *Macromolecular Symposia* 27 (1989) 139–153.
- [78] W. Balasooriya, B. Schritteser, G. Pinter, T. Schwarz, Influence of ageing on HNBR in oilfield applications, *Rubber Fiber Plastics International* 12 (4) (2017) 38–46.
- [79] H. Bender, E. Campomizzi, Improving the heat resistance of hydrogenated nitrile rubber compounds: Part 1: Aging mechanisms for high saturation rubber compounds, *KGK Kautschuk Gummi Kunststoffe* (54) (2001) 14–21.
- [80] R. Resendes, C. Hellens US 2006/0106171, 2006.
- [81] B. Alcock, T.A. Peters, R.H. Gaarder, J.K. Jørgensen, The effect of hydrocarbon ageing on the mechanical properties, apparent crosslink density and CO₂ diffusion of a hydrogenated nitrile butadiene rubber (HNBR), *Polymer Testing* 47 (2015) 22–29. <https://doi.org/10.1016/j.polymertesting.2015.07.007>.
- [82] E.C. Campomizzi, H. Bender, W. von Hellens, Improving the heat resistance of hydrogenated nitrile rubber: Part 2: Effect of a novel heat stabilizer additive on the heat resistance of HNBR, *KGK Kautschuk Gummi Kunststoffe* 54 (2001) 114–121.
- [83] J.E. Dato, E.C. Campomizzi, D. Achten, Hydrogenated nitrile for oilfield applications, *RubberNews.com* (2008).
- [84] U. Giese, I. Homeier, Y.N. Torrèjon, S. Kautz, Ageing mechanisms of elastomers and effectiveness of anti-oxidants, *Chemické Listy* 107 (2013) 3–11.
- [85] U. Giese, M. Santoso, Y.N. Torrejn, Aging of elastomers and effectiveness of antioxidants, *Chemické Listy* 65 (7) (2012) 20–23.
- [86] Y. Kamia, E. Niki, The role of Hydroperoxides in the oxidative degradation of polymers, in: R. Kerber (Ed.), H. H. G. Jellinek (Ed): *Degradation and Stabilization of Polymers*, Vol. 1. Elsevier, Amsterdam, Oxford, New York 1983. 682 Seiten, Preis: Dfl. 350,-, 1984, pp. 337–357.
- [87] P. Embury, S. Groves, J.M. Rivereau, K. Edmond, E. Ho, R. Flitney, Comparison of explosive decompression test protocols for elastomer seals in high-pressure gas service (2001).
- [88] Standard test method: Evaluating elastomeric materials in carbon dioxide decompression environments, NACE International, Houston, Tex., 2003.
- [89] NORSOK Standard, Qualification of non-metallic sealing materials and manufacturers, 2nd ed., Norwegian Technology Centre, Oslo, Norway, 2001.

I.4 Acronyms and symbols

Acronyms

RGD	Rapid gas decompression
HNBR	Hydrogenated nitrile butadiene rubbers
H ₂	Hydrogen
XDF	Explosive decompression failure
NR	Natural rubber
SBR	Styrene-butadiene copolymer
CR	Polychloroprene
NBR	Acrylonitrile butadiene rubber
IIR	Butyl rubber
FKM	Fluoroelastomer
EPDM	Ethylene propylene diene rubber
TPE	Thermoplastic elastomers
S	Sulfur
N	Nitrogen
CBS	N-cyclohexyl-2-benzothiazole sulphenamide
MBT	2-mercaptobenzothiazole
CB	Carbon black
UV	Ultraviolet
CO ₂	Carbon dioxide
H ₂ S	Hydrogen sulfide
IRHD	International Rubber Hardness Degrees
ACN	Acrylonitrile
FEPM	Tetrafluoroethylene propylene copolymer
FFKM	Perfluoroelastomer
PTFE	Polytetrafluoroethylene
PU	Polyurethane
PEEK	Polyether ether ketone
BD	Butadiene
RDB	Residual double bonds
ASTM	American Society for Testing and Materials
VMQ	Silicon rubber
HSN	Highly saturated nitrile
O ₂	Oxygen
NACE	National Association of Corrosion Engineers
NORSOK	Norsk Søkkel Konkurransesjøsion – Norwegian initiative to reduce cost on offshore projects
CH ₄	Methane
CCD	Charged coupled device
PHR	Parts per hundred rubber
NMR	Nuclear magnetic resonance
IR-ATR	Infrared in attenuated total reflection mode
SEM	Scanning electron microscope
TEM	Transmission electron microscope

Symbols

T_g	Glass transition temperature
C	Gas concentration
S	Solubility coefficient
P	Applied gas pressure
q/t	Gas permeation rate
D	Diffusion coefficient
Q	Permeation coefficient
ΔP	Pressure difference
H	Thickness of the membrane
A	Membrane surface area
P_c	Maximum pressure
E	Young's modulus
μ	Shear modulus
G	The energy release rate
a_0	Radius of an un-deformed bubble
a	Radius of a deformed bubble

PART II: STRUCTURE, CONTENT AND COLLECTION OF PAPERS

II.1 Structure and content

The elastomeric materials used as sealing components in oil and gas field applications face tremendous challenges to their functional properties as well as to their life expectancy due to various working environmental factors. The possible changes to chemical and physical properties and dimensions of the component by exposure to high-pressures, high-temperatures, and to the surrounding media during the service life and subsequently altered performance of the sealing and failure modes are primarily expected. The RGD behavior as a catastrophic component failure in high-pressure fluid handling conditions has been under discussion for decades, due to the extremely complex nature depending on various environmental factors as well as the material itself. For this reason, the effect of environmental conditions on the sealing performance, component life and RGD resistance in near service level conditions is essential information for designing purposes.

This scientific work was performed by thoroughly investigating the three main sections:

- **Thermo-oxidative aging of elastomers:** intensity of aging depending on temperature and exposure time, possible aging mechanisms, functional property degradations, etc.
- **Swelling induced aging of elastomers:** chemical resistance, the intensity of property reduction, functional property degradations, and deterioration modes.
- **Elastomer utilization in harsh environments:** RGD resistance, influence of environmental factors and additives on RGD resistance, influence of environmental factors on tribological properties in dynamic sealing applications.

The HNBR as a common elastomeric class in sealing applications, which mostly fulfills the requirements for use in oil and gas field applications, was used for

experiments in this scientific work. Further, specific HNBR grades, which were specially developed for harsh environments, for example, 36% of ACN content, peroxide cross-linked, stabilized with antioxidants, and highly filled with carbon black (85 phr), were selected for the experiments.

This section consists of a collection of four scientific journal publications, which summarize the detailed relevance of the topics, experimental setups, data reduction, and obtained results. The topics of the papers and the names of the scientific journals, where they are published, are listed below. The papers in Part II are in the originally published versions of the journals, therefore they are formatted accordingly.

Paper 1: Influence of thermo-oxidative aging of HNBR in oil field applications (Macromolecular Symposia, Wiley-VCH Verlag GmbH & Co. KGaA.)

Paper 2: Induced material degradation of elastomers in harsh environments (Polymer Testing, Elsevier)

Paper 3: Tribological behavior of HNBR in oil and gas field applications (Lubricants, MDPI) (Open access)

Paper 4: The effect of the surface area of carbon black grades on HNBR in harsh environments (Polymers, MDPI) (Open access)

II.2 Outline of papers

HNBR is widely recognized as a material with superior resistance to thermal degradation due to the total or near total saturation in the polymer backbone. However, the possible residual double bonds and the choice of the vulcanization method still influence the performance of the material class at high-temperature conditions in the presence of oxygen. Thermo-oxidative aging is a chemical degradation, which creates irreversible changes to mechanical properties and possibly limits the service life of an elastomeric seal. Therefore, the practical use of elastomers would require the understanding of material behavior under service conditions, the degradation of properties and the intensity of that degradation. The

required knowledge can be obtained by the accelerated aging methods and subsequent extrapolation techniques can reveal the behavior of the material in the real operating conditions. The possible chemical reactions of the thermo-oxidative aging of elastomers, which explain the unsaturation of the backbone involved in the radical formation and which lead up to cross-linking or chain-scission, are well understood in the literature. However, all possible reactions for HNBR as well as the influence of aging intensity on properties, which depends on several environmental factors and the ingredients in the material, are hardly found in the literature. Therefore, **paper 1** discusses the influence of thermo-oxidative aging on the properties of HNBR and the plausible underlying molecular-level reasons and structural changes. This includes the influence on the properties at different elevated temperatures and exposure times, identifying the onset of the aging process and its intensity at several stages. It is generally accepted that HNBR can be used up to 150 °C in the presence of oxygen. Therefore, in this study, 100, 150 and 170 °C were used as the aging temperatures in an air-circulated oven (ASTM E145). The conventional test methods, for example, quasi-static tensile tests, tear tests, and dynamic mechanical analysis tests were utilized for characterizing the possible changes in the physical properties. The Raman spectrum revealed the availability of unsaturated groups in the backbone of HNBR despite the hydrogenation in the material grade used. The dominance of the cross-linking or chain-scission mechanisms can be assessed by the hardening or softening behavior of the material. Further, the Double Quantum NMR (solid state) verified the intensity of the damage mechanisms. The relative microstructural changes and the involved functional groups were observed in IR spectra at ATR mode. Therefore, this research work for the HNBR grade in combination with the tests and analyzing methods to verify the possible degradation and intensity of thermo-oxidative aging is novel from the scientific point of view.

The polarity of HNBR, due to the ACN content, increases the resistance to non-polar fluids and enhances the applicability in the oil and gas field. A sealing component may absorb a liquid as a result of the liquid-elastomer interactions and in a matter of time, an equilibrium swelling state is reached, where the network forces and osmotic pressure are balanced. This process is manifested by an increase of material volume (swelling) or decrease of volume (shrinking) in case of the

extraction of soluble ingredients from the compound recipe. Generally, the degree of swelling or shrinking causes the physical and chemical effects, creates an adverse impact on the sealing performance, and is detrimental to the lifespan. Depending on the actual conditions, the sealing material faces a wide range of critical fluids, which alter the properties in reversible or irreversible manner. Therefore, **papers number 2 and 3** discuss the influence on HNBR in contact with different ASTM reference fuels, which are the laboratory equivalents for gasoline or diesel fuels, and standard testing mineral oils, which are petroleum-based solvents, according to the ASTM D471-06. Primarily, these scientific papers reveal the intensity of swelling, possible functional property changes, and the physical and chemical influences on the material in different environmental conditions.

Paper 2 further discusses the influence on RGD behavior under thermal and swelling-induced aging conditions. The swelling and RGD are two different seal failure modes, which are affected by a complex process of physical and chemical influences from the working environment. However, both of them are related to the fluid absorption and dissolution into the elastomer. Therefore, the swollen conditions may affect the gas absorption and material properties and subsequently influence the RGD behavior. Further, thermo-oxidative aging, which alters the mechanical properties of the material at elevated temperatures in the presence of oxygen, may influence the RGD resistance of the material. Therefore, this paper consists of a complete analysis of swelling-induced aging of HNBR in swollen and de-swollen conditions including the incurred influence on RGD resistance in swollen and thermo-oxidative aged conditions. The component level RGD tests were conducted in an autoclave using CO₂ as the medium and the conditions were more intense than the NORSOK standard, especially a higher decompression rate, in order to gain more information on near service level conditions. The mechanical and dynamic mechanical analysis results compared the influence on structural changes in different conditions. The volume increase in the compression phase of the RGD test revealed the effects on gas intake into the material due to the aged conditions. The NORSOK ranking rated the materials based on the internal cracks generated in the material after RGD tests observing the radial cross-sections of the cylindrical specimens. The influence of thermal and swelling induced aging on RGD resistance

is a new research field and no literature was found in this topic. Therefore, this study is novel and widens the knowledge in the field.

Moreover, **paper 3** exclusively focuses on the tribological behavior of HNBR under the influence of swelling-induced aging. As a result of swelling, the dimensional change of the sealing may increase the contact with the housing, and further, combined with the possible changes in the surface properties, can be decisive to the lifetime of the sealing, especially in dynamic conditions. There is some general literature available on the topic of lubricant and solvent effects on wear and frictional properties of the elastomer. However, the influence on the elastomers in contact with the typical liquids in oil and gas field applications, and their combined effect on the tribological properties in dynamic conditions have not been examined scientifically. For this reason, the influence on the surface properties of samples in the swollen-state as well as in the state after the sample has been dried was considered in this work and compared with un-swollen samples. The samples of the HNBR grade were tested as a specially designed disk with a precise lip geometry, which were mounted onto a rotation drive of the Tribometer so as to be in touch with a metal counterpart. The differences in the degree of wear and friction coefficient in swelling-induced aged samples were characterized including the surface analysis by IR spectra as well as by SEM analysis revealing possible structural changes. The degree of the swelling irreversibly degraded the surface and deteriorated the tribological properties; similarly, the bulk mechanical properties were also impaired, but partially regained after the drying. Concluding this study, the possible mechanisms of wearing off particles from sealings, which rub against solid counterparts, and the influence from the degree of swelling was introduced, hypothetically.

As mentioned above, the RGD is a structural failure forming blistering, internal cracks or even catastrophic collapse of a sealing component. In general, the RGD resistance is increased with the better mechanical properties of the elastomer grade. Therefore, the compound additives can offer enhanced resistance to RGD combined with good engineering properties. A filler is a main additive in the material composition, which has a high impact on material properties and offers other benefits to the compound. For this reason, **paper 4** focuses on the influence of CB,

as a most widely used reinforcing filler, on the performance of HNBR in the oil and gas field industry. In this study, the CB loading was kept constant and the primary particle size was varied in the different material grades, identifying the influence of the surface area of CB on RGD resistance. The possible differences in aggregation, agglomeration and CB distribution in the material were investigated with a transmission electron microscope (TEM). The component level RGD resistance was investigated in an autoclave using CO₂ as the medium in near service level conditions comparing the performance of different compounds. This testing procedure includes the possibility to measure the solubility of a gas into different materials during the pressurization, and the post-test inspection includes the ranking of material to RGD resistance. The supporting macroscopic and microscopic investigations revealed plausible explanations for different behaviors in differently filled conditions. The literature on the topic of the influence of fillers in elastomers on high-pressure gas solubility or RGD resistance was rarely found. The only available literature examined an EPDM elastomer in a low degree of filling condition and this in the presence of high-pressure hydrogen. Therefore, this scientific work expands the limits of research by using HNBR in highly filled conditions (85 phr), which is a specially developed material for oil and gas field applications, using CO₂ as the high-pressure medium, which works as supercritical fluid in the test conditions.

II.3 Outlook

To ensure operational safety of the facility during the use of elastomeric materials, behavioral characteristics and the good awareness of probable risks during the service life are indispensable. The gained knowledge on functional properties and the factors affecting them as well as the deterioration modes are vital in designing and deciding the acceptable operating strategies. Therefore, this information is useful in future modeling purposes of sealing function and seal lifetime. The experiments on the swelling-induced aging can be further improved by chemical analysis in mixed solvents conditions as well as solvent-rubber, solvent-lubricant, and lubricant-rubber interacting conditions for various tribological contacts. The study on material perspective as well as on component damage near the service

conditions provided more accurate information for modeling purposes, which increased knowledge on predicting seal damage for oil and gas applications. However, due to the complexity of the RGD phenomenon, more information on actual operating conditions is needed. Therefore, more tests deviating the factors, which are strongly influencing the RGD, for example, pressure, temperature, decompression rate, gas, etc., will be important. Especially, extensive studies on the RGD behavior of elastomeric materials in contact with high-pressure H₂ will benefit the future energy industry; H₂ is considered as a main future energy alternative and normally it is stored and transported in compressed form. This study assumes the gas absorption into the material by volume increase of the specimen in the compression phase. However, further measurements on thermodynamic properties related to the material and the diffusing species of gases, diffusivity (D) and solubility (S), will reveal information that is more accurate for the used gas and the material. Moreover, improvements of the component level experimental procedure will lead to a better understanding of RGD failure. One possibility would be an acoustic emission technique to observe the specimens right after the decompression phase, which can reveal precise information on crack propagation and time to release the gas fully out of the specimen. In the process of material development enhancing the RGD resistance, more tests with different CB grades (higher and lower surfaces in compositions as well as containing single CB grade in one material grade) in series of different CB loading can reckon the influence of CB surface influence in RGD resistance. Future work on the fracture mechanical approach to identify a criterion at specimen level, which can reveal the influence of mechanical properties on the RGD behavior, will provide more information on material and component development. Therefore, different testing modes, for example, strain rate-controlled, stress-controlled at different test speeds, will help to achieve a better correlation with RGD behavior in actual conditions and benefit modeling in an optimization process. Due to the still rising requirements from the applications and service conditions, not only HNBR but also other possible alternative material grade developments will enhance the limits of usage of elastomeric materials.

II.4 Collection of papers

Paper 1: Influence of thermo-oxidative ageing of HNBR in oil field applications

Winoj Balasooriya¹, Bernd Schritteser¹, Santhosh Karunakaran¹, Sandra Schlögl¹, Gerald Pinter², Thomas Schwarz³ and Zalan Kadar⁴

¹ Polymer Competence Center Leoben GmbH, Roseggerstrasse 12, 8700 Leoben, Austria.

² Department of Polymer Engineering and Science, Montanuniversitaet Leoben, Otto Glöckeltrasse 2, 8700 Leoben, Austria.

³ SKF Sealing Solutions Austria GmbH, Gabelhoferstraße 25, 8750, Judenburg, Austria.

⁴ ContiTech Rubber Industrial Kft., Budapesti ut 10, H-6728 Szeged, Hungary.

Published in *Macromolecular Symposia*, 2017, 3, 373.

DOI: 10.1002/masy.201600093

Copyright: Wiley-VCH Verlag GmbH & Co. KGaA.
Reproduced with permission.

Influence of Thermo-Oxidative Ageing of HNBR in Oil Field Applications

Winoj Balasooriya,*¹ Bernd Schritteser,¹ Santhosh Karunakaran,¹
Sandra Schlögl,¹ Gerald Pinter,² Thomas Schwarz,³ Zalan Kadar⁴

Summary: The oxidative ageing behavior of carbon black- (85 phr) filled hydrogenated nitrile-butadiene rubber (HNBR) was characterized in this study. HNBR is widely used in many oil and gas field applications for seals, hoses, down-hole packers etc., due to its intrinsic combination of good heat and excellent oil and chemical resistance, coupled with outstanding physical properties. Hence, to support the material development, it is of prime theoretical and practical importance to characterize the ageing behavior of HNBR. In this work, mechanical properties and dynamic mechanical properties of aged and un-aged material were examined using tensile, tear and dynamic mechanical analysis tests. Possible micro structural changes and functional groups involved in aging were detected using DQ NMR, Raman spectroscopy and FT-IR spectroscopy in ATR mode. The results indicated that the ageing process caused the material to deteriorate; tensile strength – strain at break, the strain at tear strength and the damping properties were decreased. Additionally, the stiffness and the glass transition temperature of the material were also raised. According to the literature, residual double bonds in HNBR are involved in forming hydro peroxide and propagating the autocatalytic oxidation process in the presence of oxygen at higher temperature. This process leads to the oxidative degradation resulting in cross-linking and in chain scissions as the predominant reactions contributing to properties. Furthermore, at ~100 °C, oxidation through the nitrile group was observed converting the cyano functional group into the imino group; but at higher temperatures, it was negligible. The results suggest that the cross-linking and the chain scission mechanisms are significant after 72 hours and 168 hours of exposure, respectively, at 150 °C. However, when aged at 170 °C, both cross-linking and chain scission were even effective after 24 hours of exposure time.

Keywords: chain scission; cross-linking; HNBR; residual double bonds; thermo-oxidative ageing

Introduction and Objectives

Acrylonitrile-butadiene rubber (NBR) is a widely used class of polymers with

resistance to oil, gasoline, solvents, etc. Basically, NBR is a copolymer of butadiene (BD) and acrylonitrile (ACN). Depending on the application, the ACN content varies from 18 – 51%.^[1,2] As depicted in Figure 1, there are two types of BD addition in the free radical polymerization process, i.e., addition in the 1,4 position which is the bulk of the BD fraction as well as addition in the 1,2 position which forms a pendant carbon-carbon double bond.^[2]

The saturation of NBR as shown in the Figure 2 to hydrogenated nitrile rubber

¹ Polymer Competence Center Leoben GmbH, Roseggerstrasse 12, 8700 Leoben, Austria

E-mail: winoj.balasooriya@pccl.at

² Department of Polymer Engineering and Science – Materials Science and Testing of Plastics, Montanuniversitaet, Otto Glöckel-Strasse 2, Leoben, Austria

³ SKF Sealing Solutions Austria GmbH, Gabelhoferstraße 25, 8750 Judenburg, Austria

⁴ ContiTech Rubber Industrial Kft., Budapesti ut 10, H-6728 Szeged, Hungary

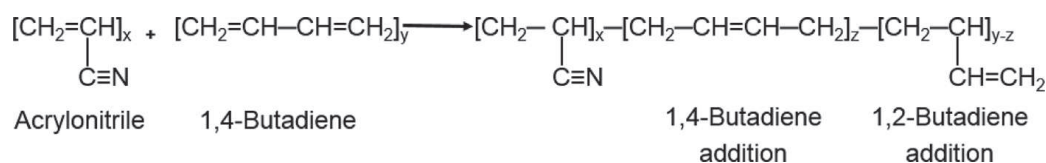


Figure 1.
NBR polymer structure.^[2]

(HNBR) eliminates nearly all the double bonds in the backbone, but slight unsaturation is expected. This process greatly improves the ageing and heat resistance which is necessary for use especially in oil field applications, where resistance to hydrocarbons at elevated temperatures is required.^[1-3]

Common uses of HNBR include down-hole packers, seals and gaskets in different industries, serpentine and synchronous belts, steel and paper mill rolls, etc.^[4] The combination of good heat, excellent oil and chemical resistance coupled with outstanding physical properties and an ease of processing make it very useful in more applications.^[1,5]

Especially, in terms of the oil and gas industry, reliability and durability of components become the limiting factor of the output and overall return for each drilling operation. Therefore, improvements have been identified in the rubber parts used in oil drilling industry, i.e., resistance to high temperature and to ageing, resistance to swelling caused by aggressive fluids and gases, resistance to rapid gas decompression, and processing properties to allow a greater freedom of compounding in new part design and production techniques.^[5]

In the present work, a carbon black-filled HNBR is introduced addressing the above-mentioned requirements in the oil field industry. Theoretically, fully

hydrogenated NBR contains no residual double bonds (RDB). However, practically, slight unsaturation causes the degradation of material.^[5,6] In this paper, totally/near totally saturated HNBR model material was tested to demonstrate the influence of thermo-oxidative ageing, to identify mechanical and dynamic mechanical properties, explaining the involved microstructure and chemistry in damage mechanisms. Special functional groups, which are contained in the material before and after ageing, were investigated using a Raman spectroscope, FT-IR in ATR mode and DQ NMR.

Properties of the HNBR depend on the ACN/BD ratio and the concentration of ACN in HNBR influences the properties of the final product. With higher ACN content, the resistance to solvents, oil and fuel will rise, but the elasticity and low temperature flexibility will be reduced.^[1,4,7-9] HNBR contains three more bonds other than the diene namely, C-H, C-C and C≡N, which have 346, 411 and 887 kJ/mol bond energies, respectively. Among them, only the C≡N part is polar and its electronegativity is relatively high, which exhibits higher bond energy compared to the other two non-polar bonds. Therefore, higher ACN content helps to increase the thermal stability and simultaneously, being polar, exerts a strong attractive force around the molecule and restrains large-scale molecular mobility or

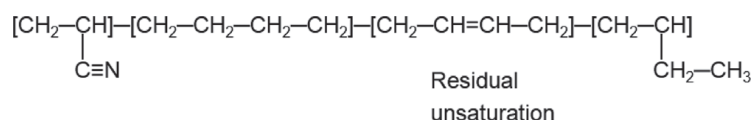


Figure 2.
HNBR polymer structure.^[2]

chain slippage affecting the flexibility of the material.^[10] The higher polarity of ACN causes the material to be better resistant to oil and fuel as well.^[1] The BD part of the rubber possesses free double bonds, existing even after vulcanization, which remain sensitive to oxygen and other reactive substances.^[1,8,10] Even small amounts of unsaturated C=C bonds reduce the performance of HNBR considerably. At a level of 3 to 5 mol% RDB, HNBR can be cross-linked with sulfur; however, this does not exhibit the environmental stability of a fully saturated HNBR.^[1,10] All polymers have tendencies to oxidize and deteriorate by molecular oxygen or other oxidizing agents in the atmosphere. Higher diene content in the backbone leads to an increase of the cross-link density, due to higher reactivity of the allylic hydrogen in a peroxide induced radical cure reaction. This is reflected by the higher stress at 100% elongation and a decreasing elongation at break with rising of BD content in cured virgin materials.^[4,6,10] Fully saturated HNBR, which is peroxide cross-linked, can even compete with FKM, due to its excellent mechanical properties in extreme environments.^[1,10]

Procedures

Material

A hydrogenated nitrile rubber (HNBR) (Terban 3629 (ACN 36%), peroxide cross-linked, stabilized with antioxidants, grade with carbon black (85 phr) was selected for these investigations. Due to constraint of confidentiality, the detailed compound ingredients are not provided here. The manufactured compound was provided as disc plates for investigations. Later, the specimens were punched out according to the test method in different dimensions. Thermo-oxidative ageing was carried out in a recirculating hot air oven according to ASTM E145 standard at 100, 150 and 170 °C for exposure times of 24, 72 and 168 hours each.

Specimens and Experimental Methods

Virgin materials and thermo-oxidative aged samples were investigated with tensile, tear and dynamic mechanical analysis (DMA) test methods. Five specimens for tensile and tear tests, and three specimens for DMA tests of each material grade were used to observe the reproducibility of results. The mean value and standard deviation of the results were calculated from these measurements and used for analysis. The specimen dimensions and test parameters are summarized below.

Tensile Test

Smooth dumbbell specimens (shape and dimensions are shown in Figure 3a) were used for the tensile experiments. These specimens have a thickness ~2 mm, width 4 mm and were clamped at a distance of 25 mm. All the tests were performed with a Zwick universal testing machine (Zwick Roell, Test expert, Ulm, Germany) with a 10 kN load cell, at a constant crosshead speed of 200 mm/min according to DIN 53504.

Tear Resistance Test

For tear resistance experiments, angled specimens with an incision (shape and dimensions are shown in Figure 3b) (no additional sharp blade notches) were used. These specimens have a thickness of ~2 mm and were clamped at a distance of 57 mm. All the tests were performed with a Zwick universal testing machine (Zwick Roell, Text expert, Ulm, Germany) with a 10 kN load cell, at a constant crosshead speed of 500 mm/min according to DIN ISO 34-1.

Dynamic Mechanical Analysis

The specimen dimensions used for the dynamic mechanical analysis experiments are as highlighted in the Figure 3c. This parallel part between the shoulders of the specimen (thickness ~2 mm, width 4 mm) was used in tension mode. The clamping distance within the machine parameters was 19.5 mm. A DMA 861/40N (Mettler Toledo GmbH, Schwerzenbach, CH) machine was

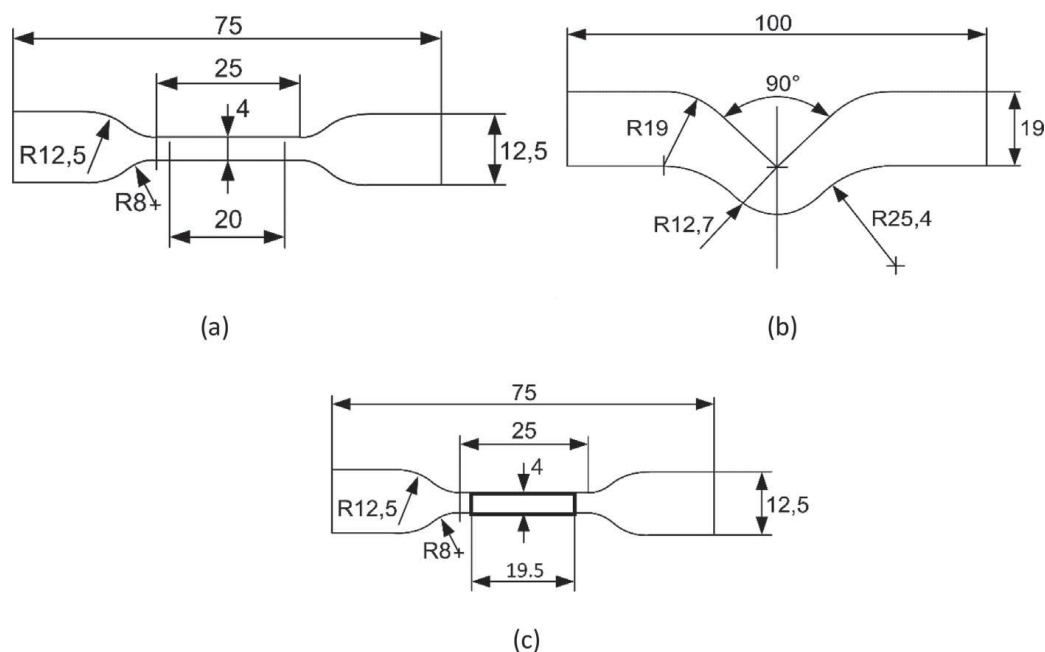


Figure 3. Test specimens and their dimensions in mm; (a) Tensile test specimen (according to DIN 53504) (b) angle specimen with incision (according to DIN ISO 34-1) (c) DMA specimen (used area is highlighted).

used with a liquid nitrogen cooling system. First, several amplitude tests were conducted at room temperature and -50°C with commonly used elastomeric parameters (2 Hz, within 1–100 μm) to figure out temperature scan test conditions. According to that, all the tests were carried out within the temperature range of -50°C to $+100^{\circ}\text{C}$, with a frequency of 2 Hz, a heating rate of 2 K/min, a dynamic amplitude of 3 μm and a static amplitude of 120%.

^1H Double Quantum NMR (DQ NMR)

NMR measurements for the samples in the study were carried on a minispec mq20 low field machine equipment operating a ^1H Larmor frequency of 20 MHz. The 90° pulse length was 2.8 μs , and the receiver dead time was 9 μs . The samples were heated with dry air whose temperature was controlled with a BVT3000 temperature controller. The measurements were made at 60°C to produce complete averaging of segmental dynamics. The samples were made as discs with a diameter 8 mm and thickness ~ 2 mm, punched out of compression-molded sheets. The discs were then stacked horizontally and positioned exactly

in the middle of the magnetic field. They were allowed a minimum of 30 minutes to equilibrate to the set temperature. Measurements of DQ NMR were carried out with the modified Baum-pines sequence.^[11,12]

Raman Microscope Test and Fourier Transmission Infra-Red (FTIR) – ATR Spectrometer Test

Small pieces were cut out as specimens from un-aged, 24 hours aged at 100°C and 168 hours aged at 170°C sheets (thickness of ~ 2 mm) for both test methods. A Horiba JY LabRAM HR 800 (HORIBA Jobin Yvon GmbH Raman Division, Bensheim, Germany) machine was used as the micro Raman spectrometer and a Spectrum GX 75611/2 (Perkin Elmer, Bucks, United Kingdom) was used as the FT-IR spectroscopy in ATR mode. The received transmittance spectrum was converted into absorbance for peak detections.

Results and Discussion

In the following section, the results from the different test methods will be discussed.

The possible microstructural changes and chemistry involved in thermo-oxidative ageing, which interpret the monitored mechanical and dynamic mechanical properties of HNBR, are discussed as well.

Oxidative Ageing Influence on Tension Properties

The change of the tensile properties of HNBR before and after ageing at different temperatures (100 °C, 150 °C and 170 °C) and exposure times (24, 72 and 168 hours) are shown in Figure 4.

The tensile strength at break (σ_R) for the different samples are shown in Figure 4a. As depicted, the strength at break slightly decreases with increasing ageing temperature as well as ageing time at a certain temperature and is reduced

compared to the virgin material in most cases. However, ageing at 100 °C shows similar or slightly improved strength at break values (especially at shorter exposure times) compared to the virgin material. Additionally, the samples aged at 150 °C for 72 hours show strength at break values similar to the virgin material and these decrease only after prolonged exposure.

In Figure 4b, the strain at break (ϵ_R) for the different samples are shown. Contrary to strength at break, strain at break for the same samples shows more pronounced ageing effects. First, at 100 °C, no clear degradation was detected with rising exposure time. However, the influence of ageing increases with the ageing temperature (and corresponding exposure times) as can be

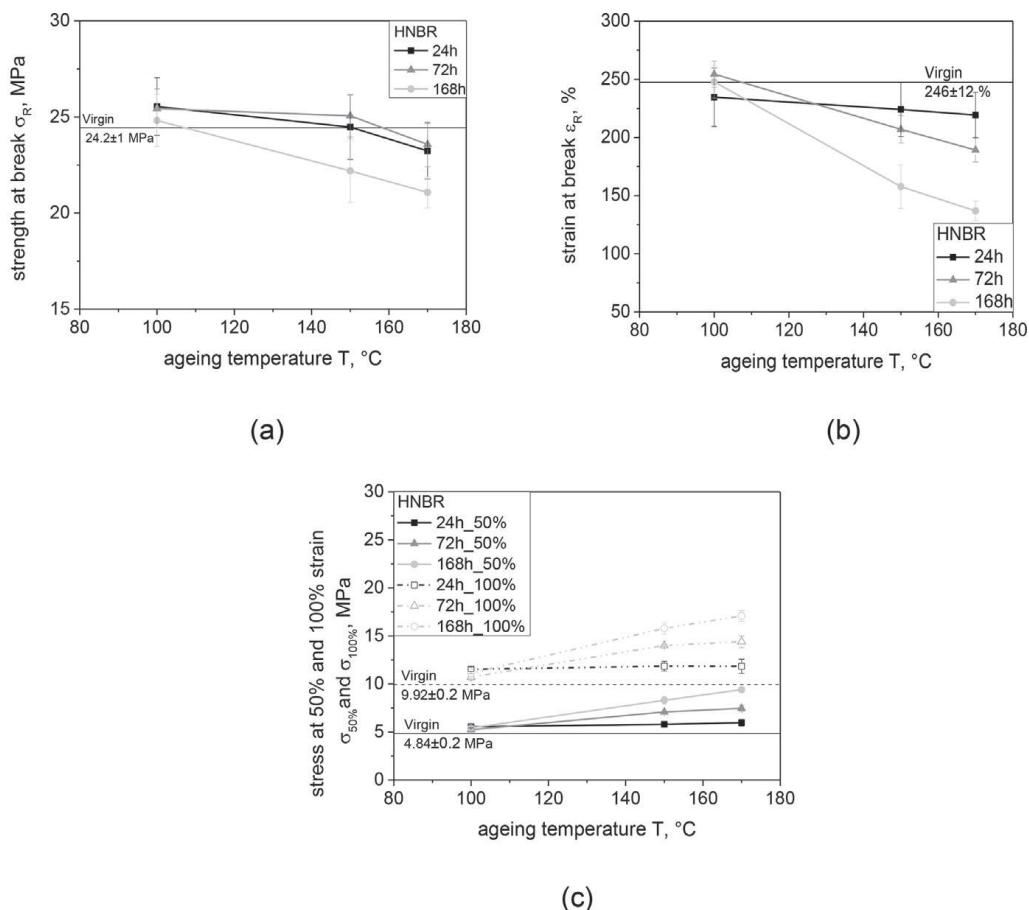


Figure 4.

Influence of ageing temperature and exposure time of HNBR on the (a) strength at break (b) strain at break (c) stress at 50% and 100% strain. The horizontal lines represent the virgin (un-aged) sample results in respective graphs.

seen from the much lower values for the samples aged at 150 °C and 170 °C. The stress at 50% and 100% strain ($\sigma_{50\%}$, $\sigma_{100\%}$) for the different samples are shown in Figure 4c.

Similar to the other material properties, ageing at 100 °C has insignificant or little influence on the rigidity of the material (as derived from stress at 50% and 100% strain). However, with higher ageing temperatures and with increasing exposure times at these temperatures, the material rigidity rises almost linearly. As expected, the highest stress at 50% and 100% strain were also observed for the most severe ageing conditions, i.e., ageing at 170 °C for 168 hours. Thus, according to the tensile results, the properties of HNBR appear to degrade with increasing severity of ageing conditions especially above 100 °C.

The influence of thermo-oxidative ageing on polymer parameters and the underlying molecular-level reasons, like structural changes, are still under discussion in the literature. According to the literature, the increase in cross-links as well as chain scission are the main possible ageing mechanisms at elevated temperatures for HNBR.^[3,4,6,12] Despite hydrogenation, RDBs on the main chain do exist and they have been identified as the strongest factors for cross-linking and chain scission mechanisms of HNBR.^[4,6,9,10,12–14] As depicted

in Figure 5, the observed Raman spectrum reflects the existence of C=C bonds from its characteristic band $\sim 1550\text{--}1650\text{ cm}^{-1}$ in HNBR. This is evidence of slight unsaturation of totally/ near totally-saturated HNBR.

The abstraction of the allylic hydrogen, which is bonded to a neighboring C atom from the RDB, leads to delocalized radicals in the polymer. They are more stable compared to alkyl radicals and are involved in the cross-linking reaction between polymer chains.^[4,6,10] This possible chemical reaction in thermo-oxidative ageing has two main steps, which are the formation of hydro-peroxides and its reactions with the main polymer. Hydro-peroxide plays a greatly important role in the oxidative degradation of polymers as the potential initiator for auto-oxidation. Stabilizers are utilized to inhibit the formation of radicals from hydro-peroxide.^[4,6,12]

A higher concentration of Hydro-peroxide could lead to a number of other reactions resulting in highly oxidized moieties, i.e., alcohols, ketones and carboxylic acids, alkoxy, peroxy and hydroxyl radicals, etc. As a result of these autocatalytic reactions, more polymer radicals are produced, and chain reactions are terminated by recombination reactions with the formation of stable compounds, i.e., the constitution of C–C or C–O–C bonds from two macro-radicals, tantamount to an increase in cross-linking density.^[4,6,15]

Such intermittent cross-linking due to ageing is known to manifest as inferior mechanical properties, especially shorter elongation at break and higher moduli.^[4,6] This is also exactly reflected in the results discussed above. Severe ageing conditions result in a more pronounced decrease of the strain at break and an increase of the rigidity, possibly due to increased cross-link density. However, the radical activated mechanism needs to cross a thermal barrier, which is achieved only at higher temperature (around 150 °C)^[14]; that explains the low influence of ageing at 100 °C.

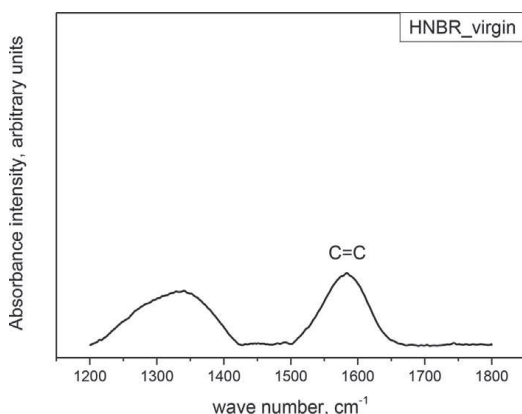


Figure 5. Detection of residual double bonds in HNBR in Raman spectrum.

The carboxylic acid groups, formed from the oxidation of the hydro-peroxides, could lead to the chain breakage. These chain scissions could occur providing more polymer radicals in the material and they could be engaged in more cross-linking reactions. Therefore, the cross-linking reactions could be more dominant on the final properties compared to chain scission starting at comparatively lower temperature levels.^[6,10,12]

These chain scission reactions in HNBR could manifest in properties as a decrease of strength at break^[4,6] as observed in Figure 4a with rising ageing temperature and exposure time. For 100 °C, the strength at break shows a slight increase compared to the virgin material (This behavior is explained later in this paper). Even a temperature of 150 °C and an exposure time of 72 hours reveal no pronounced difference in strength at break values compared to virgin material, but after 168 hours of exposure time, there is a strength at break reduction. In contrast, with a temperature of 170 °C, the chain scission is significant even after 24 hours exposure time.

In contrast to the above mentioned peroxide-based cross-linking and chain scission as ageing mechanisms, several authors discussed the effect of the cyano (–CN) functional group in ACN converting into an imino group (–CNH) due to oxidation. Especially, Bhattacharjee et al.^[16] observed a molecular weight (MW) increment at initial temperatures with a decrease after an optimum ageing time, for highly saturated NBR (ACN 37%) (MW has been measured viscosimetrically). They explained this phenomenon as a modification of –CN groups into imino groups as depicted in Figure 6.

However, in the literature, this MW increment as a result of ageing has been observed as a temporary phenomenon. Approximately, 160% increase in MW has been observed at 100 °C after ~2 hours of ageing. After this optimum ageing time, MW has gradually decreased at higher

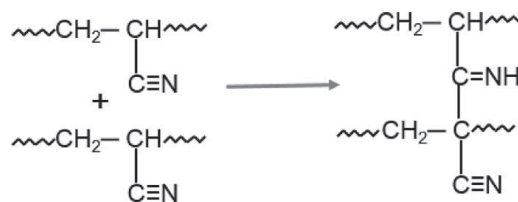


Figure 6.

Cyano group conversion to imino group and molecular weight increment.^[18]

exposure times. Similar results for an ageing temperature of 150 °C have been observed: an increment to 130 % of the MW at optimum ageing time of 30 minutes. Further, at higher temperatures, the MW increment effect has been lower and the optimum time has also decreased.^[16] Bendor and Campomissi^[6] also tried to identify the effect of –CN group conversion into –CNH as a result of oxidative ageing for aged HNBR (35% ACN). However, they did not observe characteristic peaks of imino groups, nor any decrease in the intensity of the nitrile peak or shift of the absorbed frequency in the IR spectra for their samples aged at 150 °C.^[6]

In our experiments, the FT-IR tests for un-aged, aged at 100 °C for 24 hours and aged at 170 °C for 168 hours on samples, as depicted in Figure 7, examining the effect in cyano functional groups in different aged temperatures and exposure times as a result of oxidation were conducted. The observed spectra in ATR mode for HNBR aged at 100 °C for 24 hours, Figure 7a, shows a clear decrease in the intensity of –CN functional group and an additional characteristic peak at ~1640 cm⁻¹ reflecting the newly introduced CNH group compared to the virgin material. As shown in Figure 7b, there is no clear characteristic peak intensity difference of the imino group at ~1640 cm⁻¹, nor any decrease in the intensity of the cyano peak in the IR spectra for the samples aged at 170 °C.

Summarizing the observed results and the literature, at around 100 °C, there is a sign of conversion of some amount of the cyano functional group into an imino group

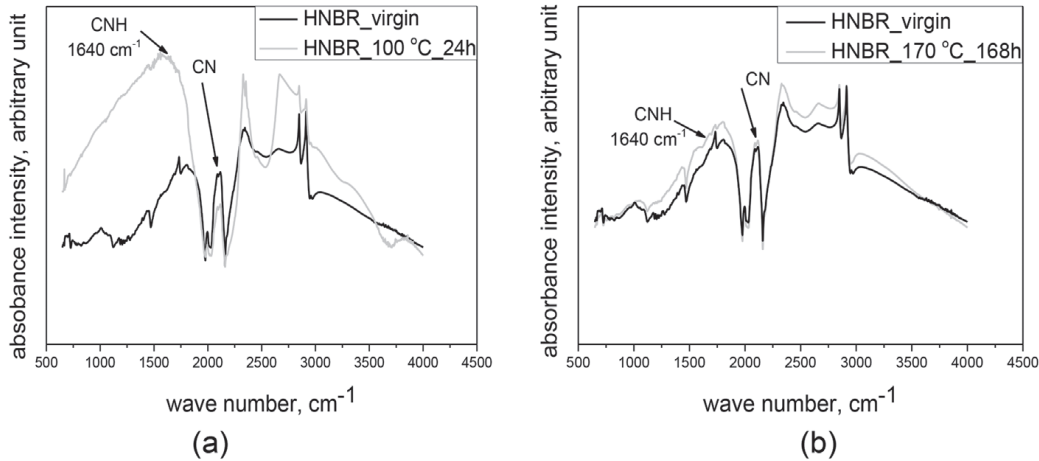


Figure 7.

Comparison of FT-IR spectra of virgin and aged HNBR samples (a) virgin material and 100 °C_24 h aged sample (b) virgin material and 170 °C_168 h aged sample.

as a result of oxidation. But at extreme ageing conditions (170 °C for 168 hours), this oxidation through cyano group only plays a secondary role as it already decomposes at elevated temperatures.^[7,8] The Observed imino group at around 100 °C is a relatively stable bond formed due to the electron-withdrawing nature of the nitrile group and this newly formed bond could increase the molecular weight of the material.^[16]

As explained before in Figure 4a, the strength at break was slightly increased at 100 °C, 24 hours exposed materials compared to its virgin state. This behavior could be ascribed to temporary bonds through imino groups between polymer chains ageing at those conditions.

In Figure 8, the ageing temperature effect after 24, 72 and 168 hours exposure times as a percentage of the virgin sample properties (σ_R = strength at break of the aged sample and σ_R = strength at break for un-aged sample, ε_R = strain at break of the aged sample, and ε_R = strain at break for un-aged sample, $\sigma_{50\%}$, $\sigma_{100\%}$ are stress at 50% and 100% strain of the aged sample and $\sigma_{50\%}$, $\sigma_{100\%}$ are the stress at 50% and 100% strain of the un-aged sample) is shown. A clear decrease of the tensile strength (about 15–20%) was observed after ageing at 170 °C for 168 hours. The breaking strain decreases to a level of

~50–60%, while the $\sigma_{50\%}/\sigma_{50\%}$ rises to 200% with the same conditions. This significant embrittlement is a clear indication of less chain scission taking place compared to increasing cross-link density as a result of thermo-oxidative ageing. At 100 °C, nearly similar properties those in virgin material were observed; only slightly higher strength at break values due to new bonds formed between chains as a consequence of cyano functional group oxidation without effective chain scissions at that temperature. Nevertheless, at 150 °C, there are already degraded properties like ~10% of strength at break, ~40% of strain at break and increased ~70% of stress at 50% of strain. Therefore, at 150 °C, already 2/3 of material property degradation was observed compared to 170 °C after 168 hours of exposure.

Stress dependency on the strain for HNBR, summarizing the tendencies after 168 hours of exposure at different temperatures compared to virgin material, is shown in Figure 9. The strain at break significantly decreases with higher ageing temperature. The strength at break is reduced as well with rising ageing temperature. In contrast to the other properties, the stiffness clearly increases with higher temperatures. The strength at break reduction is not significant compared to the embrittlement of the material. These

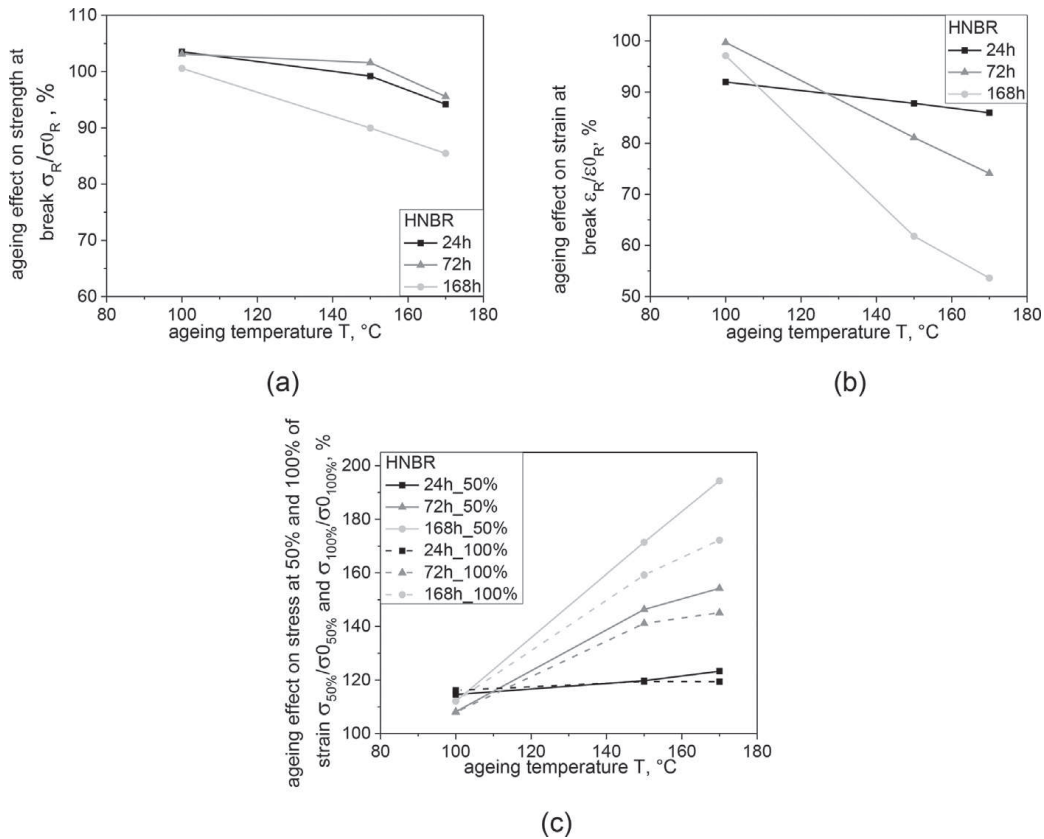


Figure 8.

Ageing temperature effect after 24, 72 and 168 hours in HNBR as a percentage of un-aged sample properties (a) strength at break (b) strain at break (c) stress at 50% and 100% strain.

results reveal a more pronounced cross-link density increment compared to chain scission influence in the material with thermo-oxidative ageing.

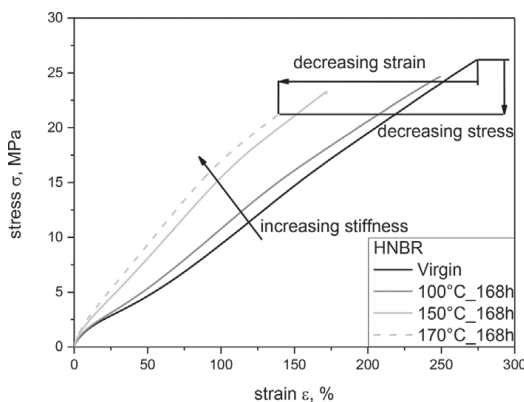


Figure 9.

Influence of the ageing temperature after 168 hours of exposure time in HNBR.

Tear Test Results

Tear properties of HNBR before and after ageing at different temperatures (100 °C, 150 °C and 170 °C) and exposure times (24, 72 and 168 hours) are compared in Figure 10. According to Figure 10a, nearly no influence on the final tear strength for the different ageing conditions were observed. At all the investigated temperature conditions, the strength at break deviated around the virgin material properties. Nevertheless, a reduction of the strain at tear strength with rising ageing temperature from 100 °C to 150 °C was observed (Figure 10b). At a temperature of 100 °C, only a minor effect on the exposure time was observed. With an increase to 150 °C, a clear decreasing strain at tear strength was observed with rising exposure time. For an increase to 170 °C, a nearly similar strain at tear strength value to samples aged at 150 °C was measured. Furthermore, at

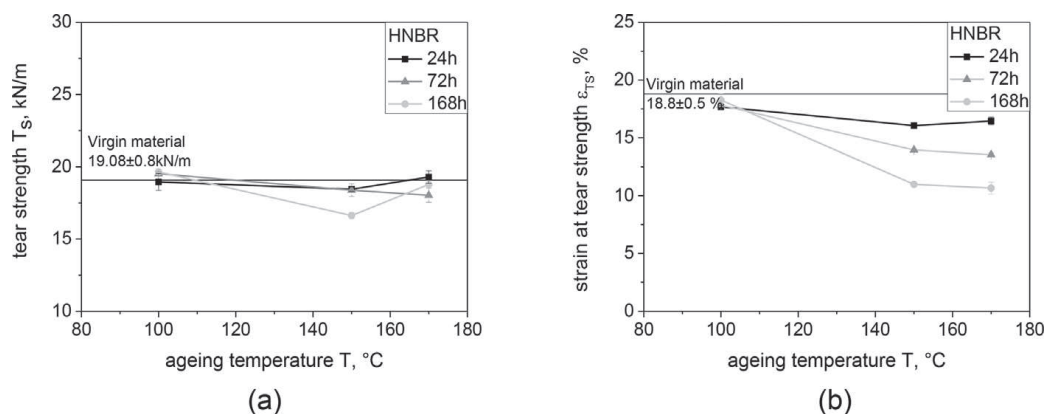


Figure 10.

Influence of ageing temperature and exposure time of HNBR on the tear results for (a) tear strength (b) strain at tear strength. The horizontal lines represent the virgin (un-aged) sample results in the respective graphs.

higher ageing temperatures, lower strain at tear strength values at higher exposure times were observed.

The tear of a rubber material is a mechanical rupture process, initiated and propagated at a site of high stress concentration caused by a cut, defect, or localized deformation reflecting tear resistance, which is proportional to a maximum force required to propagate a crack in the specimen.^[17] Theoretically, the tear strength should demonstrate the cross-link density changes in the material with ageing. However within these results (Figure 10a), no significant differences in tear strength results, compared to the virgin material properties, were observed. It can be attributed to a possible specimen geometry dominance, due to the specimen used with an angled incision. At an ageing temperature of 100 °C, the strain at tear strength seems also not influenced by the different exposure times (Figure 10b). This implies again no significant ageing at a temperature of 100 °C. Nevertheless, at 150 °C, a significant reduction of strain at tear strength and the clearly different influence of the ageing time due to increasing cross-linking density from oxidative ageing was observed. At 170 °C, the results show no clear differences from the observations at a temperature of 150 °C. These surprising phenomena could be an influence of chain scissions introduced into the material

above 150 °C, where the reduction of chain length could neutralize the effect of gained material stiffness from cross-linking for tearing.

Dynamic Mechanical Analysis

The influence of the thermo-oxidative effect on the mechanical properties of rapidly varying stress conditions over a broad range of temperatures was studied using the DMA method. The exposure time dependence on the loss factor ($\tan \delta$) for 100 °C, 150 °C and 170 °C aged samples is shown in Figure 11a, b and c respectively as a function of temperature at a frequency of 2 Hz.

No influence on the loss factor at 100 °C ageing was observed for all exposure times, revealing a peak at ~ -20 °C and similar peak maximum values (highlighted in the Figure 11a). At 150 °C, only the 24 hours exposed sample has similar loss factor intensity like the virgin material. However, a clear decrease of peak intensity as well as shifted $\tan \delta$ peak are visible for the other exposure times. All investigated samples aged at 170 °C demonstrate a $\tan \delta$ peak shifting to higher temperature and a decreasing intensity with higher exposure times. This temperature shift of $\tan \delta$ reflects the increasing glass transition temperature (T_g) with rising ageing temperature and exposure time. Moreover, the decreasing $\tan \delta$ maximum implies the changing damping properties.

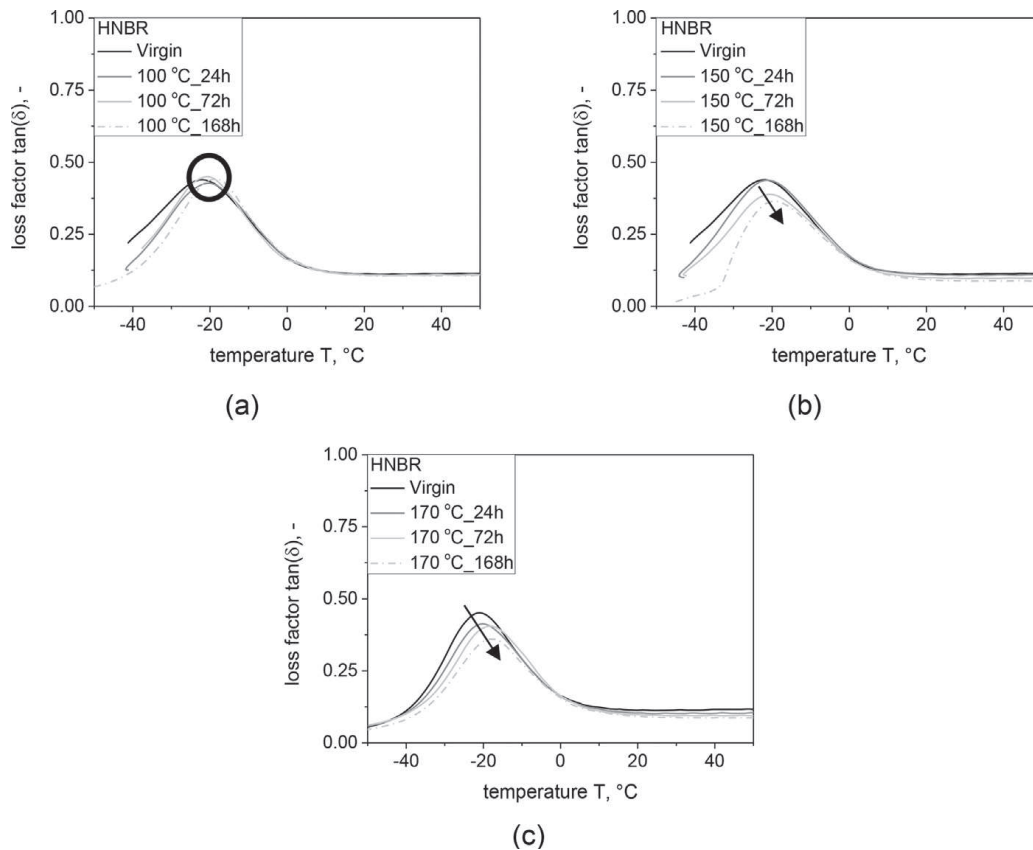


Figure 11.

Influence of the exposure time on the loss factor ($\tan(\delta)$) for HNBR at; (a) 100 °C aged (b) 150 °C aged and (c) 170 °C aged.

Several authors have investigated the ageing effects on dynamic mechanical properties of different polymeric materials, i.e., HNBR, NBR/PVC blend and PA6.^[5,7,15,16] They have observed a shifting of $\tan \delta$ curves towards higher temperatures for degradation of polymers. Moreover, the $\tan \delta$ maximum values for degraded samples reveal a lower value compared to the un-degraded samples.^[8,14,18]

Polymers aged in hot air are expected to have a higher glass transition temperature compared to the virgin materials as a result of introduced cross-linking between main chains.^[8,14,15] According to the literature, the restrictions of the mobility of the polymer main chain reflect the decreasing area under the loss factor depending on the temperature. Therefore, the intensity of the $\tan \delta$ peak at the glass transition temperature reflects the extension of the

mobility of the macromolecular chain segments.^[8,19]

As shown in the Figure 11b and c, the glass transition temperature is shifted to a slightly higher temperature after ageing for 72 hours at 150 °C. Additionally, both peak width and intensity of loss modulus of the aged samples were lower with longer exposure time. This trend is more pronounced at higher ageing temperatures. This observed behavior is attributed to the reduction of the mobility of the molecules and the damping properties at higher temperatures and higher exposure times due to more cross-links between main chains as a result of thermo-oxidative ageing of HNBR. Therefore, cross-linking visibly changes the properties after ageing 72 hours at 150 °C and 24 hours at 170 °C.

The storage modulus, E' , graphs (they are not included in this paper) were also

monitored for the above-mentioned test conditions. Similar trends were observed for T_g values taking the storage modulus transitions into account as found from the shifting of $\tan \delta$ values in Figure 11.

DQ NMR

As explained with the above results and the literature, ageing of polymers resulting in deterioration of mechanical and physical properties may involve motions that scale up to the whole chain length, yet it is usually a result of molecular-level changes, such as formation of short chains due to chain scission or additional cross-linking during ageing. In order to elucidate the structural changes that have happened due to ageing, un-aged samples and samples which were exposed for 168 hours at 170 °C were tested using double quantum NMR.

The results of the DQ measurements on the un-aged sample and the subsequent analysis to extract the defect fraction (exponential fits) are shown in Figure 12. The descriptive information of the calculations are described in the appendix.

The sum and the difference curves along with the fits for the defect fraction are shown in Figure 12a. Once the defect fractions have been determined, the double quantum build up curve, I_{DQ} , can be

normalized to I_{nDQ} as shown in Figure 12b, which reaches a plateau value of 0.5, a value that confirms the defect fraction extraction is correct. Finally, the analysis of the I_{nDQ} curve can be analyzed directly or a simultaneous analysis of I_{DQ} (not I_{nDQ}) and the sum signal after the defects have been subtracted yields D_{res} (weak residual dipolar coupling).

A gamma distribution of D_{res} (equation 1) was assumed,^[20] since the network structure is expected to be highly heterogeneous for several reasons, i.e., the structure of the HNBR (spin-system heterogeneity, i.e., different mobility of the different monomer segments),^[21] the peroxide cross-linking which is known to be heterogeneous^[22] and the ageing process that results in random chain scission and/or cross-linking.

$$I_{\text{nDQ}} = \int_0^{\infty} \frac{1}{2} \left(1 - \exp \left[-\frac{2}{5} D_{\text{res}}^2 \tau_{\text{dq}}^2 \right] \right) \times \frac{2}{\sqrt{\pi}} \sqrt{\frac{27 D_{\text{res}}}{8 D_{\text{avg}}^3}} \exp \left(-\frac{3 D_{\text{res}}}{2 D_{\text{avg}}} \right) dD_{\text{res}} \quad (1)$$

Where, τ_{dq} is pulse sequence duration and D_{avg} is the average residual coupling. For the analysis, due to the sharp decay of the I_{DQ} curve after the initial build up, a simultaneous fit of the I_{DQ} using equation 2

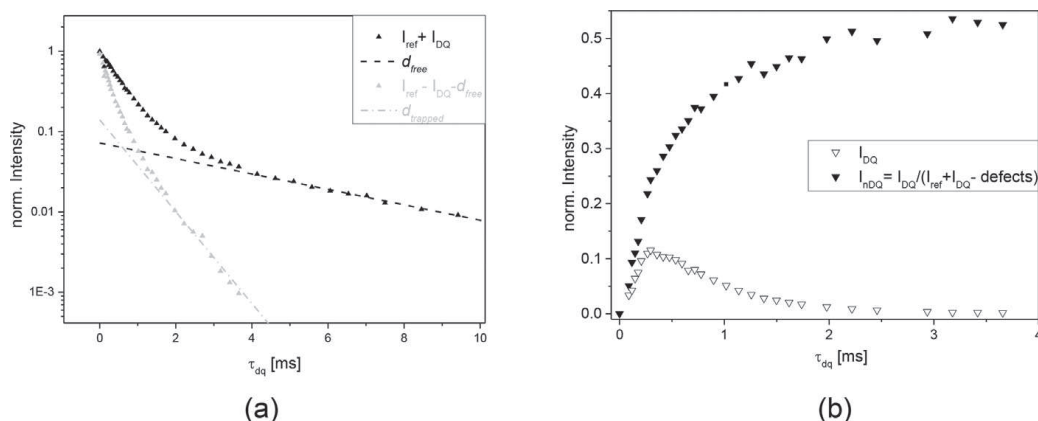


Figure 12.

DQ NMR measurement analysis for the un-aged pristine sample at 60 °C; (a) The sum and the difference curves along with the fits for the defect fraction (b) The normalized defects fraction. I_{ref} represents the reference intensity decay curve, while defects represents the summation of d_{free} (spins from free defects) and d_{trapped} (spins from constrained defects).

and the I_{sum} signal (after the subtraction of the defects) using equation 3 were used.

$$I_{\text{DQ}} = A \cdot \exp\left(\frac{-2\tau_{\text{dq}}}{T_2}\right) \cdot \int_0^\infty \frac{1}{2} \left(1 - \exp\left[-\frac{2}{5} D_{\text{res}}^2 \tau_{\text{dq}}^2\right]\right) \times \frac{2}{\sqrt{\pi}} \sqrt{\frac{27D_{\text{res}}}{8D_{\text{avg}}^3}} \exp\left(-\frac{3D_{\text{res}}}{2D_{\text{avg}}}\right) dD_{\text{res}} \quad (2)$$

$$I_{\text{sum}} = A \cdot \exp\left(\frac{-2\tau_{\text{dq}}}{T_2}\right) \quad (3)$$

In this expression, A is the fraction of detectable rigid phase in the sample and T_2 is relaxation time.

The analysis of the DQ curve for the un-aged and aged samples are given below in Table 1. From the absolute values of the average residual coupling (The width of the gamma distribution is directly related to the average), D_{avg} , it can be clearly seen that the system is highly cross-linked, as expected from the other mechanical property results. Upon ageing, there is a slight increase in the D_{res} , usually corresponding to an increase in cross-linking. Additionally, the fraction of defects (or the percentage) increases by a factor of almost 1.5 upon ageing. This shows clearly that the ageing process has an influence on the network structure with chain scission confirmed by increases in the defect fraction and a simultaneous cross-linking initiated by radical formation, confirmed by the increase in the D_{avg} . Percentage value was calculated taking all chains in to account. Some defects were detected also in the un-aged material due to mobile

non-load bearing segments such as long tails, curing additives, etc., from its curing and processing functions.

Conclusion

In this study, carbon black filled (85 phr) HNBR (ACN 36%) rubber (HNBR) was studied at different ageing temperatures and exposure times to detect thermo-oxidative degradation. It was found that with the investigation of samples aged at 100 °C, there was no significant property degradation irrespective the exposure up to 168 hours. Nevertheless, a slight increment of strength at break compared to virgin material was observed at 100 °C ageing temperature. For the samples ageing at 150 °C, up to 72 hours of exposure time, similar strength at break values to the virgin material were observed that only decreased with prolonged exposure. However, strain at break and stress at 50% strain and 100% strain for the same samples showed slight degradation starting from 24 hours of exposure time followed by more pronounced ageing effects at prolonged exposure. Strain at tear strength was reportedly reduced at 150 °C compared to the virgin materials and retained the approximately similar values until 170 °C aged temperature. However, nearly no influence on the final tear strength for the different ageing conditions were observed. The glass transition temperature was shifted slightly to higher temperatures at 150 °C ageing temperature from 72 hours of exposure time compared to virgin material. Moreover, at 170 °C, the influence of ageing was visible starting from 24 hours of exposure time for dynamic mechanical properties.

The results indicated that the oxidative degradation is the predominant reaction contributing to properties in this study. Degradation of the sample occurred in the tensile strength – strain at break, strain at tear strength and damping properties as well as the raising of the stiffness and the

Table 1.

Analysis of the DQ curve for the un-aged and the most aged sample. The defect fraction i.e. the fraction of chains that do not contribute to the load bearing properties of the network and the network density were estimated according to the analysis explained above.

Sample	D_{avg}/Π [kHz]	% Defects
Un-aged	7.13 ± 0.43	21%
Aged (170 °C_168 h)	8.14 ± 0.59	30%

glass transition temperature of the material.

From all the test results, it is clear that HNBR degradation is a combination of chain scission and cross-linking. The nitrile group in the polymer conversion in-to the imino group as a result of oxidation is negligible at higher ageing temperatures and higher exposure times. However, at $\sim 100^\circ\text{C}$, the slight increment of strength at break compared to un-aged material is due to temporary nitrile group oxidation. Residual double bonds in nearly total saturated HNBR undergo a thermo-oxidative aging process. Hydro-peroxide, which initiated through the unsaturation, plays a very important role as the potential initiator of auto oxidation. This process introduces stable radicals that drive the process causing more cross-linking and chain scission in the polymer.

The cross-linking effect visibly changes the material properties at 150°C ageing for 72 hours of exposure time. When aged at 170°C , the cross-linking effect is already visible after 24 hours of exposure time. This behavior was revealed from tensile strain at break, stress at 50% and 100% strain, strain at tear strength and DMA results. However, the chain scission becomes more clearly visible in the material properties only after 168 hours of exposure time at 150°C aged temperature. When aged at 170°C , chain scission starts to be effective from 24 hours of exposure time. This implies from the reduction at strength at break and behavior from tear results. Therefore, 150°C is already seemed influential for the physical properties of HNBR, where it shows cross-linking after 72 hours of exposure and chain scission after 168 hours of exposure.

Thermo-oxidative ageing effects on properties of HNBR model material and the possible microstructural changes were discussed in this paper. The future work will be focused on the other relevant damage mechanisms for HNBR in oil and gas industry applications, i.e., the resistance to rapid gas decompression, the resistance to swelling by aggressive

fluids and gases, etc., under thermally aged and un-aged conditions.

Acknowledgements: The research work was performed at the Polymer Competence Center Leoben GmbH (PCCL, Austria) within the framework of the COMET-program of the Federal Ministry for Transport, Innovation and Technology and Federal Ministry for Economy, Family and Youth with contributions by material science and testing of polymers of the Montanuniversitaet Leoben, SKF Sealing Solutions Austria GmbH and ContiTech Rubber Industrial Kft. The PCCL is funded by the Austrian Government and the State Governments of Styria, Lower Austria and Upper Austria.

Appendix

Background of DQ NMR

Protons (^1H), bound to molecular chains (segments), can interact through space in the presence of a magnetic field, an interaction that is known as dipolar interaction or dipolar coupling (DC). This depends primarily on the inter-nuclear distance of the interacting spins and instantaneous average orientation of the dipolar tensor of a given $1\text{H}-1\text{H}$ pair with respect to the magnetic field. This interaction is averaged to zero in the case of fast isotropic motion but settles to a small finite value D_{res} when motion is restricted and remains anisotropic. In the case of elastomers, at short times, the motion is isotropic and fast rendering an averaging effect to the coupling; however for longer periods due to the motional hindrances posed by cross-linking, entanglements and filler-interactions, the D_{res} settles to a small finite value. The finite value D_{res} given by equation 4 is then characteristic of the motional hindrance that, in the case of elastomers, is due to cross-linking, entanglements and filler interactions.

$$D_{\text{res}} \propto \frac{1}{2} \langle 3\overline{\cos^2\theta} - 1 \rangle \propto \frac{3}{5N} \quad (4)$$

Here $\langle \dots \rangle$ denotes the average over all conformations of the chain segments and $\langle \dots \rangle$ denotes the average over all the segments in the network, the angle θ stands for the instantaneous segmental orientation with respect to the end-to-end vector and N denotes the number of segments between two cross-link points (or other similar constraints). Thus, determining D_{res} reliably becomes a key to network structure determination. It should be noted that in weakly cross-linked systems, N would be a composite of entangled as well as network chains ($N^{-1} \propto M_{\text{crosslinks}}^{-1} + M_{\text{entanglement}}^{-1}$). However, in commercial systems such as the ones used in the study, it is dominated by network chains due to the high cross-link density.

Double Quantum NMR (or multiple quantum NMR) is known as the method of choice for determining D_{res} in different systems.^[22,23] Technically, the method involves exciting two signals as a function of the excitation time: (i) signal coming from the interacting spins (to a good approximation neighboring spin pairs specially at short excitation times, hence double quantum (DQ)) which are usually a part of motionally restricted segments of the network chains in the case of elastomers, henceforth denoted as I_{DQ} and (ii) a signal consisting of all the rest of the protons that are not excited in the first signal are simply denoted I_{ref} . The sum of these two will then constitute the whole system of spins.^[11] Ensuing effects are the most mobile non-load bearing segments, i.e., long tails, curing additives, etc., (free defects or d_{free}) which appear as a slowly decaying tail in this sum signal which can be extracted with an exponential fit of the signal decay at long times. Analogously, the constrained defects such as loops, short dangling ends etc., (d_{trapped}) appear as a tail in the difference signal after removal (subtraction) of component d_{free} . Finally, a simple point-by-point division of the I_{DQ} and I_{sum} after subtraction of the defects results in a normalized DQ signal ($I_{\text{nDQ}} = I_{\text{DQ}}/I_{\text{sum-defects}}$). This signal then excludes any relaxation contribution from defect

segments while it is characteristic only of the network segments; D_{res} can be extracted using a suitable fit from the normalized signal or alternately from simultaneous fits of I_{DQ} and $I_{\text{sum-defects}}$ resulting in a reliable description of the actual network, cross-link density, its distribution and the defect fraction. However, in certain cases, the relaxation processes can affect the I_{DQ} considerably, in such cases, a simultaneous fit of the I_{DQ} and the I_{sum} signal after removal of defects can be used to extract D_{res} .^[21]

Note that it is also important to measure at high enough temperatures in order to accurately determine the network properties, (empirically $>T_{\text{g}}^{\text{DSC}} + 50^\circ\text{C}$), where the segmental motion has enough thermal energy, hence enough degrees of freedom, to cover the entire conformational space resulting in complete averaging. In this study, experiments were carried out taking this into account.

- [1] W. Hofmann, *Rubber Technology Handbook*, 2nd Ed., Hanser publishers, Munich-Vienna-New York **1989**.
- [2] R. C. Klingender, *Handbook of Specialty Elastomers*, Taylor & Francis Group, Boca Raton-London-New York **2008**.
- [3] Properties And Applications Of Hydrogenated Nitrile-Butadiene Rubber, International Institute of Synthetic Rubber Producers, azom.com 2013, Accessed 7/13/2015, <http://www.azom.com/article.aspx?ArticleID=1724>.
- [4] Y. Kamiya, E. Niki, in *Degradation and Stabilization of Polymers*, H. H. G. Jellinek, Ed., Elsevier publishers, Amsterdam-Oxford-New York **1983**, p. 337.
- [5] R. A. Chaudhry, I. A. Hussein, M. B. Amin, B. F. Abu Sharkh, *J. Appl. Polym. Sci.* **2005**, 97, 1432.
- [6] H. Bender, E. Campomizzi, *KGK Kautschuk Gummi Kunststoffe* **2001**, 54, 14.
- [7] J. E. Dato, E. C. Campomizzi, D. Achten, Rubber-News.com, **2008**, Accessed 7/14/2015, <http://www.rubbernews.com/article/20080519/ISSUE/305199964>
- [8] U. Giese, I. Homeier, Y. Navarro, S. Torr ejon, S. Kautz, *Chem. Listy.* **2013**, 107, 3.
- [9] B. Schritteser, G. Pinter, T. Schwarz, Z. Kadar, T. Nagy, *Rubber Fiber Plastics Int.* **2016**, 11, 40.
- [10] A. Chaudhry, A. F. Bhowmick, C. Ong, M. Soddemann, *Polym. Eng. Sci.* **2010**, 50, 1389.
- [11] K. Saalw achter, *Prog. Nucl. Magn. Reson. Spectrosc.* **2007**, 51, 1.
- [12] D. J. Carlsson, S. Chmela, D. M. Wiles, *Makromol. Chem. Macromol. Symp.* **1989**, 27, 139.

- [13] U. Giese, M. Santoso, Y. Navarro, *Chem. Listy.* **2011**, 105, 233.
- [14] E. Campomizzi, H. Bender, W. von Hellens, *KGK Kautschuk Gummi Kunststoffe* **2001**, 54, 114.
- [15] U. Giese, I. Homeier, Y. N. Torr jon, S. Kautz, *Chem. Listy.* **2013**, 107, 3.
- [16] S. Bhattacharjee, A. K. Bhowmick, B. N. Avasthi, *Polym. Degrad. Stabil.* **1991**, 31, 71.
- [17] Standard Test Method for Tear Strength of Conventional Vulcanized Rubber and Thermoplastic Elastomers, Annual Book of ASTM Standards **2000**.
- [18] B. Likozar, M. Krajnc, *e-Polymers* **2007**, 131.
- [19] M. C. S. Perera, U. S. Ishiaku, Z. A. M. Ishak, *Polym. Degrad. Stabil.* **2000**, 68, 393.
- [20] J. L. Valent n, D. L pez, R. Hern ndez, C. Mijangos, K. Saalw chter, *Macromolecules* **2009**, 42, 263.
- [21] M. A. Malmierca, A. Gonz lez-Jim nez, I. Mora-Barrantes, P. Posadas, A. Rodr guez, L. Ibarra, *Macromolecules* **2014**, 47, 5655.
- [22] T. Saleesung, D. Reichert, K. Saalw chter, C. Sirisinha, *Polymer* **2015**, 56, 309.
- [23] W. Chass , S. Schl gl, G. Riess, K. Saalw chter, *Soft Matter* **2013**, 9, 6943.

Paper 2: Induced material degradation of elastomers in harsh environments

Winoj Balasooriya¹, Bernd Schrittester¹, Gerald Pinter² and Thomas Schwarz³

¹ Polymer Competence Center Leoben GmbH, Roseggerstrasse 12, 8700 Leoben, Austria.

² Department of Polymer Engineering and Science, Montanuniversitaet Leoben, Otto Glöckeltrasse 2, 8700 Leoben, Austria.

³ SKF Sealing Solutions Austria GmbH, Gabelhoferstraße 25, 8750, Judenburg, Austria.

Published in *Polymer Testing*, 2018, 69, 107.

DOI: 10.1016/j.polymertesting.2018.05.016



ELSEVIER

Contents lists available at ScienceDirect

Polymer Testing

journal homepage: www.elsevier.com/locate/polytestPOLYMER
TESTING

Material Behaviour

Induced material degradation of elastomers in harsh environments

Winoj Balasooriya^{a,*}, Bernd Schritteser^a, Gerald Pinter^b, Thomas Schwarz^c^a Polymer Competence Center Leoben GmbH, Roseggerstrasse 12, 8700, Leoben, Austria^b Department of Polymer Engineering and Science, Montan University Leoben, Otto Glöckelstrasse 2, 8700, Leoben, Austria^c SKF Sealing Solutions Austria GmbH, Gabelhoferstrasse 25, 8750, Judenburg, Austria

ARTICLE INFO

Keywords:

Oil and gas
HNBR
Rapid gas decompression
Swelling
Thermal ageing

ABSTRACT

The elastomeric components used in oil drilling operations, especially sealing solutions, are experiencing hardships from high pressure, high temperature and in contact with fluids. Therefore, the present work contributes to identifying the behaviour of hydrogenated nitrile butadiene rubber (HNBR) in contact with solvents and gases, and the ageing effect on resistance to rapid gas decompression (RGD). The swelling behaviour of HNBR was measured in different solvents and the tensile properties in different swollen conditions, i.e., unswollen, swollen and de-swollen, were tested. RGD resistance was investigated in virgin and aged conditions. Deteriorated properties were observed in swollen states and the degradation magnitude was correlated with the degree of swelling; in fully de-swollen states, the un-swollen properties were regained. In RGD measurements, a relatively lower gas permeation was seen in swollen samples as well as the lowest volume increase during the decompression phase. However, crack observation based NORSOK ranking rates the RGD resistance in thermo-oxidative aged HNBR to be best followed by swollen and virgin samples, respectively.

1. Introduction and basic considerations

The oil and gas industry is still to play a major role in the present and the foreseeable future in global energy requirement, as alternative energy sources are yet to be fully developed. Today, oil and natural gas respectively deliver ~31% and 21% of the total world energy supply [1]. Therefore, wells are being drilled in increasingly hostile environments, for instance, high pressure, high temperature (HPHT) and ultra-HPHT in the deep waters of the Gulf of Mexico [2]. In these conditions, as the aid of drilling operations, the operating well environment engages with gaseous and liquid hydrocarbons, carbon dioxide (CO₂), hydrogen sulphide (H₂S), brines, inhibitors, solvents, etc., [2,3]. Consequently, the elastomeric components in oil and gas field equipment, i.e., different seals, packers, etc., where each tool application requires specific elastomer properties, are challenged in operation to perform as expected [4].

Especially, the sealing function is reportedly impaired by seal hardening, chemical degradation, excessive seal swelling or shrinkage, seal extrusion and fragmentation due to high pressure and RGD [3–5] causing costly financial, safety and environmental implications for the operators and equipment suppliers [4,6,7]. The identified failure mechanisms are encountered in the diffusion of fluid into the elastomer, changes to the internal rubber structure, and modification of physical properties [6]. At elevated temperatures, the altering the mechanical

properties and accelerating the damage mechanisms can be expected [8,9].

Elastomers interacting with liquid may result in the absorption of liquid by the elastomer (swelling), extraction of soluble constituents from the elastomer or chemical reaction with the elastomer. According to the situation, these phenomena can be combined [10]. After a certain time, the equilibrium swelling state is established and the change of volume could be identified gravimetrically or by measuring the change of dimensions; the volume change could be varied from shrinking effect to a quite large volume swell up to 150% and more [10–13]. Elastomer-liquid interacting behaviour is based on several variables; mainly, a polymer's chemical structure, crystallinity, and the presence of cross-links (chemical or associative) [14]. Among them, the monomer of the elastomer determines the elastomer-liquid affinity for liquid absorption and the polarity of elastomers is vital for elastomer-liquid compatibility [13,15,16]; it is explained with the solubility parameter “ δ ”, which is a thermodynamic property related to the energy of attraction between molecules. When substances with same or similar δ values are inter-mixed, they are likely to have an affinity for each other. Therefore, if the liquids have the same or close δ compared with the elastomer, the possibility to be absorbed into the elastomer increases and vice versa [17].

Crosslinking limits liquids entering into the material because of additional tie points [14]. Considering reinforced elastomers, fillers

* Corresponding author.

E-mail address: winoj.balasooriya@pccl.at (W. Balasooriya).<https://doi.org/10.1016/j.polymertesting.2018.05.016>

Received 2 February 2018; Received in revised form 30 April 2018; Accepted 14 May 2018

Available online 15 May 2018

0142-9418/ © 2018 Elsevier Ltd. All rights reserved.

could reduce the movement of rubber molecules. Therefore, the amount of filler in the material has an adverse effect on the absorption process [17]. In addition to these material structural factors, the amount of absorption depends also on other characteristics of the solvents, i.e., the molecular weight, the molar volume as well as the increasing temperature [11,18,19]. Viscoelastic nature of the rubber increases the mobility of long chains with increasing the temperature. Therefore, higher working temperatures increase the diffusion of solvent molecules (even bigger solvent molecules) into gaps between polymer chains [19,20]. Moreover, other external parameters like the agitation of the solvent and exposure to radiation can also have an influence on the interaction [11,18].

The presence of absorbed fluid in sufficient quantities can weaken the polymer, where the fluid molecules push the polymer molecules apart; these phenomena could lead to disentangling the tie points, detaching the polymer-filler adsorption bonds and also have a plasticizing effect [17,21]. If the fluid molecules were just physically present between the polymer chains, by fully removing them, for example by evaporation, the original properties would be almost restored, if the effects on the physical network were not considered [9,17,21,22]. However, the absorbed fluid is hostile and changes the chemical structure of the elastomer, so that the properties of the material are irreversibly deteriorated and still affected after fully drying out. Elastomers with considerable levels of unsaturation in their backbone are susceptible to degrade through chemical attacks during the swelling process; moreover, the functional groups could also be chemically attacked [17,23]. Leaching out of the soluble constituents from the elastomer could manifest itself as a decrease in volume or could be physically invisible, before fully drying out, if the softening effect is higher compared with the stiffening effect [10]. In operation, the volume shrinkage can impair the sealing function resulting in leakage of system [15].

Major elastomeric materials used in oil and gas applications are classified in Table 1, according to their polarity and saturation [17,24].

The swelling ability of elastomers is being utilized as a favourable feature as well. In industry, the swellable elastomers, “smart materials”, are used as production separation packers replacing the conventionally or hydraulically set packers, establishing zonal isolation in linear completions, where normally a cement column would be used as an expandable open hole clad [5,13,25,26].

RGD or explosive decompression (ED, EXD) is generally found in the oil and gas industry as well as in any fluid handling application, when dealing with a rapid gas pressure drop [7,27]. In the literature, this process is explained in steps; gas diffuses into the elastomer in the presence of high pressure and temperature until reaching the equilibrium state. In this state, the whole system is stable and pressure and concentration differentials are formed. If the pressure is released rapidly, the compressed gas can nucleate at voids, softly bonded particles or other imperfections leading to an expansion within the elastomer and there can also be structural failure in the form of blistering, internal cracking and splits [7,27–29]. This damage might also occur internally in the material, and would not be visible on the surface [27]. The seal failure process due to rapid gas decompression is extremely complex and it depends on several factors, i.e., polymer type, gas type/mix, pressure, rate of decompression, temperature, compounding, mixing and processing, levels of squeeze and grove fill, number of pressure

Table 1
General classification of elastomers used in oil and gas industry [17,24].

Non-polar elastomers		Polar elastomers		
Slightly unsaturated	saturated	unsaturated	Slightly unsaturated	saturated
IIR	EPM	NBR CR	HNBR	FKM, FEPM, FFKM, TPU MVQ, CPU

cycles as well as the seal cross-section [7,27].

As a chemically aggressive gas, H₂S could chemically attack some elastomers causing seal degradation; however, it has a relatively secondary effect on RGD in comparison with the CO₂ environment [7,30]. Nevertheless, the CO₂ can be favourable too, if it is injected back into the reservoir to reduce the viscosity of the oil, assisting to improve the yield [30,31].

Over the years, a huge amount of work and research at the laboratory level has been conducted to identify the effects on elastomers in the oil and gas industry [3,7,27,29,32]. However, there is still a need to discuss the ageing effects of elastomers combined with rapid gas decompression. HNBR, a widely used class of polymers in oil and gas industry due to its intrinsic properties [33,34], is being used as a model material for investigations. In the previous research [8,9], the influence of ageing behaviour of HNBR in harsh environments was discussed by these authors. The objective of the present work is to address the effects, when HNBR is in contact with solvents and gases, and the ageing effect on its resistance to rapid gas decompression.

2. Experimental procedures

2.1. Material

An HNBR (ACN 36%) grade, peroxide cross-linked, stabilized with anti-oxidants, filled with carbon black (85 phr), was selected for these investigations. The manufactured compound was provided as disc plates and cylinders for investigations.

The specimen dimensions and test parameters are summarized below.

2.1.1. Swelling test

The swelling tests were conducted for HNBR in toluene, IRM 901, IRM 903 and iso-octane/toluene mixture (70:30, V%), according to ASTM D471-06 [35]. The rectangular shaped specimens, which were cut out from the plates, were immersed in solvents (IRM 901 and IRM 903 at 100 °C, iso-octane/toluene mixture at 70 °C or toluene at room temperature) in fully closed small glass test bottles. The immersed samples were taken out of the glass bottles after 24, 48, 72 and 168 h to measure the volume changes over the time. Sample surfaces were dried using paper towels and this was followed by measuring the weight and density. A balance and a density kit (XS205DU, Metler Toledo, Switzerland) were utilized measuring the weight (in the air to the nearest 1 mg) and the density (by the buoyancy method). The density was measured submerging in distilled water and the samples which were swollen in highly volatile solvents found difficulties measuring the quite precise density and volume measurements, but viable reproducibility was achieved. The mean value and standard deviation of the results were calculated from these measurements and used for analysis.

2.1.2. Tensile test

Smooth dumbbell specimens (S2) (DIN 53504) were punched out from plates (un-swollen, swollen and de-swollen conditions) for the tensile experiments. These specimens possessed a thickness ~2 mm, width 4 mm and gauge length of 25 mm. All the tests were performed with a Zwick universal testing machine (Zwick Roell, Test expert, Ulm, Germany) with a 1 kN load cell, at a constant crosshead speed of 200 mm/min according to DIN 53504. Tensile properties of HNBR in different swollen conditions, i.e., un-swollen (no contact with solvent), swollen (equilibrium state) and de-swollen (after removing the solvent from the material) samples were tested. For tensile tests, swollen samples were prepared by immersion in toluene for 24 h at room temperature, in IRM 903 at 100 °C and iso-octane/toluene mixture at 70 °C for 168 h. At the end of the exposure times, they were taken out of the solvent and punched out to obtain tensile test specimens. To obtain the de-swollen samples, the swollen samples were dried in an air-circulating oven; samples immersed in toluene and iso-octane/toluene

mixture were dried in an air-circulated oven at 70 °C for 7.5 h and 22 h respectively, while the samples immersed in IRM 903 were dried in a vacuum oven at 70 °C for 3.5 h. The drying time was determined by repeatedly measuring the weight of the specimens until the equilibrium state was reached. Thereafter, the samples were punched out for the tensile tests. The other swollen specimens were rushed for sample preparation and testing. Five specimens of each condition were used to ensure reproducible results.

2.1.3. Rapid gas decompression test

The bulk deformation behaviour of HNBR virgin state (un-aged) and aged stages (immersed in liquid or thermally aged) under highly confined conditions, the crack initiation and crack growth under high deformation rates were tested in the RGD measurements. The tests were performed on specimens, which were machined to cylinders (similar to a cross-section of an O-ring). The cylinders were aged in an air-circulating oven at 150 °C for 168 h or immersed in IRM 903 at 100 °C for 168 h.

The RGD resistance experiments were performed in a high-pressure autoclave test system (SITEC, Sieber Engineering AG, Zürich, CH) with pure CO₂ at 90 °C, 150 bar and a de-pressurisation rate of 100 bar/min. The system is comprised of a high-pressure autoclave (500 cm³), a heating unit with controls and a data acquisition system, which could test a pressure of 350 bar, temperature of 200 °C and decompression rates up to 25 bar/second with carbon dioxide (CO₂), methane (CH₄). This experimental set up is further explained in the literature [27,32]. Cylindrical specimens (diameter 8 mm and height 8 mm) were utilized in un-constrained conditions on a freely standing position on the ground of autoclave for ~ 21 h. The changes in the cylindrical specimens were measured in situ with a camera. The Tracker software package (Tracker 4.95, Douglas Brown physlets.org/tracker) was employed to calculate dimensional changes in different states (pressurising, equilibrium and de-pressurising) based on the continuously captured pictures.

After the tests, a visual observation and assessment of the specimens were carried out according to the NORSOK rating system (see Table 2) [36]. Each cylindrical specimen was examined at three radial cut sections by light microscope for internal cracks, and the samples were rated for RGD damage according to the number and length of any cracks observed. Every test condition was reproduced with three specimens.

2.1.4. Dynamic mechanical analysis

The possible microstructural changes of HNBR in thermally aged conditions were investigated with DMA measurements. The samples aged at 150 °C for different exposure times were compared. For the experiments, a DMA 861/40N testing device (Mettler Toledo GmbH, Schwerzenbach, Switzerland) was used with a liquid nitrogen cooling system. All tests were carried out within the temperature range of -50 °C to 100 °C. The parallel parts between the shoulders of the dumbbell specimens (thickness approximately 2 mm, width 4 mm) were

Table 2
The seal failure rating criteria according to NORSOK testing standard [35].

Description	Rating
No internal cracks, holes, or blisters of any size	0
Less than 4 internal cracks, each shorter than 50% of the cross-section, with a total crack length less than the cross-section	1
Less than 6 internal cracks, each shorter than 50% of the cross-section, with a total crack length of less than 2.5 times the Cross-section	2
Less than 9 internal cracks of which max. 2 cracks can have a length between 50% and 80% of the cross-section	3
More than 8 internal cracks, or one or more cracks longer than 80% of the cross-section	4
Crack(s) going through the entire cross section or complete separation of the seal into fragments	5

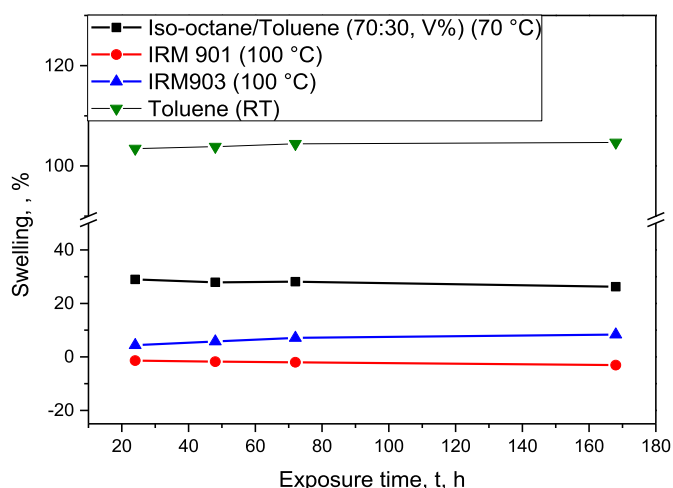


Fig. 1. HNBR swelling behaviour (volume increase) with main solvents; IRM 901 at 100 °C, IRM 903 at 100 °C, iso-octane/toluene mixture at 70 °C and toluene at RT.

used as the specimens in tension mode. The detailed information of the DMA test method and the complete analysis of the thermal ageing performance of the HNBR material can be found in previous research work [8,9].

3. Results and discussion

In the following section, the swelling behaviour, the property changes of swollen samples and the ageing effect on RGD resistance are compared. The possible microstructural changes and the chemistry involved with interacted solvents, which affect the monitored mechanical properties of HNBR, are discussed as well.

3.1. Swelling behaviour of HNBR in different solvents

The variation of volume changes of HNBR as a function of immersed duration in IRM 901, IRM 903, iso-octane/toluene mixture and pure toluene are shown in Fig. 1. According to the results, toluene seems to be the most compatible solvent with HNBR compared with the other solvents. HNBR swells in toluene up to 105% of initial volume and the equilibrium swelling is eventually reached from ~ 24 h of exposure. The volume of HNBR increases up to ~ 30% in contact with iso-octane/toluene mixture for 24 h. When HNBR is immersed in IRM 903, the swelling amount is increased from 24 h until 72 h exposure at a moderate rate into the equilibrium state of ~ 9% volume increase. However, when HNBR is exposed to IRM 901, the volume is even decreased compared with the un-swollen state. This behaviour is slightly increased up to ~ -3% after 168 h.

Pure toluene and iso-octane/toluene mixtures (ASTM reference fuels) which encounter gasoline or diesel fuels in service seemingly show more compatibility with the used HNBR. Solubility parameters (δ), for toluene and iso-octane, are indicated in the literature as 8.97 and 6.9 (cal/cm³)^{1/2} respectively. In terms of petroleum base, IRM 901 and IRM 903, standard test mineral oils possess δ values of ~ 13.9 and 16.9 (cal/cm³)^{1/2} respectively while HNBR has the δ ~ 9.7 (cal/cm³)^{1/2} (δ range 9.0–12 (cal/cm³)^{1/2}) [6]. Toluene as an aromatic based, low viscous, volatile solvent [35] contains a closer solubility parameter in contact with HNBR and reveals an exceptionally high swelling effect. The mixture of iso-octane and toluene has the next closer solubility parameter to HNBR compared with the other solvents. However, IRM 901 has a closer solubility parameter compared with IRM 903 to HNBR, even showing a material shrinkage in contact with the polymer. In general, oils having a similar aniline point display similar effects on rubber: the lower the aniline point, the more pronounced is the swelling

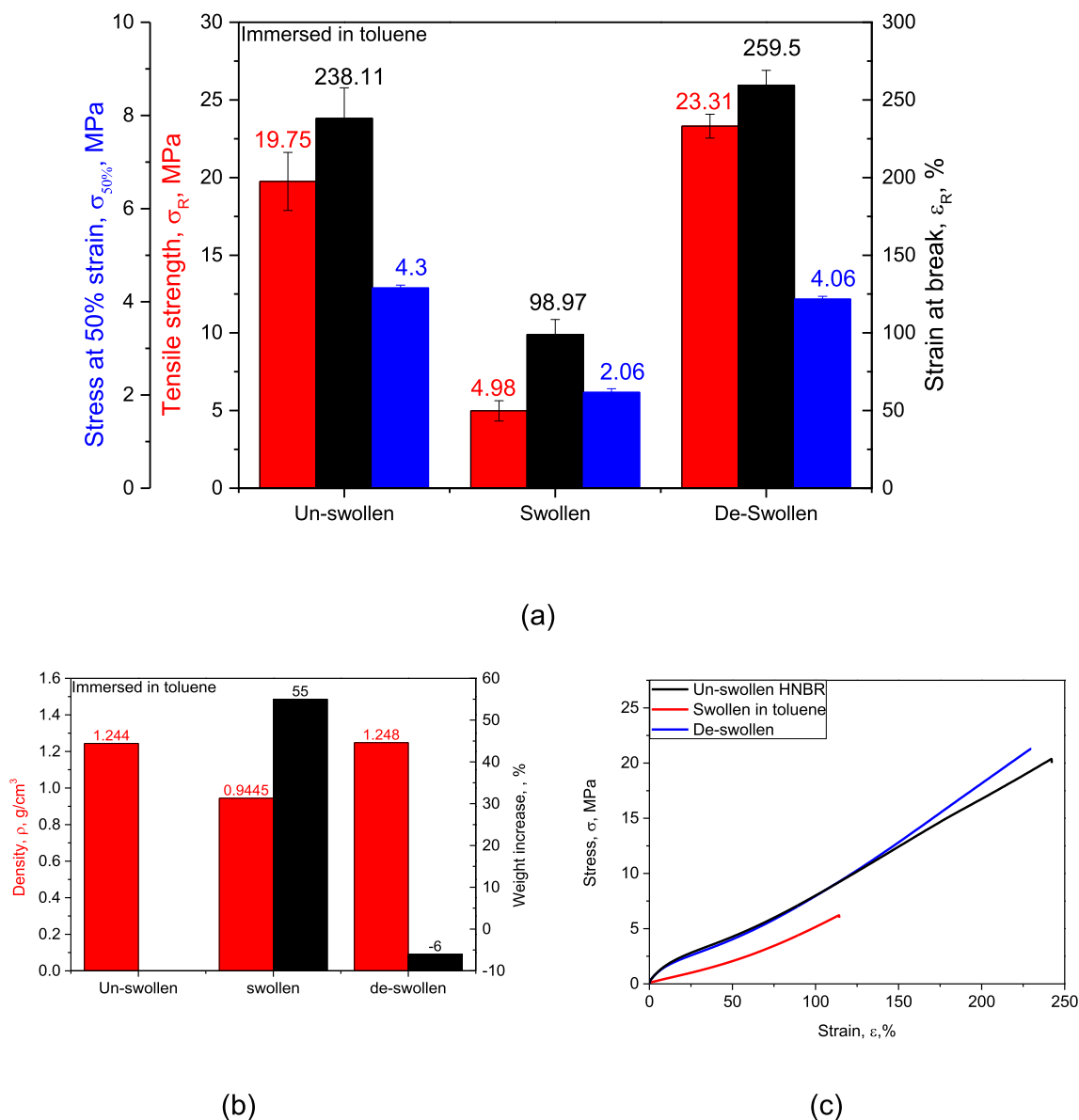


Fig. 2. Comparison of the influence of swelling of HNBR in toluene at room temperature for 24 h and after de-swelling compared with un-swollen samples (a) tensile strength, strain at break and stress at 50% strain, (b) density and weight increase in percent, (c) stress-strain behaviour.

action [37]. Thus, IRM 901 (A higher content of aliphatic components), having a high aniline point (124 °C), causes a slight swelling or shrinkage, while IRM 903 oil has a low aniline point (70 °C) and causes relatively large swelling of seals [23]. The shrinking effect could be also explained as an extraction process, where the contacting fluid leaches out the plasticizers and other additives of the elastomer's recipe [23]. As the samples were seemingly saturated after 24 h in every solvent and the immersed time in distilled water at room temperature for density measurement was trivial, the swelling effect from distilled water in every condition is negligible. In general, HNBR is considered as a water resistant elastomeric grade and especially in low temperature, it lowers the diffusion gradient as well [13,24].

3.2. Influence of swelling on tensile properties

The influence on the tensile properties of HNBR in swollen and de-swollen conditions after immersion in toluene at room temperature for 24 h, iso-octane/toluene at 70 °C for 168 h and in IRM 903 at 100 °C for 168 h are compared with the un-swollen sample properties in Figs. 2–4, respectively. The tensile strength (σ_R), the strain at break (ϵ_R) and the

stress at 50% strain ($\sigma_{50\%}$) deviation in different swelling conditions are shown in every graph (Figs. 2a, 3a and 4a). Furthermore, the density and weight changes (Figs. 2b, 3b and 4b) as well as the stress-strain behaviour (Figs. 2c, 3c and 4c) are reported for the samples immersed in the tested solvents.

As depicted in Fig. 2a, when HNBR is immersed in toluene, the σ_R values in the swollen state drastically decrease from its original values (down to ~25% of σ_R). However, after de-swelling, the σ_R values are fully restored to the un-swollen values. Similarly, the ϵ_R shows a reduction of the original values right after swelling (down to ~42% of ϵ_R) and after de-swelling, it is recovered or even slightly higher compared with the un-swollen material. Due to the swelling, the $\sigma_{50\%}$ was also reduced to ~48% from the un-swollen values and after de-swelling it is mostly recovered with a slight loss.

As shown in Fig. 2b, after immersion in toluene, the weight increases in the swollen state by ~55% and after de-swelling, the absorbed solvent is fully evaporated, recording a weight loss. The density is reduced in the swollen state by ~25%; however, it is restored in the de-swollen state. The stress-strain behaviour shows a considerable softening of the swollen material (Fig. 2c); however, the original

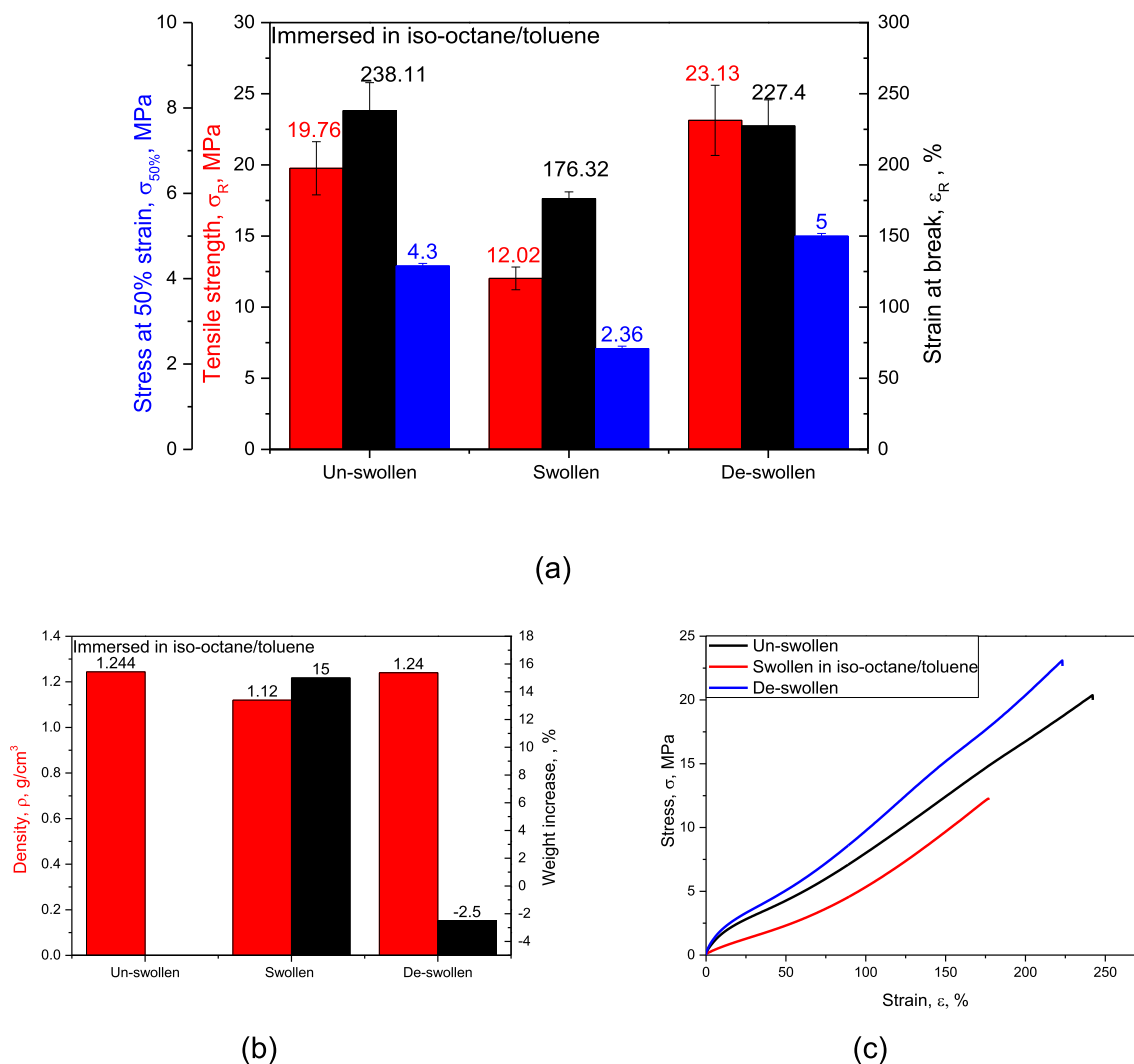


Fig. 3. Comparison of the influence of swelling of HNBR in iso-octane/toluene at 70 °C for 168 h and after de-swelling compared with un-swollen samples (a) tensile strength, strain at break and stress at 50% strain, (b) density and weight increase in percent, (c) stress-strain behaviour.

properties are nearly fully restored in the de-swollen state along the strain.

When samples were immersed in iso-octane/toluene, the tensile properties in the swollen state were decreased compared with the un-swollen (Fig. 3a), however at a lesser magnitude with respect to the property degradations in pure toluene; the σ_R , ϵ_R and $\sigma_{50\%}$ were decreased up to 60%, 74%, and 55%, respectively from their un-swollen properties. These properties were all restored in de-swollen condition and σ_R and $\sigma_{50\%}$ values are even higher than the un-swollen.

After swelling in iso-octane/toluene, the sample weight is increased up to ~15% and after de-swelling, a slight weight loss is recorded as shown in Fig. 3b. The density is also slightly reduced due to the solvent uptake; however, it is recovered after full evaporation. The stress-strain behaviour shows a considerable softening of the swollen material (Fig. 3c). But, the material is even stiffer in the de-swollen state than in the un-swollen state.

As shown in Fig. 4a, the σ_R , ϵ_R and $\sigma_{50\%}$ of HNBR have not deteriorated much after immersing in IRM 903 nor in the de-swollen state. As shown in Fig. 4b, the swelling increases the weight slightly ~5.6% and it stays mostly (~4.9%) in the material even after the evaporation, and the density also changes in accordance. As the other mechanical properties proved, the stress-strain behaviour (Fig. 4c) was not changed considerably by samples in contact with IRM 903.

The comparison of the stress-strain behaviour of HNBR in different

swollen conditions, i.e., un-swollen, swollen in IRM 903, swollen in toluene and swollen in iso-octane/toluene is shown in Fig. 5. The volume increase in the swollen states compared with the un-swollen condition is stated in the brackets. There is not a large difference in un-swollen and swollen in IRM 903 which had a 9% volume increase, but only slight stiffness reduction. With 30% of volume increase, the HNBR swollen in iso-octane/toluene has shown significant material softness and reduced strain at break compared with the un-swollen condition. However, with ~105% of volume increase in toluene, it shows relatively similar stiffness reduction with a significant reduction of strain at break. Seemingly, the stiffness reduction deteriorated after a certain amount of swelling, but strain at break reduction continued with increasing swelling.

The flexible nature of polymers, particularly elastomers, reflect the existence of the free volume within the polymer chains, which leads to moving macromolecules during the external loading [7,11]. When elastomers are in contact with the solvents, they swell through the absorption process of solvent molecules, i.e., water swells elastomer through the mechanism of osmosis and oils swell elastomer through a diffusion-controlled process [38–40]. The swelling process of elastomers through the diffusion can be illustrated as shown in Fig. 6. As depicted, initially the solvent is absorbed at the elastomer surface and penetrated into the polymer occupying the porous and free volume and then solvent molecules are diffused into the polymer. The material

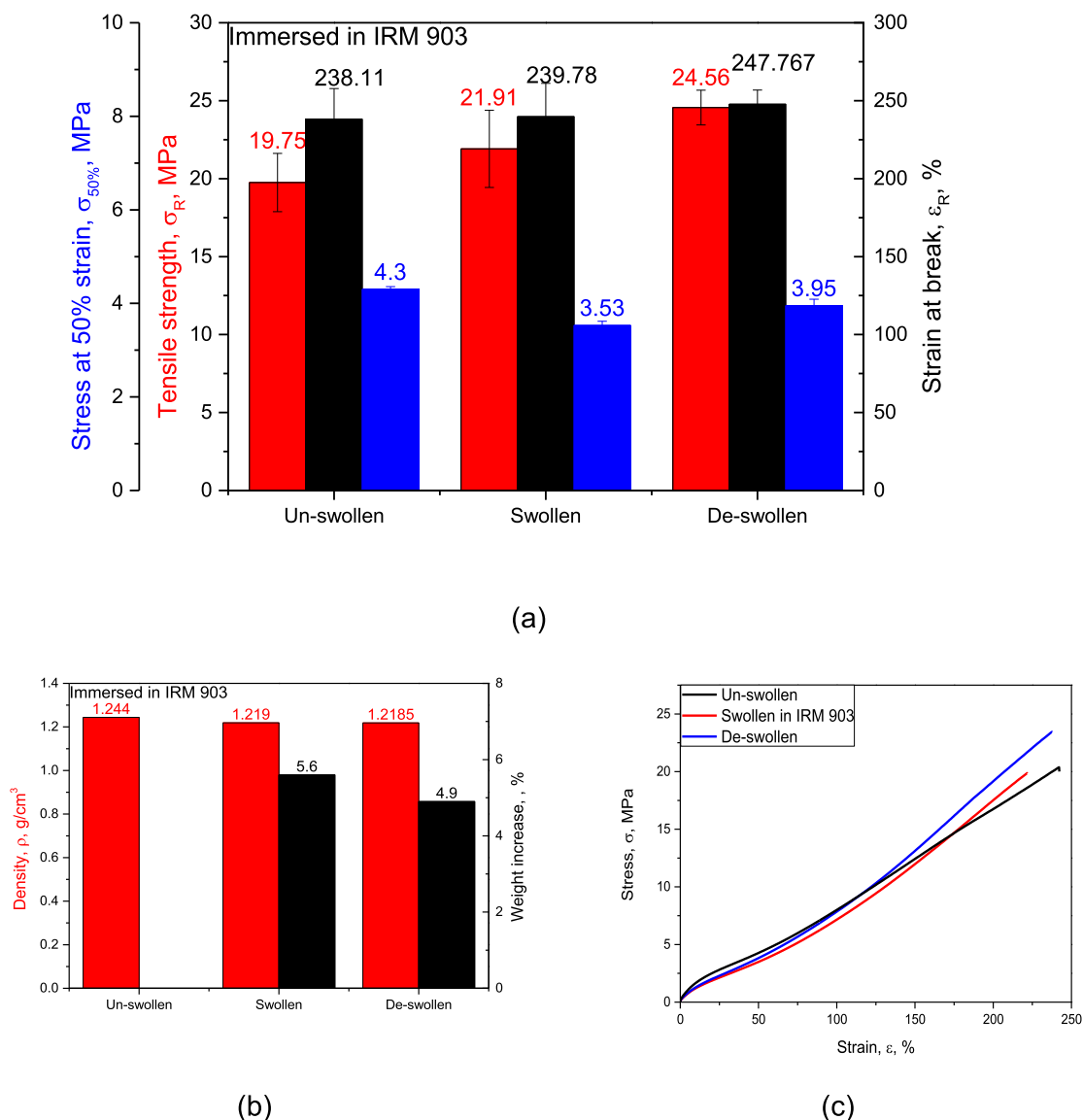


Fig. 4. Comparison of the influence of swelling of HNBR in IRM 903 at 100 °C for 168 h and after de-swelling compared with un-swollen samples (a) tensile strength, strain at break and stress at 50% strain, (b) density and weight increase in percent, (c) stress-strain behaviour.

swells as a result of trapped solvent molecules in the pores penetrate into the network of the polymer chains [19,20,22,39–41].

With the presence of solvent molecules between the polymer chains, the distance of the chains increases. The diffusion rate and the amount of solvent could lead to disentangle the polymer chains, de-bonding of the elastomer-filler interaction and even plasticizing of the chains [19,21,22,40]. Maximum effect from these phenomena are expected in the equilibrium swelling state, where the rubber-solvent interaction is maximised, and the rubber-rubber interaction decreases [22].

In general, the filler-rubber adsorption bonds can be recreated at another place along the molecule chain after sliding over the surface of the filler [21]. However, this regeneration process could be hindered by liquid present in the swollen state [9].

The tensile behaviour of swollen specimens is mainly based on the intra-molecular motions of segments and the molecular motions involving the adjustments and the shifting of chain entanglements, elastomer-filler de-bonding and plasticizing [21,22]. These micro structural changes could possibly be attributed to the lower σ_R and lower $\sigma_{50\%}$ in swollen samples. The stretched molecules, due to increased volume, could yield the lower ϵ_R of the swollen samples. These property reductions were observed with every tested solvent and the degradation

was significant with the degree of swelling.

With the starting of the de-swelling process, the amount of liquid within the molecules decreases and a segmental chain motion becomes easier. Therefore, the flexibility of the molecules increases and it leads to a higher strain at break [9,21]. After the fully de-swelling process, the conformations and entanglements return to their original state and the interaction of the filler-rubber is reintroduced leading to new physical bonds. Therefore, the fully dried samples after swelling have regained all of their properties (see Figs. 2 and 3). Nevertheless, the samples immersed in iso-octane/toluene show even higher σ_R and $\sigma_{50\%}$ values in the de-swollen condition compared with un-swollen. Relatively viscous oils, like IRM 903, were found to be difficult to remove from the specimens by conventional drying methods without yielding erroneous test results [35]. Therefore, within the tested conditions, the IRM 903 is not ideal for finding the de-swelling effect in mechanical property comparison tests, but for other test series where it needs the solvent within the material to investigate the swollen effect, for example the influence swollen effect on RGD behaviour.

ASTM reference fuels in the de-swollen state exhibit a weight reduction in comparison to the un-swollen sample (see Figs. 2b and 3b). This phenomenon could be explained as a leaching out of the

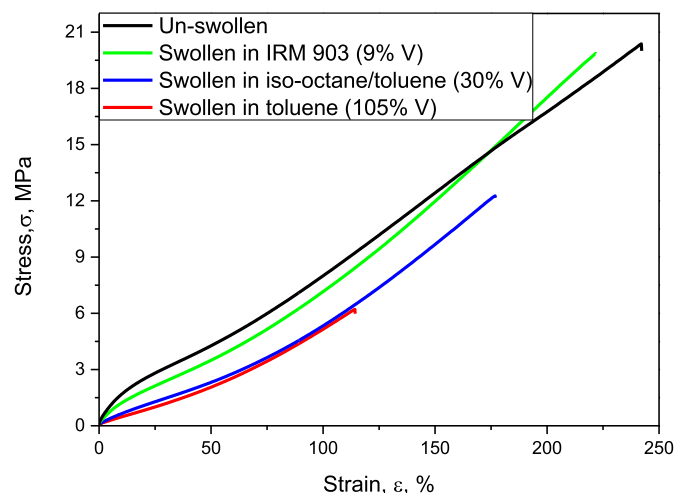


Fig. 5. The stress-strain behaviour comparison of HNBR in un-swollen, swollen in IRM 903, swollen in toluene and swollen iso-octane/toluene. The volume increase in swollen condition compared with the un-swollen state is shown in brackets.

plasticizers, stabilizers or other additives from the elastomer by the solvents. The weight loss is greater in pure toluene compared with the iso-octane/toluene mixture, where a higher degree of swelling was recorded as well. In every tested solvent, the % change in volume is greater than the % change in mass and the swollen sample density is lighter because the solvents are lighter than the elastomers [18].

3.3. Ageing effect on rapid gas decompression

For the comparison of the effect of different ageing conditions on the RGD resistance, the data from the autoclave tests were reduced to two specific values, i.e., the maximum observed volume change during the compression phase (the difference of volume at saturation phase to initial volume) (ΔV_C), and the maximum observed volume change during decompression (volume expansion compared with saturated volume) (ΔV_D). The ageing effect of HNBR on the volume change during the compression phase for HNBR at a saturation pressure of 150 bar with pure CO_2 and the relative volume change during the depressurization at a rate of 100 bar/min are summarized in Fig. 7a. While optical microscope pictures for observing damage are shown in Fig. 7b for the cylindrical specimens, the NORSOK ranking results from reproducible measurements for every ageing condition are shown to the left of the microscope picture of the sample.

As depicted in Fig. 7a, in the compression phase, virgin and thermo-oxidative aged (150 °C for 168 h) samples show similar ΔV_C (~10%). However, the samples immersed in IRM 903 at 100 °C for 168 h have relatively less ΔV_C (~3%) during the compression phase. In the decompression phase, virgin HNBR records highest ΔV_D (~40%), while

thermally aged samples and swollen samples show relatively less ΔV_D , ~33%, and 27%, respectively. The swollen samples possessed ~9% of volume increase compared with the virgin state before testing. The radial cross-section observation based NORSOK ranking (Fig. 7b) reveals better RGD resistance in aged samples compared with the virgin samples. Interestingly, the thermally aged sample showed the highest resistance in RGD performance followed by the swollen sample and virgin sample. In particular, major cracks were observed in virgin HNBR, which was more than 80% of the cross-section; while in swollen samples, some significant cracks amounting to between 50%–80% of the cross-section and some relatively fewer internal cracks in the thermally aged sample were detected.

Additionally, the dynamic mechanical analysis of HNBR revealing the exposure time influence on thermally aged samples at 150 °C is shown in Fig. 8. As depicted, a sample with 24 h of exposure time did not deviate from the virgin material properties, but at higher exposure times, both peak width and intensity of loss modulus were lower and the glass transition temperature (T_g), which correlates the peak temperature, increased. Especially, at 168 h exposure time the property degradation is significant compared with virgin material properties. This observed behaviour is attributed to the reduction of the mobility of the molecules and the damping properties due to more cross-links between main chains as a result of the thermo-oxidative ageing of HNBR [8,9].

RGD is a permeation/fracture phenomenon where tears, splits or blisters initiate from gas accumulations within the elastomer after pressure is suddenly released. Therefore, a good knowledge of gas permeation in elastomers is an essential prerequisite for identifying the RGD resistance [6]. The free volume, small imperfections or cavities in the elastomer matrix, are filled and expanded during the pressurisation until saturation is reached [27,29]. Even in these testing conditions, the absorbed IRM 903 is expected to be in the material (as shown in Fig. 4) minimizing the permeation of CO_2 into the material. Consequently, a relatively lower volume increase during the compression state of the swollen sample could be expected. During the decompression phase, the high rate of elastic expansion of the voided volume is followed by a tearing process in the elastomer bulk as well as some macroscopic crack initiation and growth within the matrix/filler interfaces [6,27,29]. Therefore, the resistance to RGD is increased if the permeability of gases into the material is lower and the physical properties (tear resistance, tensile strength) are as high as possible [34]. Consequently, interpreting the results in Fig. 7, the lowest volume expansion is recorded in the swollen sample at the decompression phase due to the lower gas intake during the compression phase. However, considering the NORSOK ranking and crack observation, the thermally aged sample shows the best performance, followed by swollen and virgin samples, respectively. The thermo-oxidative ageing increases the crosslink density of HNBR and increases the T_g , stiffness and tear resistance of the material [8,9]. This could possibly explain the fewer cracks, less crack propagation in the thermally aged sample. The swollen sample would become softer due to the presence of a solvent. Consequently, a

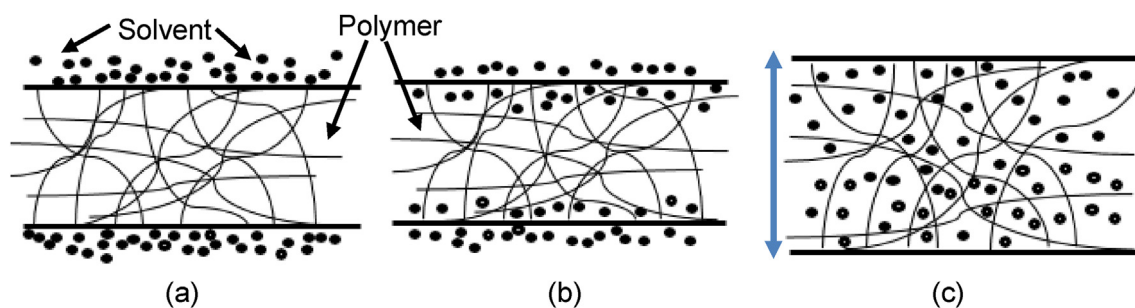


Fig. 6. Elastomer-hydrocarbon based solvent swelling mechanism through a diffusion process. (a) the absorption of solvent (b) penetration of solvent (c) swollen material due to the expansion of molecules.

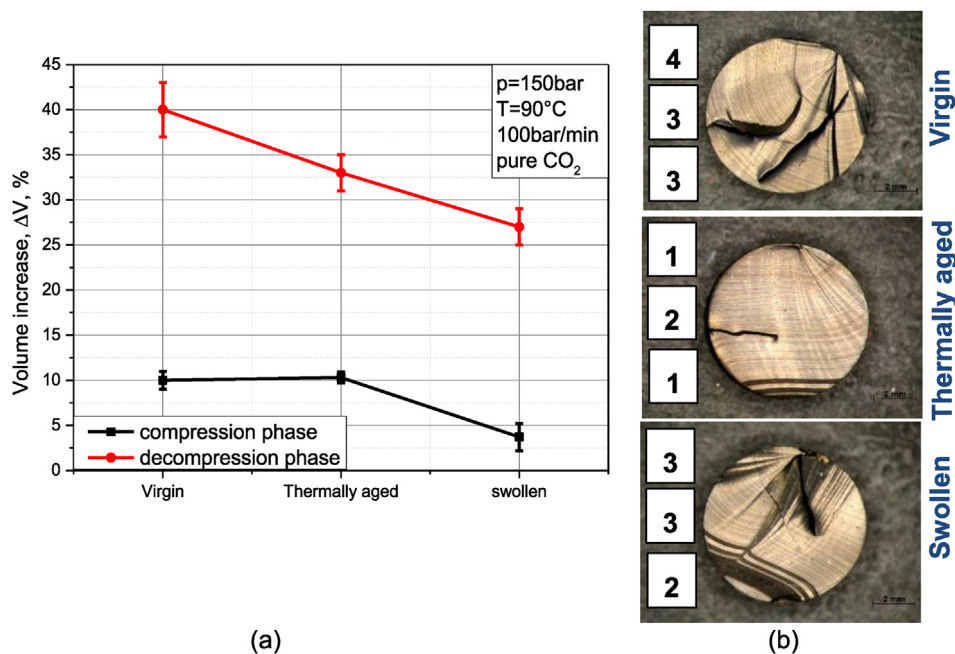


Fig. 7. Influence of ageing conditions on RGD performance of HNBR (a) Volume increase during compression (ΔVC) and decompression (ΔVD) (b) Visual observation of cylindrical specimens and the Norsok material ranking (every number on the left represents a different measurement).

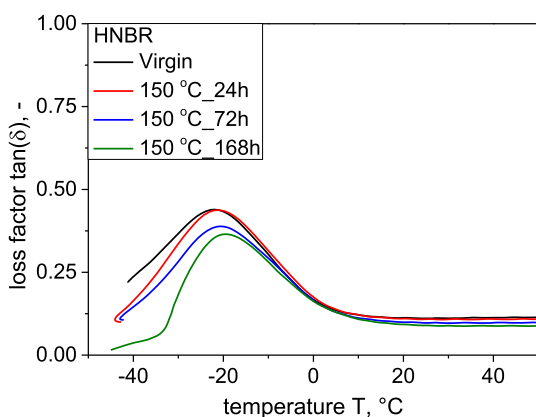


Fig. 8. Influence of the exposure time on the loss factor at 150°C .

relatively greater crack growth could be expected in depressurization, irrespective of lesser gas intake during compression. Therefore, RGD resistance appears to be a combination of many factors including gas permeation and mechanical properties.

4. Summary and conclusions

The aim of this paper was to study the behaviour of HNBR in contact with solvents and gases, and the ageing effect on resistance to RGD. Tests were conducted to measure the swelling behaviour HNBR in toluene, IRM 901, IRM 903 and iso-octane/toluene mixture (70:30, V%) and the tensile properties in different swollen conditions, i.e., unswollen, swollen and de-swollen. Further, the resistance to RGD was tested in virgin state and aged stages (immersed in liquid or thermally aged), under highly confined conditions. The greatest degree of swelling of HNBR in toluene was experienced followed by iso-octane/toluene mixture and IRM 903, and even a shrinking behaviour was observed in IRM 901. Solubility parameters, solvent viscosity and aniline points of solvents explain the swelling behaviour. Softer material properties were observed in the presence of the solvent in the material and the degradation magnitude was correlated with the degree of

swelling; in fully de-swollen states, the unswollen properties were regained. In swollen states, disentanglements of the polymer chains, debonding of the elastomer-filler interaction and even plasticizing of the chains could be expected, however, the altered physical reactions were seemingly restored in fully de-swollen conditions. In RGD tests, a relatively lesser volume increase during compression was experienced in the swollen sample; during the decompression phase, the lowest volume increase was recorded with the swollen sample, followed by thermo-oxidative aged and virgin samples. However, considering the Norsok ranking and cracks observation, the thermo-oxidative aged sample reveals the best performance followed by swollen and virgin samples. Thermo-oxidative aged HNBR is expected to introduce higher crosslink density in the material and with respect to increasing of the T_g , stiffness and tear resistance. These phenomena could probably explain the relatively greater resistance to RGD in thermo-oxidative aged HNBR, irrespective of lesser gas intake in swollen samples. Therefore, rapid gas decompression resistance is seemingly a combination of many factors including gas permeation and mechanical properties.

Acknowledgment

The research work was performed at the Polymer Competence Center Leoben GmbH (PCCL, Austria) within the framework of the COMET-program of the Federal Ministry for Transport, Innovation and Technology and Federal Ministry of Economy, Family and Youth with contributions from the material science and testing of polymers of the Montanuniversität Leoben and SKF Sealing Solutions Austria GmbH. The PCCL is funded by the Austrian Government and the State Governments of Styria, Lower Austria and Upper Austria.

References

- [1] Future of oil and gas, Global Agenda Council on the Future of Oil & Gas, World economic forum, Geneva, Switzerland, 2016.
- [2] A. Belani, S. Orr, A systematic approach to hostile environments, *J. Petroleum Technol.* 60 (2008) 34–39.
- [3] D.L. Hertz, Oil and Gas Industry Seals and Sealing - Success and Failure, ERG Fall Technical Meeting, Texas, Houston, September 18, 1996.
- [4] V. Bodepudi, J.M. Wilson, A. Patel, Drilling fluid type affects elastomer selection, *J. Oil Gas* 96 (1998), <http://www.ogj.com/articles/print/volume-96/issue-43/in-this-issue/drilling/drilling-fluid-type-affects-elastomer-selection.html>.

- [5] Z. Qamar, M. Akhtar, T. Pervez, M.S.M. Al-Kharusi, Mechanical and structural behavior of a swelling elastomer under compressive loading, *J. Mater. Design* 45 (2013) 487–496.
- [6] A. Stevenson, R. Shepherd, An overview of the requirements for seal life prediction, Part 1-static seals, *J. Sealing Technol.* 13 (1995) 9–12.
- [7] E. Ho, *Elastomeric Seals for Rapid Gas Decompression Applications in High-pressure Services*, BHR Group limited for the health and safety executive, 2006.
- [8] W. Balasooriya, B. Schritteser, S. Karunakaran, S. Schlögl, G. Pinter, T. Schwarz, Z. Kadar, Influence of thermo-oxidative ageing of HNBR in oil field applications, *J. Macromol. symposia* 3 (2017) 373–389.
- [9] W. Balasooriya, B. Schritteser, G. Pinter, T. Schwarz, Influence of HNBR ageing in oil field applications, *J. Rubber Fiber Plastics Int.* 4 (2017) 250–257.
- [10] L.P. Smith, *The Language of Rubber*, Butterworth-Heinemann, Oxford, 1993.
- [11] E.V. Takeshita, F.A. Piantola, S.M.A.G.U. de Souza, R.C.R. Nunes, A.A.U. de Souza, Quantification of styrene-butadiene rubber swelling as a function of the toluene content in gasoline: a new method to detect adulterations of fuels, *J. Appl. polymer sci.* (2012), <http://dx.doi.org/10.1002/APP.37643>.
- [12] B. Schritteser, G. Pinter, T. Schwarz, Z. Kadar, T. Nagy, Impact of the acrylonitrile content on the mechanical performance of elastomeric materials, *J. Rubber Fiber Plastics Int.* 1 (2016) 11–40.
- [13] R. Seyger, S. Resink, H. Harms, R. Hibberd, The future of swelling elastomers: an elastomer manufacturer's view of swelling elastomer developments and market trends, *J. Eng. Res.* 10 (1) (2013) 50–64.
- [14] A.O. Patil, T.S. Coolbaugh, *Elastomers: a literature review with emphasis on oil resistance*, *J. Rubber Chem. Technol.* 78 (03) (2005) 516–535.
- [15] M. Rinnbauer, *Technical elastomers: the basis of high-tech sealing and vibration control technology solutions*, Technische Elastomerwerkstoffe, SV corporate media GmbH, Munich, 2007.
- [16] H. Zhang, A. Cloud, *Research Progress in Calenderable Fluorosilicone with Excellent Fuel Resistance*, Arlon: Arlon Silicone Technologies Division, (2007), pp. 1–7.
- [17] R.P. Champion, B. Thomson, J.A. Harris, *Elastomers for fluid containment in offshore oil and gas production: guidelines and review*, *J. Health Saf. Exec.* 320 (2005).
- [18] M.S. Seehra, M. Yalamanchi, V. Singh, *Structural Characteristics and Swelling Mechanism of Two Commercial Nitrile-butadiene Elastomers in Various Fluids* vol. 26506, West Virginia University, Department of Physics, Morgantown, VA, 2012.
- [19] S. Gopakumar, M.R. Gopinathan Nair, Swelling characteristics of NR/PU block copolymers and the effect of NCO/OH ratio on swelling behavior, *J. Polymer* 46 (2005) 10419–10430.
- [20] A. Mostafa, A. Abouel-Kasem, M.R. Bayoumi, M.G. El-Sebaie, Effect of carbon black loading on the swelling and compression set behavior of SBR and NBR rubber compounds, *J. Mater. Design* 30 (2009) 1561–1568.
- [21] J. Diani, B. Fayolle, P. Gilormini, A review on the Mullins effect, *J. Eur. polymer* 45 (2009) 601–612.
- [22] S.C. George, M. Knörger, S. Thomas, Effect of nature and extent of crosslinking on swelling and mechanical behavior of styrene-butadiene rubber membranes, *J. Membr. sci.* 163 (1999) 1–17.
- [23] E. Vidović, Development of lubricating oils and their influence on the seals, *Goriva i maziva* 53 (3) (2014) 220–235.
- [24] T. Schwarz, *Material Data Sheet*, (2001) <http://files8.webydo.com/92/9259947/UploadedFiles/E6F89B2F-8E5C-81A7-1842-14500807AAEA.pdf>.
- [25] B.H. Harold, J.E. Edwards, S. Oman, R.V. Kuijk, B. Froelich, F. Marketz, R.W.F. Welling, C. Leuranguer, Evaluating expandable tubular zonal and swelling elastomer isolation using wireline ultrasonic measurements, IADC/SPE Asia Pacific Drilling Technology Conference and Exhibition, Bangkok, Thailand, 13–15 November 2006, 2006.
- [26] T. Pervez, S.Z. Qamar, R.A. Siddiqui, M. van de Velden, Effect of exposure on material response of a swelling elastomer, *Archives of Mater. Sci. Eng.* 37 (2) (2009) 77–84.
- [27] Z. Major, K. Lederer, M. Moitz, M. Mitterhuber, T. Schwarz, R.W. Lang, Development of a test and failure analysis methodology for elastomeric seals exposed to explosive decompression, 5th International MERL Conference, London, England, 29–30 March 2006, 2006.
- [28] S. Atkinson, Decompression modelling of elastomer seals promises to eliminate downtime, *J. Sealing Technol.* 12 (2002) 8–11.
- [29] B. Schritteser, G. Pinter, T. Schwarz, T. Nagy, M. Urbán, Fracture and fatigue behavior of elastomers used in the oil and gas industry, High Performance for Oil and Gas Conference, Houston, USA, 10–12 April 2013, 2013.
- [30] P. Warren, S. Winterbottom, A. Douglas, Rapid gas decompression resistance of elastomeric o-rings to supercritical CO₂, High Performance Polymers for Oil & Gas Conference, Edinburgh, Scotland, 15–16 April 2014, 2014.
- [31] G. Morgan, *Testing and Qualifying Advanced Elastomers for Deepwater Oil Exploration*, <https://www.element.com/nucleus/2016/07/14/testing-and-qualifying-advanced-elastomers-for-deepwater-oil-exploration>.
- [32] B. Schritteser, G. Pinter, T. Schwarz, Z. Kader, Rapid gas decompression performance of elastomers – a study of influencing testing parameters, *J. Procedia Structural Integrity* 2 (2016) 1746–1754.
- [33] W. Hofmann, *Rubber Technology Handbook*, second ed., Hanser Publishers, Munich Vienna New York, 1989.
- [34] D. Achten, Next generation HNBR grades – new materials for oilfield application, Oilfield Engineering with Polymers Conference, London, England, 29–30 March 2006, 2006.
- [35] ASTM standard D-471-06, Standard test method for rubber property - effect of liquids, *ASTM Int.* (1998).
- [36] NORSOK Standard M-710, Rev. 2, Norwegian technology centre, Qualification of non-metallic Sealing Materials and Manufacturers (2001).
- [37] R.A. Chaudhry, I.A. Hussein, M.B. Amin, B.F. Abu Sharkh, Influence of molecular parameters and processing conditions on degradation of hydrogenated nitrile butadiene rubbers, *J. Appl. polymer sci.* 97 (4) (2005) 1432–1441.
- [38] B.H. Harold, J.E. Edwards, R.V. Kuijk, B. Froelich, F. Markets, R.W.F. Welling, C. Leurangular, Evaluating expandable tubular zonal and swelling elastomer isolation using wireline ultrasonic measurements, IADC/SPE Asia Pacific Drilling Technology Conference, Thailand, Bangkok, 13–15 November 2006, 2006.
- [39] M. Zielińska, R. Seyger, W.K. Dierkes, D. Bielinski, J.W.M. Noordermeer, Swelling of EPDM rubbers for oil-well applications as influenced by medium composition and temperature Part I. Literature and theoretical background, *J. Elastomery* 20 (2) (2016) 6–17.
- [40] M. Abdul Kader, A.K. Bhowmick, Thermal ageing, degradation and swelling of acrylate rubber, fluoro-rubber and their blends containing polyfunctional acrylates, *J. Polymer Degrad. Stabil.* 79 (2003) 283–295.
- [41] O.M. Farid, *Investigating Membrane Selectivity Based on Polymer Swelling* (PhD thesis), University of Nottingham, 2010.

Paper 3: Tribological behavior of HNBR in oil and gas field applications

Winoj Balasooriya¹, Bernd Schritteser¹, Chao Wang¹, Andreas Hausberger¹, Gerald Pinter² and Thomas Schwarz³

¹ Polymer Competence Center Leoben GmbH, Roseggerstrasse 12, 8700 Leoben, Austria.

² Department of Polymer Engineering and Science, Montanuniversitaet Leoben, Otto Glöckeltrasse 2, 8700 Leoben, Austria.

³ SKF Sealing Solutions Austria GmbH, Gabelhoferstraße 25, 8750, Judenburg, Austria.

Published in *Lubricants*, 2018, 6, 20.

DOI: 10.3390/lubricants6010020



Article

Tribological Behavior of HNBR in Oil and Gas Field Applications [†]

Winoj Balasooriya ^{1,*}, Bernd Schrittester ¹, Chao Wang ¹, Andreas Hausberger ¹, Gerald Pinter ² and Thomas Schwarz ³

¹ Polymer Competence Center Leoben GmbH, Roseggerstrasse 12, 8700 Leoben, Austria; Bernd.Schrittester@pccl.at (B.S.); Chao.Wang@pccl.at (C.W.); Andreas.Hausberger@pccl.at (A.H.)

² Department of Polymer Engineering and Science—Materials Science and Testing of Plastics, Montanuniversitaet Leoben, 8700 Leoben, Austria; gerald.pinter@unileoben.ac.at

³ SKF Sealing Solutions Austria GmbH, 8750 Judenburg, Austria; Thomas.Schwarz@skf.com

* Correspondence: Winoj.Balasooriya@pccl.at; Tel.: +43-3842-429-6232

[†] This paper is an extended version of our paper published in 6th World Tribology Congress, Beijing, China.

Received: 10 January 2018; Accepted: 11 February 2018; Published: 13 February 2018

Abstract: The common usages of elastomeric components in oil and gas field applications are in dynamic atmospheres; especially sealing appliances that are in relative motion when interacting with surfaces. Therefore, their performance and service life mainly depend on the wear and friction characteristics in use. The objective of this scientific work is to identify the effect of swelling-induced ageing on the tribological properties and surface damage mechanisms of hydrogenated nitrile butadiene rubber (HNBR) in contact with different liquids. Furthermore, the investigation of the co-relation between mechanical properties and surface properties in the tested conditions is indispensable. In the swollen state, deteriorated mechanical properties were observed; however, in de-swollen conditions, the mechanical properties were restored. As far as the surface characterization is concerned, when the HNBR was swollen by a standard IRM 903 solvent, its wear was greater compared with the un-swollen specimen (1.1 times) despite the lower coefficient of friction (COF) (reduced by ~25%) and surface temperature (reduced by ~2.4 °C). In the de-swollen condition, wear was even greater (6 times), but the COF and surface temperature were situated in between those recorded in the swollen and un-swollen conditions. With swelling, greater wear damage and lower COF were observed; higher surface ageing (softness), which eases crack growth, created bigger debris. Under the conditions used, in the de-swollen states, the bulk mechanical properties were almost recovered, in contrast to the surface properties, which were still significantly impaired.

Keywords: elastomeric materials; HNBR; swelling-induced ageing; mechanical and tribological characterization; surface analysis

1. Introduction

Elastomers are a popular class of materials in oil field applications for sealing, down-hole packers, gaskets, etc. due to their soft, nearly elastic, and incompressible nature [1]. Especially, seals prevent the leakage of fluids and/or gas from a machine and contamination of the environment [2]. However, their performance and service life depend on the wear and friction characteristics in use [3]; therefore, tribology (the study of wear, friction, and lubrication) is an important factor for the seal performance and the overall efficiency of a machine [2,3]. It is necessary to reduce the coefficient of friction (COF) and wear rate of rubber composites for better performance [4]. The tribology of rubber is a complex phenomenon and depends mainly on the configuration of the tribo-testing rig, sliding speeds, applied loads, surface properties of the counterpart, sliding mode, contact area, etc. [5].

Wear in rubber materials is expected as a result of two processes: tearing (local mechanical rupture) and smearing (general decomposition of the molecular network to a low molecular weight material) [6,7]. These are affected by crack growth behavior, the mechanical properties of the rubber, chemical ageing, and the thermal conductivity of the composite [8]. Wear mechanisms can be classified as abrasive wear, fatigue wear, and roll formation. Abrasive and fatigue wear occur frequently on harsh and blunt surfaces, respectively, and roll formation occurs on relatively smooth surfaces of the abrading counterpart and for relatively smooth and soft elastomers [8]. Therefore, wear resistance is the ability of a material to resist mechanical actions, such as rubbing, scraping, or erosion, that tend progressively to remove material from its surface, which is related to the structural unit, localized stresses of the rubber, or initial substrate failure due to flaws in the rubber [8]. The viscoelastic nature of elastomers results in shear wave propagation along the surface of rubber during sliding, where it increases the surface area; these waves are known as “Schallamach waves” [8]. Therefore, with increasing applied normal force the wear due to the increased contact area rises [9]. Moreover, adding fillers rather than gum to elastomers seems to increase the abrasion resistance due to increased mechanical properties [10].

Rubber friction is considered to be based on two main components: adhesion and hysteresis behavior. While adhesion creates the stick-slip action between the rubber and the counter surfaces, hysteresis is a bulk phenomenon within the body of the rubber [8,11–13]. Additionally, the lubrication between surfaces has a crucial effect on frictional behavior, because it reduces both the adhesion and hysteresis components of friction. The smoothed surfaces possess reduced viscoelastic deformation from surface asperities, which leads to lower friction levels [2].

Adhesion is generally recognized to consist of the creation and breaking of junctions at a molecular level (attach to counter surface, stretch, detach, relax, and re-attach), which occurs at asperity peaks, where the fluid film (if available) is extremely thin and has properties distinct from the bulk lubricant in the voids [2,12,13]. For the majority of polymers, the Van der Waals and hydrogen bonds are typical [11]. If the interfacial bonding is stronger than the cohesion of the weaker material, the material is fractured and wearing takes place. Otherwise, the fracture occurs at the interface [11]. During the rapid detachment and relaxation phases of the rubber molecules and their counterparts in each cycle, the elastic energy stored in the polymer chains is dissipated as heat, and this is assumed to be the origin of the adhesion component of friction [12,13]. The adhesion friction, which is expected to occur more on smooth elastomer surfaces [12,13] sliding over a hard surface, decreases with a decrease in Young’s modulus and it is a function of the viscoelastic properties of the elastomer depending on the temperature and the sliding velocity [2].

A sliding elastomer can flow readily over the asperities of the counterpart and comply with their contours. This flowing action produces the deformation component of friction, which is called hysteresis [2]. The interface hysteresis occurs as a result of energy loss incorporated with the internal damping within the viscoelastic body (internal friction) [2,13]; however, the hysteresis increases with a decreasing Young’s modulus [2].

Most oil and gas industry operations are in the presence of fluids, and the elastomeric seals, in static and dynamic applications, interact with liquids. Therefore, the determination of the tribological performance of elastomers both in contact with a solvent and under dry conditions is indispensable to understand the material’s behavior [2,3,14]. The interaction of liquid with elastomers may result in an absorption process by the elastomer (swelling), which could change the chemical and physical material properties [9,15]. The chemical changes are expected to deteriorate irreversibly and still affect the properties after the solvent has fully dried out [15]. The monomers of the elastomer and their polarity determine the affinity for liquid absorption, where polar solvents are more compatible with polar substances and non-polar solvents are more compatible with non-polar substances and more likely to be dissolved [16–18]. The solubility parameter (δ), which is a thermodynamic property related to the energetic interaction between the liquid and the elastomer molecules, seems to explain mainly the liquid–elastomer interaction. When substances with the same or similar δ values are in

contact, they are likely to have an affinity for each other. Therefore, if the liquids have the same or closer δ values compared to the elastomer, the possibility to become absorbed into the elastomer increases and vice versa [15]. Additionally, the glass-transition temperature (T_g), crosslinking structure, amount of filler, working temperature, and specimen geometry influence this interaction [15,19]. In the equilibrium swelling state, the rubber–solvent interaction is maximized, whereas the rubber–rubber interaction decreases, leading to a total change in the conformation of polymer segments and chain entanglements [20]. Additionally, liquid intake into the material leads to a detachment process of the filler–rubber bonds, which are physically bonded [21], or even to a plasticizing effect [20,21]. Therefore, the properties are expected to be increasingly modified with the amount of swelling, which could be measured with the volume increase or the weight change after immersion.

There are very few published works dealing with the evaluation of the tribological performance after the swelling-induced ageing of elastomers. Mofidi et al. [2,22] tested the tribological behavior of elastomers aged in different oils (mineral, ester-based, and poly-alpha-olefin (PAO)) [2] and the influence of lubrication on abrasive wear [22]. They observed a higher COF reduction after ageing in ester-based synthetic oils compared with the mineral oils or PAOs for their nitrile butadiene rubber (NBR) used in the experiments [2], and in the lubricated conditions, they observed lower wear and a lower COF [22]. Although hydrogenated nitrile butadiene rubber (HNBR) is a widely used material in the oil and gas industry [1], some previous research efforts examining the effect of swelling-induced ageing on the tribology properties of HNBR are hard to find. However, there are some published works separately addressing the tribological properties of HNBR [23–27] and the influence of the swelling-induced ageing of HNBR on a change of the material's properties [16,19,28]. For example, Roche et al. [23] studied the influence of ageing on the tribological behavior of HNBR that was surface modified by ion implantation. They experienced greatly improved tribological properties by introducing a high-hardness coating layer to HNBR. Felhös et al. [24] experimented on the tribological properties of peroxide-cured HNBR with different multiwall carbon nanotube (MWCNT) and silica contents under dry sliding and rolling conditions against steel, and they observed that the filler amount has a progressive effect on the COF and wear resistance, while the MWCNT is a much better filler than silica. Similarly, Xu et al. [26] tested the friction and wear of HNBR with different fillers under dry rolling and sliding conditions and they experienced that the carbon black (CB)-containing and MWCNT-containing HNBR compounds possessed higher wear resistance compared with a silica-filled HNBR. Yuqin et al. [27] researched on the impact, friction, and wear properties of HNBR composites filled with silane-treated silicon carbide (SiC) and graphite. They experienced that the friction and wear behavior of the filled composites improved mostly when graphite-treated and silane-treated SiC were added together due to the synergistic effect between them. Karger-Kocsis et al. [25] conducted tests identifying the mechanical and tribological properties of rubber blends composed of HNBR and in-situ produced polyurethane and they found that the resistance to wear increased with Polyurethane (PU) hybridization into HNBR.

Therefore, the objective of this scientific work is to identify the effect of the combined action of swelling-induced ageing and tribological properties of HNBR in swollen and de-swollen conditions. This helps in improving its wear resistance and extending its service life under various conditions related to oil and gas field applications. Furthermore, the scientific paper focuses on the investigation and correlation between mechanical properties and surface properties in different environments. A clear understanding of the failure mechanism provides better insight to predict the service life of rubber products.

2. Experiments

2.1. Materials

An HNBR model material, which has 36% acrylonitrile (ACN) content, is peroxide cross-linked, and is filled with carbon black (85 phr) and plasticizers in a common amount, was selected for these

investigations. The manufactured compound was provided as disk plates and as specially designed disk specimens.

2.2. Specimens and Experimental Methods

In order to investigate the tensile properties of HNBR in different swelling conditions, un-swollen (no contact with solvent), swollen (immersed in a solvent until the equilibrium state), and de-swollen (swollen and then dried to remove the solvent out of the material) samples were tested. The swelling tests were conducted by exposing HNBR to standard solvents according to ASTM D471-06, i.e., IRM 903 at 100 °C and an iso-octane/toluene mixture (70:30, vol %) at 70 °C for 168 h [16]. To obtain the de-swollen state, the samples which were swollen in IRM 903 were placed in a vacuum oven at 50 °C for 4 h, and the samples which were swollen in the iso-octane/toluene mixture were placed in an air-circulating oven at 50 °C for 26 h. The drying time was determined by repeatedly measuring the weight of the specimens until the equilibrium state was reached. The other swollen specimens were rushed to sample preparation and testing. For each condition, five tensile test specimens were used to ensure reproducibility. Besides the mechanical performance, the swelling amount and density were measured in different swelling test setups. A balance and density kit (XS205DU, Mettler Toledo, Greifensee, Switzerland) measured the weight (in air to the nearest 1 mg) and the density (by the buoyancy method). The mean value and standard deviation of the results were calculated from these measurements and used for analysis.

The surface properties of HNBR in the un-swollen, swollen, and de-swollen states were investigated through tribological measurements. The swollen (in IRM 903 or in the iso-octane/toluene mixture) and de-swollen conditions were achieved with similar steps as explained above. The weight before swelling, after swelling, and after the tribological tests was measured to the nearest 1 mg.

The worn surface morphologies were analyzed by scanning electron microscopy (SEM) to obtain a better understanding of the friction and wear behavior and special damage mechanisms at every test stage. The specimen surfaces were analyzed with FTIR in ATR mode to identify the possible chemical and structural changes due to swelling-induced ageing.

In the following sections, the specimen dimensions and test parameters are summarized.

2.2.1. Tensile Tests

Smooth dumbbell specimens (S2) (DIN 53504) were punched out from plates (in un-swollen, swollen, and de-swollen conditions) just before the tensile tests. These specimens possess a thickness of ~2 mm and a width of 4 mm. All of the tests were performed with a Zwick universal testing machine (Zwick Roell, Test expert, Ulm, Germany) with a 1 kN load cell at a constant crosshead speed of 200 mm/min and a gauge length of 25 mm according to DIN 53504.

2.2.2. Tribological Tests

All tests were conducted in a rotational Tribometer TE93 (Phoenix Tribology Ltd., Newbury, UK) under a 50 N load at 118 rpm speed for 168 h. The specially designed disk specimen (with inner and outer diameters of 21 mm and 62 mm, respectively) contains a homogeneous lip geometry for the investigation of the friction behavior in line contact with the counter surface. The test parameters and the specimens were improved by previous research work [29]. The specimen's front view and a sketch of the cross-section and lip geometry are shown in Figure 1a,b, respectively. The specimen was mounted onto the rotational drive of the machine, whereas the counterpart was in the static state. The counterpart is a hollow cylindrical steel disk with 54 mm and 38 mm outer and inner diameters, respectively; the average surface roughness (R_a) was measured utilizing a non-contact Profilometer (Microprof, FRT GmbH, Bergisch Gladbach, Germany). The surfaces of the counterpart were polished using a grinding pass, giving them nearly identical surface roughness structures, $R_a \sim 0.03 \mu\text{m}$. Every test was conducted with similar amounts of Vitrea 68 (~80 mg) in liquid form as

the lubricant between the counterpart and the specimen. The tested samples were carefully washed with diluted iso-propanol before measuring the sample weight and before surface observations.

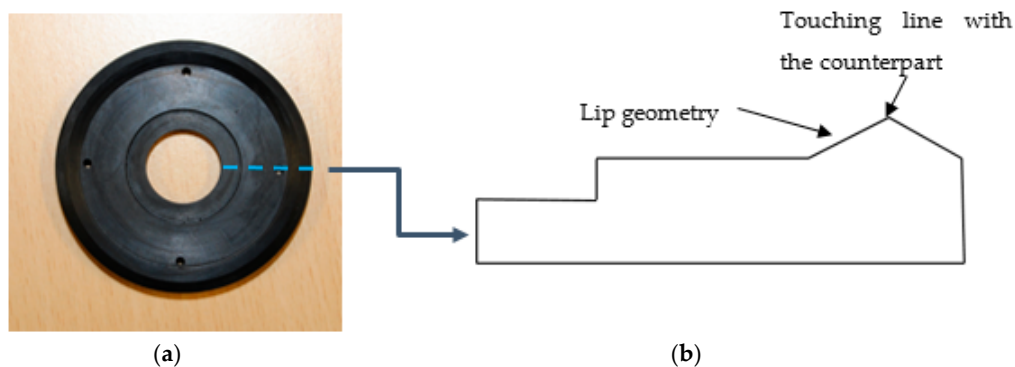


Figure 1. The tribology specimen: (a) the front view and (b) a sketch of the radial cross-section of the specimen.

2.2.3. Surface Observation

The surface topography of every fresh specimen was investigated to maintain the accuracy of the contact surfaces and lip geometry by optical microscope (Alicona Infinite Focus, Graz, Austria). The wear surfaces of the tribo-tested samples were inspected by utilizing SEM (Tescan VEGA-II, Brno, Czech Republic) and a light microscope.

2.2.4. Fourier Transmission Infra-Red (FTIR) Spectrometer Test

The surface layer of the lip geometry of tribo-tested samples was analyzed with FT-IR spectroscopy in ATR mode using a Spectrum GX 75611/2 (Perkin Elmer, Liantriasant, UK) in the spectra range of 600–4000 cm^{-1} .

3. Results and Discussion

In the following section, the swelling behavior, the bulk property changes of the swollen samples, and the swelling-induced ageing effects on tribological properties are compared. The possible microstructural changes and the chemistry involved in the interaction with the solvents, which affect the bulk properties, surface properties, and SEM-assisted surface analysis, are discussed as well.

The influences of the swelling-induced ageing on the tensile properties of HNBR are shown in Figures 2 and 3 for the samples immersed in iso-octane/toluene and IRM 903, respectively. The tensile strength (σ_R), the elongation at break (ϵ_R), and the stress at 50% strain ($\sigma_{50\%}$) are compared in Figure 2a. As depicted, the σ_R values are drastically decreased in the swollen state compared with the un-swollen, up to 60%; however, after de-swelling, the σ_R values are fully restored. A similar behavior was observed for ϵ_R , where the swollen values show a reduction from the un-swollen values (up to ~74%), and after de-swelling they are recovered or even higher compared with the un-swollen properties. Due to swelling, the $\sigma_{50\%}$ is also reduced by up to half of its un-swollen values, ending up in a fully recovered state after de-swelling or with even slightly higher values. The swelling amount (density and weight) changes, as well as the stress-strain behavior, are shown in Figure 2b,c, respectively, for the samples which were immersed in iso-octane/toluene. In the swollen state, the sample weight is increased by up to ~15%, and after de-swelling, a slight weight loss is recorded and the density is changed accordingly (the volume change in the swollen condition (~30%) is more significant compared to the change of the weight). By contrast, as Figure 3a summarizes, for samples immersed in IRM 903, the σ_R , ϵ_R , and $\sigma_{50\%}$ of the HNBR did not deteriorate much; they also did not deteriorate much in the de-swollen state. As shown in Figure 3b,c, swelling increases the weight slightly (~5.6%), and this effect mostly persists (~4.9%) in the material even after the evaporation and no significant density change

was recorded. As the other mechanical properties proved, the stress-strain behavior (Figure 3c) is not changed significantly in samples in contact with IRM 903. The equilibrium swelling was reached after 24 h of immersion time, and the volume increase was recorded as 27% and 9% in the iso-octane/toluene mixture and the IRM 903, respectively.

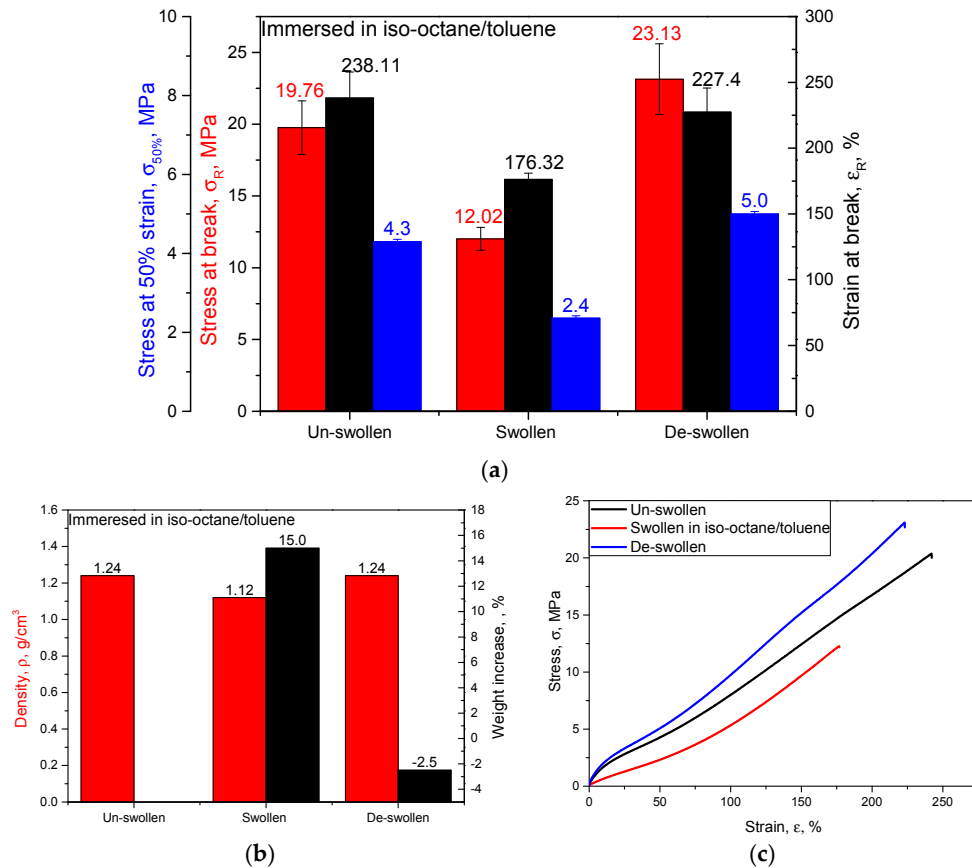


Figure 2. Influence of swelling of hydrogenated nitrile butadiene rubber (HNBR) in iso-octane/toluene at 70 °C for 168 h and after de-swelling compared with un-swollen samples: (a) strength at break, strain at break, and stress at 50% strain; (b) density and weight increase in percent; (c) stress-strain behavior.

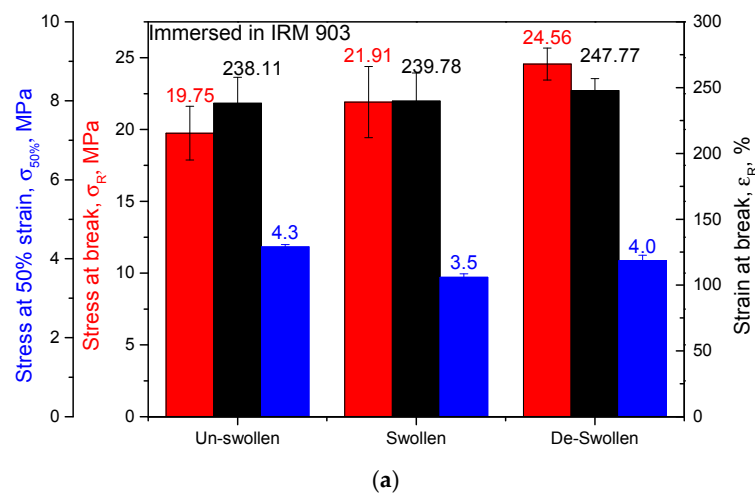


Figure 3. Cont.

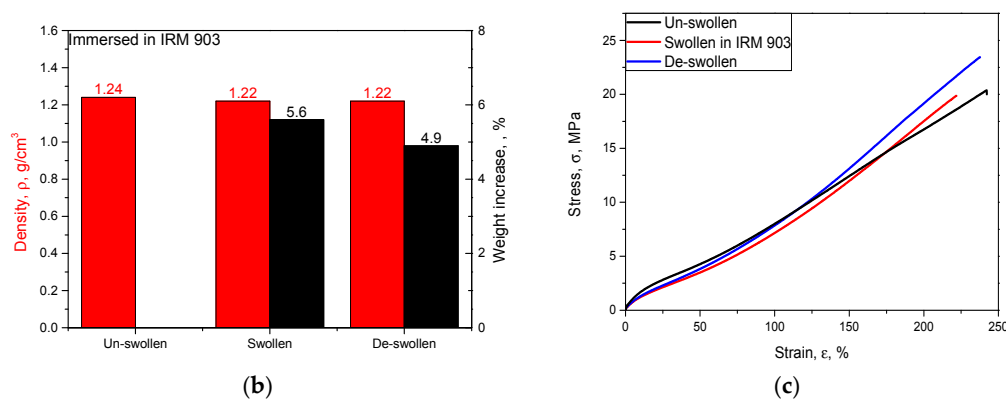


Figure 3. Influence of swelling of HNBR in IRM 903 at 100 °C for 168 h and after de-swelling compared with un-swollen samples: (a) strength at break, strain at break, and stress at 50% strain; (b) density and weight increase in percent; (c) stress-strain behavior.

Swelling is mainly responsible for the intra-molecular motions of segments and rearranging the long molecular chains, including the shifting of chain entanglements, elastomer-filler de-bonding, and even plasticizing [16,20,21]. Therefore, the observed results in the swollen states, the degraded strength at break, and the decreased stiffness could be attributed to released entanglements, the elastomer-filler de-bonding mechanism, and plasticizing. The elastomers possess free volume within the molecules, which gives molecules the freedom to rearrange during external loading. However, in the swollen state, the presence of solvents in the material stretches the molecules and that results in reduced strain at break or decreased ductility in the swollen state. Nevertheless, the physically impaired tensile properties are fully restored in the de-swollen states of those samples that were swollen in iso-octane/toluene due to re-arranging entanglements, possible elastomer-filler bonding, and regained free volume within the molecules in fully dried-out conditions. The HNBR seems more compatible to the contact with the iso-octane/toluene mixture compared with IRM 903, which are equivalent to gasoline or diesel fuels and petroleum, respectively. Solubility parameters (δ) for the toluene and iso-octane were identified in the literature as 8.97 and 6.9 (cal/cm^3)^{1/2}, respectively, and meanwhile, the IRM 903 and HNBR have δ as 16.9 (cal/cm^3)^{1/2} and 9.7 (cal/cm^3)^{1/2}, respectively [30]. Therefore, iso-octane and toluene as aromatic, low viscosity, volatile solvents, which possess closer solubility parameters to HNBR, exhibit a greater swelling effect in contact with the HNBR samples [31]. However, the HNBR swells only slightly in IRM 903 due to the low compatibility between the solubility parameters based on a polarity mismatch and higher viscosity. Greater swelling correlates with the degree of tensile properties' reduction in swollen conditions in these two solvents. Additionally, the butadiene part of HNBR and the higher viscosity of IRM 903 create difficulties in removing IRM 903 from the sample by conventional drying methods to obtain the de-swollen condition [1,31]. Therefore, IRM 903 would not be ideal for finding the de-swelling effect on mechanical properties, but it is suitable to analyze the effects of swelling.

A typical test result from the TE 93 test machine is shown in Figure 4, which displays the friction coefficient, the temperature on the specimen surface and on the counterpart, and wear in terms of dimensional change with test time. The results show that the COF and the specimen surface and counterpart temperatures are stabilized after a running-in time.

The surface properties of the tested HNBR specimens in different swollen conditions (un-swollen, swollen in IRM 903, swollen in IRM 903 and de-swollen, swollen in iso-octane/toluene and de-swollen) are summarized in Figure 5, comparing: (a) the wear (mass and dimensional) losses, (b) the friction coefficients (COFs), as well as (c) the specimen surface temperature. The tribological properties after swelling in the iso-octane/toluene mixture were not tested due to the highly volatile nature of that solvent, but the samples immersed in IRM 903 were tested in both swollen and de-swollen conditions.

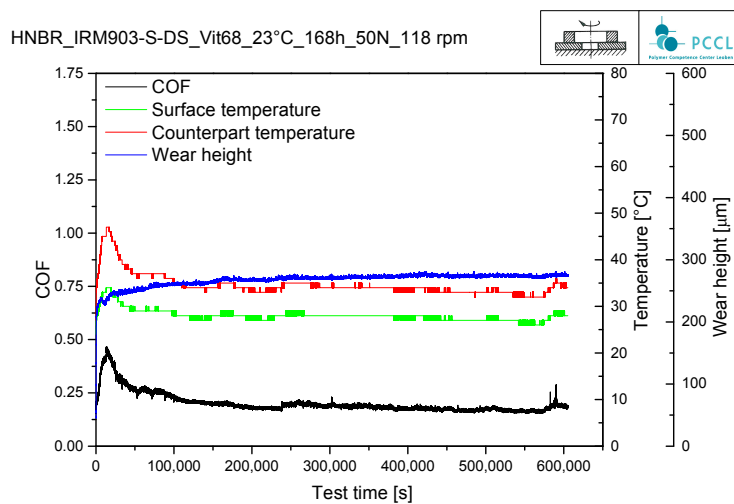


Figure 4. A typical surface analysis test result from TE 93: a result of sample swollen in IRM 903, which shows COF, specimen surface temperature, counterpart temperature and wear in terms of dimensional change with testing time.

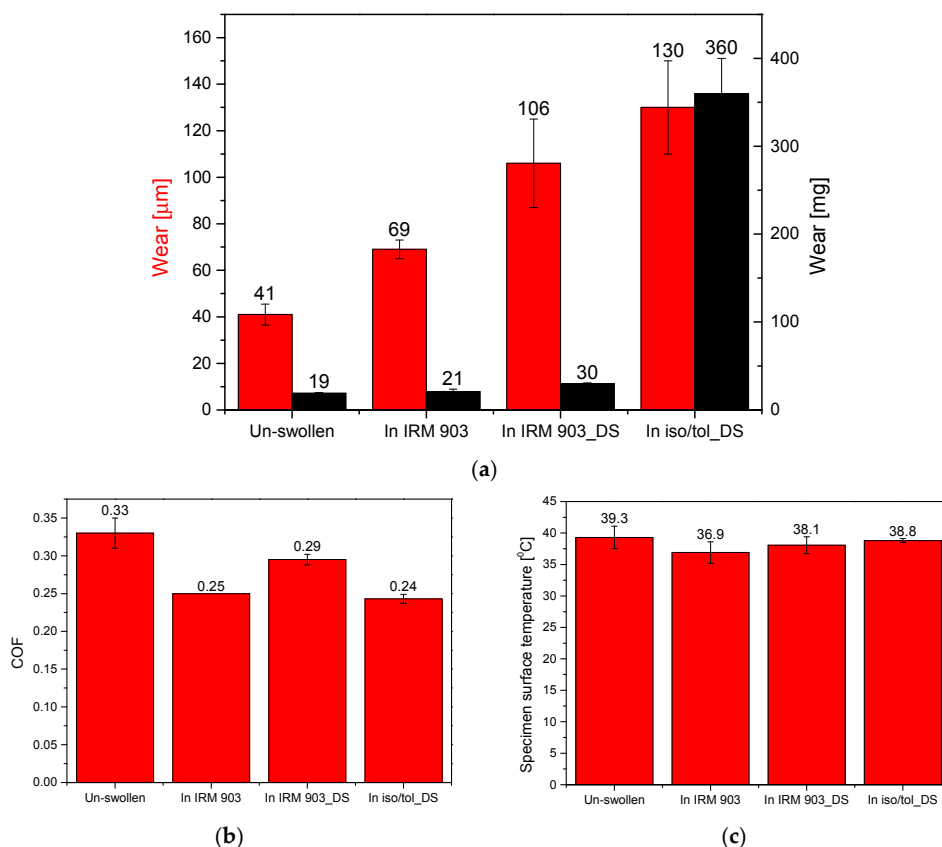


Figure 5. Tribological property changes of HNBR in different conditions; un-swollen, swollen in IRM 903 at 100 °C for 168 h and after de-swelling, swollen in iso-octane/toluene at 70 °C for 168 h and subsequently de-swollen: (a) Wear losses (weight and dimensional); (b) COF; and (c) specimen surface temperature.

As depicted in Figure 5, the un-swollen samples demonstrate the lowest wear losses in dimensions and weight, but the highest friction coefficient and the highest specimen surface temperature compared with the other tested conditions. The samples, which were swollen in IRM 903, show a relatively

higher wear, lower COF, and lower specimen surface temperature compared with the un-swollen condition; in the de-swollen state, the wear is even greater than that in the swollen state; however, the COF and the specimen surface temperatures are in between those of the swollen and un-swollen results. Nevertheless, the highest wear loss was recorded for the samples in de-swollen conditions after swelling in iso-octane/toluene, irrespective of the lowest COF. As shown in Figure 5a, the greatest magnitude of wear losses, in weight and dimensions, was recorded in the swollen and de-swollen conditions compared with the un-swollen state. For example, the weight losses of samples swollen in IRM 903 and those of the de-swollen samples that had previously been immersed in IRM 903 and in iso-octane/toluene are 1.1, 6, and 18 times greater, respectively, compared with the weight loss of the un-swollen sample. Evidently, the extent of material removal in the de-swollen samples immersed in iso-octane/toluene was remarkably higher as compared to the other conditions.

In between the samples and counterparts, a similar amount of Vitrea 68 was used for lubrication in every tribology test, maintaining the same condition for every test. This high viscosity-index mineral oil was specially chosen due to its ability to provide superior lubrication and its good compatibility with HNBR, where minimal swell, hardness, and change of oil viscosity over the temperature range are expected in service [32]. Therefore, a minimum effect from the lubricant on the chemical changes of the material and among different tests are expected. The specimens were gently cleaned with diluted iso-propanol after the tribology measurements, as it is widely used as a cleaning agent due to its ability to dissolve mineral oils and its highly volatile nature. Therefore, only the removal of the lubricant on the surface, and no effect on the final weight measurements, is expected. After washing, the specimens were dried again in an air-circulated oven at 50 °C until the weight was constant, implying that no residuals of oil or of the iso-propanol itself should be left on the sample surfaces. Thereafter, the weight measurements and surface analysis of the tested samples were conducted.

In order to understand the mechanisms of wear involved in testing different conditions, the specimen surfaces were examined by scanning electron microscope. The surface texture of the un-swollen samples before testing and after testing are compared in Figure 6a,b, respectively. The surface morphologies of the worn tracks of samples immersed in IRM 903, in IRM 903 then de-swollen, and in iso-octane/toluene then de-swollen are displayed in Figures 7–9, respectively. The surface texture of the un-swollen samples after the sliding test (Figure 6b) seems worn off (some small particles) compared with the sample before testing (Figure 6a); however, in general, it still looks smooth and dense.

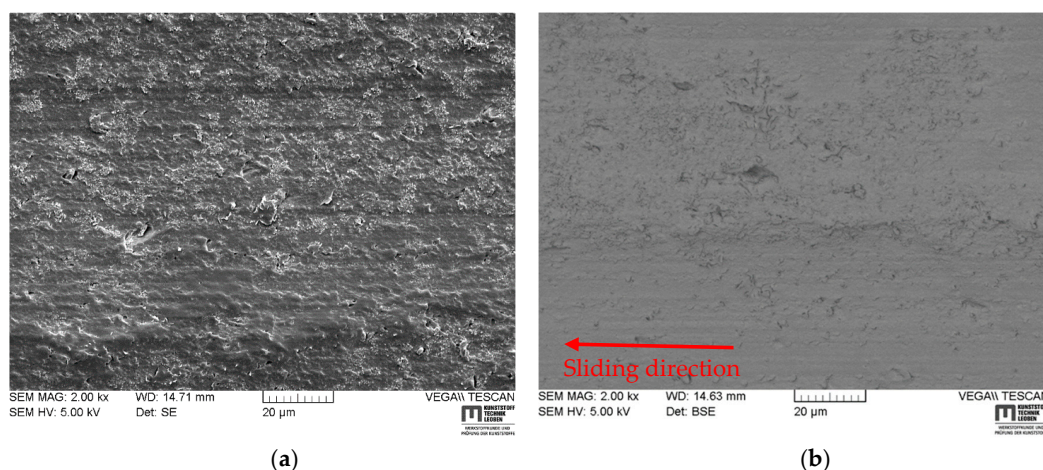


Figure 6. Typical SEM images of HNBR un-swollen samples: (a) before the tribo-test; (b) after the tribo-test.

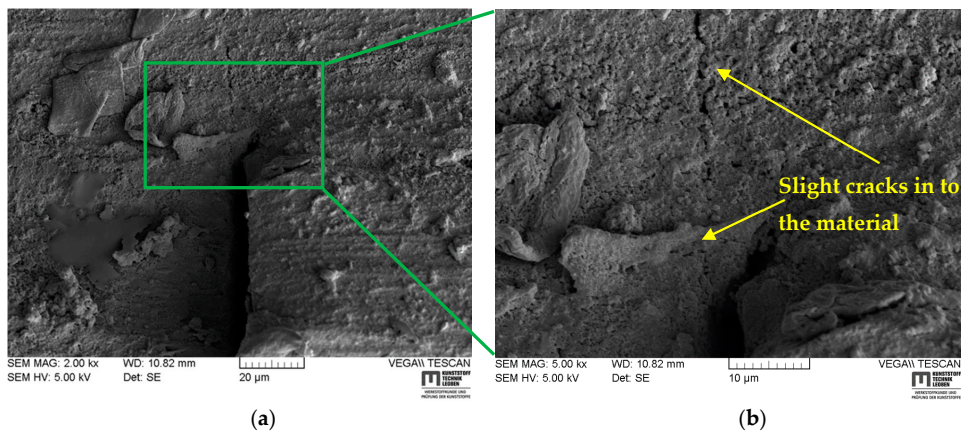


Figure 7. Typical SEM images after the tribo-tests of samples immersed in IRM 903: (a) tearing cracks perpendicular to the sliding direction and removal of small particles; (b) magnified area around the vicinity of a crack.

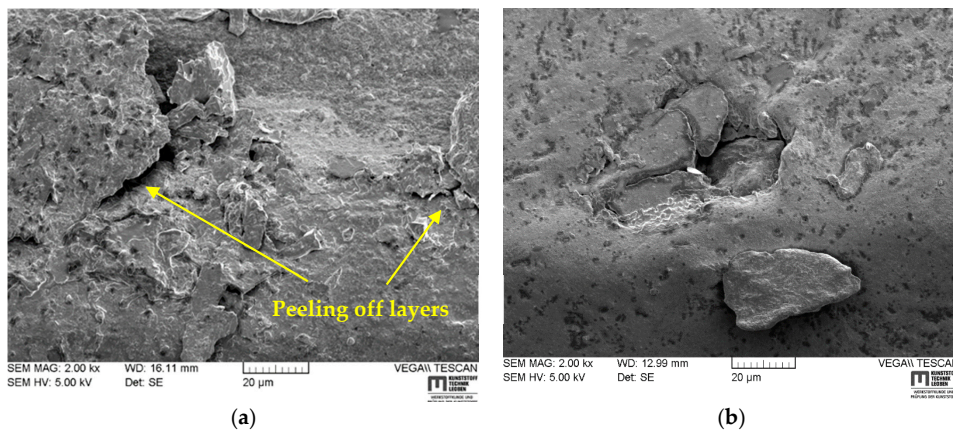


Figure 8. Typical SEM images after the tribo-tests of samples immersed in IRM 903 and de-swollen: (a) wear behavior in a manner of the peeling off of layers; (b) wear behavior in a manner of removing bigger particles from the surface.

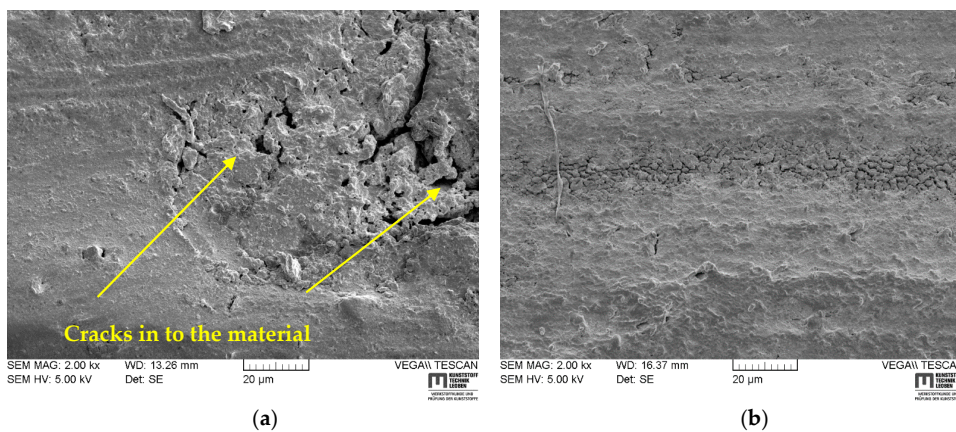


Figure 9. Typical SEM images after the tribo-tests of samples immersed in iso-octane/toluene and de-swollen: (a) a large wear surface with pitting morphology and cracks into the material; (b) deep worn tracks and cracks into the material.

The swollen samples in IRM 903 exhibit ruptures perpendicular to the sliding direction, including relatively larger debris, as shown in Figure 7a and in the magnified view (Figure 7b), where slight cracks around the rupture and uneven surface roughness can be seen. Lamellar structures, originating from the peeling of surface layers, were apparent on the worn surface of samples swollen in IRM 903 and subsequently de-swollen, as visible in Figure 8a. Additionally, some larger spallings were observed as shown in Figure 8b. Larger worn-off surfaces with pits and a greater density of defects penetrating into the material were evident in samples swollen in iso-octane/toluene and subsequently de-swollen (Figure 9a). Further, the surface contains worn-off tracks with a larger number of cracks as shown in Figure 9b.

With respect to the observed results, the surface properties and the surface analysis through the SEM images are in good agreement. The absorbed solvent could emerge to the surface with the applied force and act as an additional lubricant between the sample and the counterpart; this could explain the relatively lower COF measured with the IRM 903 swollen samples compared with the samples in an un-swollen condition. An additional test series where IRM 903 was used as a lubricant, instead of Vitrea 68, revealed a higher COF compared with Vitrea 68 used in the same amount as a lubricant. For example, the un-swollen HNBR with IRM 903 (naphthenic base oil) as lubricant showed a COF of 0.41 instead of a value of 0.33 with Vitrea 68 (paraffinic base oil). Mofidi et al. [2] observed a similar trend with their tests comparing the COF of NBR in the presence of different base fluids. IRM 903 has a middle range of viscosity compared with Vitrea 68, which has high viscosity (the kinematic viscosities of Vitrea 68 and IRM 903 are $68 \text{ mm}^2/\text{s}$ and $32 \text{ mm}^2/\text{s}$, respectively, at $40 \text{ }^\circ\text{C}$) [2,32,33]. However, Mofidi et al. [2] did not find any correlations between the viscosity of the lubricant and the COF. Therefore, IRM 903 is in fact a lubricant, though less effective than Vitrea 68, and its release from a swollen sample can contribute towards further reduction in friction compared to the un-swollen or de-swollen samples as witnessed in Figure 5b. However, the chemical reactions between those highly viscous, anti-oxidative paraffinic and naphthenic base oils [32,33] were not considered in this study, which was expecting a minimal effect. The increased wear in terms of weight and dimension loss in the swollen condition could be attributed to the decrease in the shearing strength of the rubber surface as a result of the weak properties of swollen rubbers [34]. The observed larger tearings/ruptures could also confirm this behavior (Figure 7). The swelling of rubber alters the molecular network with disentanglements, the de-bonding of physical bonds, and even a plasticizing effect [16,20,21]. Additionally, in swollen states, decreased density values were observed as a result of the liquid's penetration, including a slightly porous morphology on the surface, as shown in Figure 7b. These phenomena indicate the lower wear resistance and the relatively larger debris on the surface of samples in a swollen condition compared with those in an un-swollen condition. A lower specimen temperature is expected in swollen samples with respect to the lower COF, lower energy dissipation, and better thermal conductivity with some additional oil in the material [2,35]. Under the test conditions, the samples swollen in IRM 903 were not fully de-swollen; however, a surface dryness was expected. Therefore, the COF and the surface temperature of de-swollen samples could be anticipated to be intermediate between those of swollen and un-swollen samples. However, a higher wear loss was recorded compared with both samples in the swollen state and samples in the un-swollen state. This tendency was revealed in the SEM images with worn-off layers and relatively bigger worn-off particles as shown in Figure 8. In the swollen conditions, the specimen surface was offered some lubrication by absorbed solvent as a viscous protective film and this could alleviate the local concentrations of tearing force, which could presumably be responsible for the detachment of particles [7]. The samples in a de-swollen state after being swollen in iso-octane/toluene showed the highest wear; for instance, wear is ~18 times and 12 times greater compared with the un-swollen samples and the samples in de-swollen conditions after being swollen in IRM 903, respectively, while showing the lowest COF in the present test conditions. The SEM-assisted analysis also revealed deep and larger pits on the contact surface, with densified cracks into the material on worn-off surfaces (Figure 9). Iso-octane and toluene, being low molecular weight and highly volatile aromatic solvents, swell HNBR to a relatively higher degree (~30% in

volume and 15% in weight) compared to IRM 903, a highly viscous, non-volatile mineral oil (~9% in volume and 5.7% in weight), as shown in Figures 2 and 3. Therefore, the larger swelling seemingly adversely affected the wear resistance of the HNBR while lowering the COF.

Therefore, an additional FTIR-ATR analysis was conducted to gain knowledge about any chemical structural changes introduced to the materials' surfaces as a result of swelling-induced ageing which remained even after the de-swelling. Figure 10 illustrates the typical IR spectra of HNBR after the tribo-tests in different swelling-induced ageing conditions (de-swollen state after being swollen in IRM 903 and iso-octane/toluene) compared with the un-swollen state. As depicted, every condition shows HNBR signature peaks, i.e., the peaks in the range of 2800–3000 cm^{-1} corresponding to C–H stretching vibrations, the peak at 2238 cm^{-1} for –CN, and the peak at 1433 cm^{-1} for –CH₂ groups. Additionally, the peaks at 1733, 1169, and 1108 cm^{-1} were apparent in the un-swollen samples, which could be attributed to the C=O stretching vibration, the C–O–C stretching vibration, and the –CH₃ group, respectively. This could reveal the presence of additives in the used HNBR, i.e., stearic acids, acyl esters, aliphatic acids, rubber anti-oxidants (TMQ), and curing agents [36–39]. The peaks corresponding to additives were seemingly reduced to some extent in the de-swollen states compared with the un-swollen states. The peaks in the range of 2800–3000 cm^{-1} were also reduced, which could also be attributed to some level of paraffin (a typical processing agent used in rubber) [37,38] in the material and a reduction in de-swollen conditions. Therefore, it seems that the solvents extracted the soluble additives, which is a physiochemical process [38], from the material, and this could be also seen from the weight loss (Figure 2b) or hardened bulk properties in samples in a de-swollen condition (Figures 2c and 3c). However, additive extraction is seemingly adversely affecting the surface properties, because the additive breakdown from the material matrix creates a non-uniform density distribution and a porous nature on the surface [36]. The SEM-based surface observation proved a similar behavior (Figures 7–9). Therefore, higher swelling causes a higher surface degradation/softness and this condition persists even in de-swollen conditions. Similar behavior was observed in the literature for fluoro-elastomers with swelling-induced ageing [34].

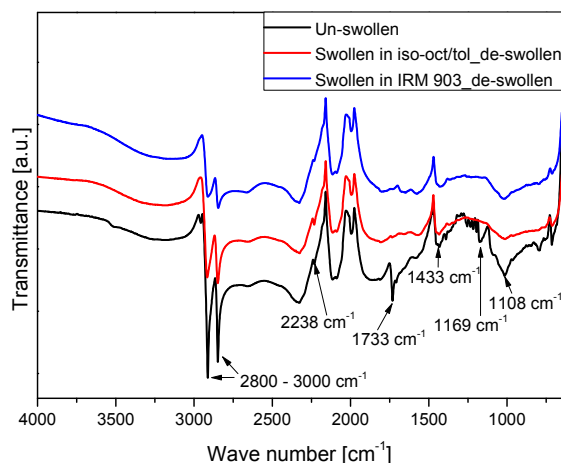


Figure 10. The FTIR spectra in ATR mode of the tribo-tested samples in different conditions.

The friction and wear properties of the HNBR that was used are rather complex, because the specimen in the test setup rotates continuously and stress and strain apply in the normal and the tangential directions on the counter surface. Owing to the curved and entangled nature of rubber molecules, they can withstand considerable lateral deformations without fracture by the stretching and twisting of chains [4,8]. Wear is generally based on tearing or smearing: small particle removal from the surface by frictional forces (smearing) and subsequent removal of larger particles by tearing. When the shear stress surpasses the cohesive strength of the polymer chains, a fracture initiates by the propagation of the crack along the root of the contact area [8,10]. If crack initiation is more

difficult to achieve, the whole wearing process is retarded. Thus, overall wear is dependent upon crack initiation [10].

Under the present test conditions, sliding occurred on a relatively smooth surface, so friction was expected through the stick-slip mechanism (adhesion). During adhesion, at the interface, the shear stress increases continuously with time and the crack grows when the local shear stress reaches the critical value [12]. The damage mechanisms of the un-swollen sample surface (Figure 6b) correlate with the smearing wear mechanisms, where small particles were worn off due to a relatively hard counterpart surface without any swelling-induced ageing. The swollen samples in IRM 903 showed a relatively aged surface with some tiny pores on the surface and some relatively larger worn off particles. Friction due to adhesion is retarded to some extent with IRM 903 on the surface in the swollen condition. In both de-swollen states, the samples show higher wear, forming lamellar spallings and a pit-like surface with particles rolling off. Therefore, this damage mechanism could be explained as shown in Figure 11.

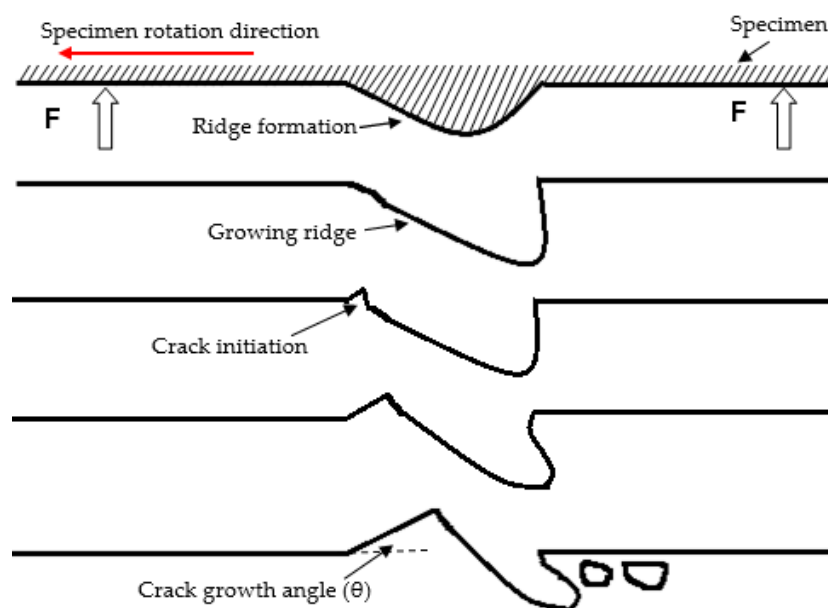


Figure 11. Schematic illustration of the possible mechanism of the wearing off of particles in rubber sliding against a solid counterpart. Stages of ridge formation and crack growth on the specimen's surface when stresses exceed the weakened polymer chain strength. Specimen rotation direction and force (F) direction on the surface from the counterpart are as illustrated.

When the stress is transferred to a softer surface, for instance, due to the swelling effect, the lower modulus of the material can increase the normal deformation, which could increase the contact area and the shear effect on the material, intensifying the wear degradation [4]. Additionally, as shown in Figure 11, the repeated deformation accumulates in the surface layers into a roll formation, i.e., ridges. The swelling of HNBR, especially in iso-octane/toluene, results in cracks and voids on the surface (Figure 9). As the FTIR spectra revealed (Figure 10), some additives are extracted from the surface, creating small voids in the elastomer and acting as a possible initiator of internal failure as a result of unbounded elastic expansion [9]. Based on the density of the surface defects, the thickness of ridges is attenuated or increased; severely impaired surfaces initiate the cracks at larger angles (θ) and drive the crack deeper into the material as illustrated in Figure 11. Additionally, Lv et al. [34] observed a reduction of cross-link density and an increase in the proportion of tail suspension chain (%) in their NBR material with the degree of swelling. The swelling-induced ageing lead to surface softness through voids and molecular structure destruction and it drives chain elongation and even

easy chain breakage [9]. Therefore, the worn surface further shows the formation of grooves and the removal of material as chunks (bigger particles).

4. Summary and Conclusions

In the present work, an HNBR model material was used to identify the tribological and mechanical behavior under certain swollen conditions. A greater degree of swelling of the HNBR in an iso-octane/toluene (70:30, vol %) mixture was experienced compared with a relatively lower effect in IRM 903. Weaker mechanical properties were observed in the presence of solvent in the material, and the degradation magnitude was correlated with the degree of swelling; in fully de-swollen states, the un-swollen properties were regained. In swollen states, the material surface properties were impaired with a lower friction coefficient and higher wear loss, and in de-swollen conditions, the wear loss magnitude was even greater. The presence of the solvent increased the wear loss, and the degree of swelling correlated with the surface property degradation, where higher mechanical property degradation was experienced with the degree of swelling. However, an even higher degree of wear was experienced in de-swollen conditions due to the permanently altered surface as a result of swelling, but the absence of solvent releasing from the material in the de-swollen condition could add further lubrication to the surface. In un-swollen conditions, wear through smearing was witnessed, but in swollen and de-swollen conditions, bigger particles were worn off through tearing. Surface defects due to swelling-induced ageing could more easily initiate cracks on the ridges, which accumulated as a result of constant sliding, and the degree of swelling could determine the intensity of the soft surface, which would help the crack to grow deeper in to the material. Under the tested conditions, in the de-swollen states, the bulk mechanical properties were almost recovered, in contrast to the surface properties, which were greatly impaired. The present study could be improved by adding deeper investigations of the effects of swelling-induced ageing from different solvents in different conditions and considering effects with lubricant at different temperatures. Furthermore, tribological properties with a simulation method for predicting the service life of lip seals will be implemented in a future work.

Acknowledgments: The research work was performed at the Polymer Competence Center Leoben GmbH (PCCL, Austria) within the framework of the COMET-program of the Federal Ministry for Transport, Innovation, and Technology and the Federal Ministry of Economy, Family, and Youth with contributions from the material science and testing of polymers of the Montanuniversität Leoben and SKF Sealing Solutions Austria GmbH. The PCCL is funded by the Austrian Government and the State Governments of Styria, Lower Austria, and Upper Austria.

Author Contributions: Andreas Hausberger developed the tribology test setup and the test procedure, including the specimen geometry; Winoj Balasooriya conducted the tests and Chao Wang helped implement the tribology test procedure; Winoj Balasooriya, Bernd Schrittester, Chao Wang, and Andreas Hausberger analyzed the data and discussed the results; Thomas Schwarz contributed the materials and specially designed specimens; Gerald Pinter consulted on the research work and held scientific discussions; Winoj Balasooriya conducted the literature research and wrote the paper.

Conflicts of Interest: The authors declare no conflicts of interest.

References

1. Hofmann, W. *Rubber Technology Handbook*, 2nd ed.; Hanser: Munich, Germany; Vienna, Austria; New York, NY, USA, 1989.
2. Mofidi, M.; Kassfeldt, E.; Prakash, B. Tribological behavior of an elastomer aged in different oil. *Tribol. Int.* **2008**, *41*, 860–866. [[CrossRef](#)]
3. Chandrasekaran, M.; Batchelor, A.W. In situ observation of sliding wear tests of butyl rubber in the presence of lubricants in an X-ray micro focus instrument. *Wear* **1997**, *211*, 35–43. [[CrossRef](#)]
4. Tayeb, N.S.M.E.; Nasir, R.M. Effect of soft carbon black on tribology of de-proteinised and polyisoprene rubbers. *Wear* **2007**, *262*, 350–361. [[CrossRef](#)]
5. Wang, L.L.; Zhang, L.Q.; Tian, M. Mechanical and tribological properties of acrylonitrile butadiene rubber filled with graphite and carbon black. *Mater. Des.* **2012**, *39*, 450–457. [[CrossRef](#)]

6. Gent, A.N.; Pulford, C.T.R. Mechanisms of rubber abrasion. *Appl. Polym. Sci.* **1983**, *28*, 943–960. [[CrossRef](#)]
7. Smith, G.C.; Park, D.; Titchener, K.J.; Davies, R.E.; West, R.H. Surface studies of oil-seal degradation. *Appl. Surf. Sci.* **1995**, *90*, 357–371. [[CrossRef](#)]
8. Myshkin, N.K.; Petrokovets, M.I.; Kovalev, A.V. Tribology of polymers: Adhesion, friction, wear, and mass-transfer. *Tribol. Int.* **2005**, *38*, 910–921. [[CrossRef](#)]
9. Guo, F.; Jia, X.; Lv, M.; Wang, L.; Salant, R.F.; Wang, Y. The effect of aging in oil on the performance of a radial lip seal. *Tribol. Int.* **2014**, *78*, 187–194. [[CrossRef](#)]
10. Pandey, K.N.; Setua, D.K.; Mathur, G.N. Material behavior Fracture topography of rubber surfaces: An SEM study. *Polym. Test.* **2003**, *22*, 353–359. [[CrossRef](#)]
11. Gent, A.N. A hypothetical mechanism for rubber abrasion. *Coll. Polym. Sci. Polym. Eng. Univ. Akron* **1988**, *62*, 750–756. [[CrossRef](#)]
12. Persson, B.N.J.; Volokitin, A.I. Rubber friction on smooth surfaces. *Eur. Phys. J.* **2006**, *21*, 69–80. [[CrossRef](#)] [[PubMed](#)]
13. Persson, B.N.J. On the theory of rubber friction. *Surf. Sci.* **1998**, *401*, 445–454. [[CrossRef](#)]
14. Muller, H.K. *Fluid Sealing Technology: Principles and Applications*; CRC Press: New York, NY, USA, 1998.
15. Champion, R.P.; Thomson, B.; Harris, J.A. *Elastomers for Fluid Containment in Offshore Oil and Gas Production: Guidelines and Review*; Health and Safety Executive: Liverpool, UK, 2005.
16. Balasooriya, W.; Schrittmesser, B.; Pinter, G.; Schwarz, T. Influence of HNBR ageing in oil field applications. *Rubber Fiber Plast. Int.* **2017**, *4*, 250–257.
17. Rinnbauer, M. *Technical Elastomers, the Basis of High-Tech Sealing and Vibration Control Technology Solutions*; SV Corporate Media GmbH: Munich, Germany, 2007.
18. Zhang, H.; Cloud, A. *Research Progress in Calenderable Fluoro-Silicone with Excellent Fuel Resistance*; Arlon Silicone Technologies Division: Bear, DE, USA, 2007.
19. Vidović, E. Development of lubricating oils and their influence on the seals. *Goriva I Maziva* **2014**, *53*, 220–235.
20. George, S.C.; Knörgenb, M.; Thomas, S. Effect of nature and extent of crosslinking on swelling and mechanical behavior of styrene-butadiene rubber membranes. *Membr. Sci.* **1999**, *163*, 1–17. [[CrossRef](#)]
21. Diani, J.; Fayolle, B.; Gilormini, P. A review on the Mullins effect. *Eur. Polym. J.* **2009**, *45*, 601–612. [[CrossRef](#)]
22. Mofidi, M.; Prakash, B. The influence of lubrication on two-body abrasive wear of sealing elastomers under reciprocating sliding conditions. *Elastom. Plast.* **2010**, *43*, 19–31. [[CrossRef](#)]
23. Roche, N.; Heuillet, P.; Janin, C.; Jacquot, P. Mechanical and tribological behavior of HNBR modified by ion implantation, influence of aging. *Surf. Coat. Technol.* **2008**, *209*, 58–63. [[CrossRef](#)]
24. Felhös, D.; Karger-Kocsis, J.; Xu, D. Tribological testing of peroxide cured HNBR with different MWCNT and silica contents under dry sliding and rolling conditions against steel. *Appl. Polym. Sci.* **2008**, *108*, 2840–2851. [[CrossRef](#)]
25. Karger-Kocsis, J.; Felhös, D.; Xu, D. Mechanical and tribological properties of rubber blends composed of HNBR and in situ produced polyurethane. *Wear* **2010**, *268*, 464–472. [[CrossRef](#)]
26. Xu, D.; Karger-Kocsis, J.; Schlarb, A.K. Friction and wear of HNBR with different fillers under dry rolling and sliding conditions. *Express Polym. Lett.* **2009**, *3*, 126–136. [[CrossRef](#)]
27. Yuqin, T.; Wang, X.; Chi, Y.; Liu, H.; Zhou, T. Research on the impact and friction and wear properties of acrylonitrile butadiene rubber composites filled with SiC and graphite. *J. Thermoplast. Compos. Mater.* **2014**, *27*, 1013–1021.
28. Trakarnpruk, W.; Porntangjitlikit, S. Palm oil biodiesel synthesized with potassium loaded calcined hydrotalcite and effect of biodiesel blend on elastomer properties. *Renew. Energy* **2008**, *33*, 1558–1563. [[CrossRef](#)]
29. Hausberger, A.; Godor, V.; Grün, F.; Pinter, G.; Schwarz, T. Development of Ring on Disc tests for elastomeric sealing materials. In Proceedings of the International Tribology Conference, Tokyo, Japan, 16–20 September 2015.
30. Stevenson, A.; Shepherd, R. An overview of the requirements for seal life prediction Part 1—Static seals. *Seal. Technol.* **1995**, *13*, 9–12. [[CrossRef](#)]
31. *ASTM Standard D-471-06*; ASTM International: Conshohocken, PA, USA, 1998.
32. Shell Vitrea Oils, Premium Quality Industrial Oils. Available online: <http://www.dayanoilco.com/upload/product/1451803762.pdf> (accessed on 10 July 2017).
33. Base Oil Handbook, NYNAS. Available online: http://www.engnetglobal.com/documents/pdfcatalog/NYN001_200412073535_Base%20oil%20handbookENG.pdf (accessed on 3 August 2017).

34. Lv, X.R.; Wang, H.M.; Wang, S.J. Effect of swelling nitrile rubber in cyclohexane on its ageing, friction and wear characteristics. *Wear* **2015**, *328–329*, 414–421. [[CrossRef](#)]
35. Simmons, G.F.; Mofidi, M.; Prakash, B. Friction evaluation of elastomers in lubricated contact. *Lubr. Sci.* **2009**, *21*, 427–440. [[CrossRef](#)]
36. Lou, W.; Zhang, W.; Liu, X.; Dai, W.; Xu, D. Degradation of hydrogenated nitrile rubber (HNBR) O-rings exposed to simulated servo system conditions. *Polym. Degrad. Stab.* **2017**, *144*, 464–472. [[CrossRef](#)]
37. Yang, R.; Zhao, J.; Liu, Y. Oxidative degradation products analysis of polymer materials by pyrolysis gas chromatography mass spectrometry. *Polym. Degrad. Stab.* **2013**, *98*, 2466–2472. [[CrossRef](#)]
38. Zhao, J.; Yang, R.; Iervolino, R.; Barbera, S. Changes of chemical structure and mechanical property levels during thermo-oxidative aging of NBR. *Rubber Chem. Technol.* **2013**, *86*, 591–603. [[CrossRef](#)]
39. Sanches, N.B.; Cassu, S.N.; Dutra, R.C.L. TG/FT-IR characterization of additives typically employed in EPDM formulations. *Polímeros* **2015**, *25*, 247–255. [[CrossRef](#)]



© 2018 by the authors. Licensee MDPI, Basel, Switzerland. This article is an open access article distributed under the terms and conditions of the Creative Commons Attribution (CC BY) license (<http://creativecommons.org/licenses/by/4.0/>).

Paper 4: The effect of the surface area of carbon black grades on HNBR in harsh environments

Winoj Balasooriya¹, Bernd Schritteser¹, Gerald Pinter², Thomas Schwarz³, and Lucia Conzatti⁴

¹ Polymer Competence Center Leoben GmbH, Roseggerstrasse 12, 8700 Leoben, Austria.

² Department of Polymer Engineering and Science, Montanuniversitaet Leoben, Otto Glöckeltrasse 2, 8700 Leoben, Austria.

³ SKF Sealing Solutions Austria GmbH, Gabelhoferstraße 25, 8750, Judenburg, Austria.



⁴ National Research Council, ISMAC Genova, Via De Marini 6, 16149 Genova, Italy.

Published in *Polymers*, 2019, 11, 61.

DOI: 10.3390/polym1101006

Article

The Effect of the Surface Area of Carbon Black Grades on HNBR in Harsh Environments

Winoj Balasooriya ^{1,*}, Bernd Schrittester ¹ , Gerald Pinter ², Thomas Schwarz ³ and Lucia Conzatti ⁴ 

¹ Polymer Competence Center Leoben GmbH, Roseggerstrasse 12, 8700 Leoben, Austria; Bernd.Schrittester@pccl.at

² Department of Polymer Engineering and Science, Montanuniversitaet Leoben, Otto Glöckeltrasse 2, 8700 Leoben, Austria; Gerald.Pinter@unileoben.ac.at

³ SKF Sealing Solutions Austria GmbH, Gabelhoferstrasse 25, 8750 Judenburg, Austria; Thomas.Schwarz@skf.com

⁴ National Research Council, ISMAC Genova, Via De Marini 6, 16149 Genova, Italy; Lucia.Conzatti@ge.ismac.cnr.it

* Correspondence: Winoj.Balasooriya@pccl.at; Tel.: +43-3842-429-6232

Received: 5 December 2018; Accepted: 28 December 2018; Published: 4 January 2019



Abstract: Concerning the still rising demand for oil and gas products, the development of new reliable materials to guarantee the facility safety at extreme operating conditions is an utmost necessity. The present study mainly deals with the influence of different carbon black (CB) filled hydrogenated nitrile butadiene rubber (HNBR), which is a material usually used in sealing applications, on the rapid gas decompression (RGD) resistance in harsh environments. Therefore, RGD component level tests were conducted in an autoclave. The supporting mechanical and dynamic mechanical property analysis, the microscopic level investigations on the material and failure analysis were conducted and are discussed in this work. Under the tested conditions, the samples filled with smaller CB primary particles showed a slightly lower volume increase during the compression and decompression phases; however, they steered to a significantly lower resistance to RGD. Transmission electron micrographs revealed that the samples filled with smaller CB particles formed larger structures as well as densified filler networks including larger agglomerates and as a consequence a decrease effective matrix component around the CB particles. Apparently, at higher loading conditions, which already deliver a certain level of mechanical stresses and strains, the densified filler network, and especially a lower amount of effective matrix material composition, adversely affect the RGD resistance. SEM-based fracture analysis did not identify any influence of the CB grades tested on the crack initiation site; however, it revealed that the cracks initiated from existing voids, hard particles, or low strength matrix sites and propagated to the outer surface.

Keywords: oil and gas; elastomers; HNBR; carbon black; rapid gas decompression

1. Introduction

The durability and the performance of elastomers are greatly affected by the working environment. Especially in harsh conditions, for example, elastomeric materials are exposed to high pressure, high temperature, and different media, and as a result, their properties deteriorate significantly and even component failure occurs [1]. Therefore improving the material properties to face the challenges in use are of utmost interest among materials scientists. The specific catastrophic failure phenomenon, the rapid gas decompression (RGD), which occurs in almost every fluid-handling elastomeric component as a result of sudden pressure release, is well-known, but is still under

discussion even after decades [2–9]. This failure leads to high volume increase, crack initiation, crack growth, and the complete destruction of the component. The whole process can be divided into the pressurization and the depressurization phases. The first occurs due to the penetration of different media (mainly in gas conditions) at high-pressure and high-temperature atmospheres; it leads to a volume increase, strongly depending on the temperature, the pressure, and the media used [6,9,10]. The latter is a highly complex phase, where a high volume change of the component due to the pressure reduction occurs at ambient conditions. A stress-state change is expected in nominal stresses from compression to tension during the decompression cycle. The high volume change of gas leads to a three-dimensional pneumatic tension state in the material and it creates an additional and complementary assumed uniform body stress in the sample [2,6,11]. The compressed gas nucleates at voids or loosely bonded filler/rigid inclusion surfaces during rapid gas decompression; the voids inflate resulting in tensile stresses or strains in the void walls. This can lead to surface blisters or cleavage cracks, according to the permeability of gases into the material and induced stress levels [2,12].

Furthermore, during the compression phase, with high-pressure gas exposure, mainly two effects can be expected: (i) the plasticization of the polymer matrix leading to increased free volume and subsequent backbone movement and (ii) the compression of the polymer matrix. The first occurs mainly with highly soluble gases with a high boiling point (e.g., CO₂) and the second mainly with gases with lower boiling points (e.g., N₂). The nature of the gas and the applied pressure define the dominance of these opposite effects in the material and lead to a change of the mechanical and thermal properties [4]. Therefore, the permeation and solubility of gas strongly influences the material behavior. Additionally, the interacting media has a significant effect as well. Many previous research efforts could be found in the literature dealing with the media and permeation processes [8,13,14]. Especially, carbon dioxide (CO₂) can become a supercritical fluid and therefore a good solvent at relatively moderate pressure and temperature [15]. This concerns the elastomeric components in use when CO₂ is present. Especially in the oil and gas fields, the existence of a moderate amount of CO₂ in the reservoir can induce a failure in elastomeric seals that otherwise perform well in high-pressure gases [15]. This is because carbon dioxide has a small, permanent dipole with uneven charge distributions and it is capable of multiple types of associations, especially with polar elastomers. For example, in CO₂, the swelling is higher for fluoroelastomer (FKM) and hydrogenated nitrile butadiene rubber (HNBR) compared with ethylene propylene diene monomer (EPDM) [4,10,16].

The RGD phenomenon of elastomers is common in harsh environments and this rather complex process is seemingly a combination of many factors. Several authors have made efforts to identify the RGD behavior in different aspects dealing with the influence of testing parameters, fracture mechanical approaches and simulation models [2–11]. However, it is still of prime interest to identify the influence of the material composition, especially of the reinforcing fillers. Carbon black (CB) is an essential ingredient of most rubber formulations and has a considerable influence on the performance of the final product. This is especially true for RGD behavior, including the high probability of crack initiation in rubber matrix–filler interface, and considering the space between particles where the matrix is highly constrained [3]. Hence, it is vital to understand how the RGD and the related performance of the materials are affected by the nature of the CB grades used. Therefore, the aim of this research work is to consider mainly the RGD performance of HNBR filled with different CB grades in contact with CO₂ in conditions near the service level and to delve more deeply into the reinforcement mechanism of the CB filler system.

The use of CB in elastomers is common to achieve a reasonable range of mechanical properties required for a great variety of modern applications. It increases stiffness, modulus, rupture energy, tear strength, tensile strength, cracking resistance, fatigue resistance and abrasion resistance [17–19]. At the beginning of the 19th century, CB was accidentally identified as a substance to eliminate the inherent stickiness of rubber after zinc oxide had long been used [20]. CB as a reinforcing filler also reduces the cost of the end product and modifies the electrical and optical properties of the polymer matrix and is one of the most stable chemicals [17,19,20].

Considering CB as a reinforcing media, it relies on several factors, i.e., the primary particle size (specific surface area), the structure (the degree of irregularity of the filler unit) and the surface activity [18–20]. These factors evolve from the source or processing characteristics, and they are named accordingly; for example, furnace black, lampblack, thermal black, acetylene black, and channel black [20,21]. ASTM nomenclature uses the letter “N” to indicate a normal curing rate of typical furnace black which has had no special modification to alter the influence of the curing rate of rubber, followed by three numbers indicating the reinforcing character [20,22]. The first number refers to the average typical size of the elementary particle size. Therefore, a lower number refers to a lower particle diameter and higher surface area, for example N550 has a higher primary particle size and a lower surface area compared with N330 or N110 [21]. The last two digits of the number refer the structure of the aggregate and its reinforcing character, for example, N340 is a better reinforcing grade compared with N327 while in the same primary particle size diameter range [21,22]. The primary particles do not exist as separate particles, but they are fused together to form aggregates and this three-dimensional arrangement designates the “structure” of the CB grade [20–22]. A high degree of branching or clustering of the aggregates characterizes a “high structure”, and vice versa [20,23]. Additionally, the branched aggregates create porous structures and a higher surface area compared with the compact dense spherical particle structures. This creates additional filler surfaces available to interact with rubber and results in better reinforcing capabilities [21,23,24].

With regards to the particle size, particles up to 100 nm diameter are responsible for the reinforcement, irrespective of the particle structure [22]. However, particles larger than 10^3 nm are hardly responsible for reinforcing effects but used to increase viscosity by a hydrodynamic effect [23]. A smaller particle size, which gives higher surface area, manages to create a higher degree of cross-links with the elastomer and has a positive effect on the tensile strength, elastic modulus, the hardness of the elastomers as well as the compression set [19,23,24]. Mainly the filler–rubber cross-links are of a physical nature (physisorption), but the surface chemistry of CB has an effect on the vulcanization behavior of filled compounds [18]. Therefore, it is generally accepted that the surface area has a significant effect on increasing vulcanization reactions and mechanical properties [17,19].

The anisometric nature of the aggregate has a progressive influence on creating the entanglements of rubber molecules with the CB and their attachment (mechanical interlocking) [19]. Furthermore, the primary particle size correlates to the structure, for example, smaller primary particle size CB grades tend to create higher structural CB aggregates and vice versa [23]. A low structure may contain less than 20 primary particles per aggregate; a high structure may consist of up to 200 particles [21]. The aggregate is the smallest form of a given CB grade because they flocculate together to form weak, giant secondary aggregates called agglomerates [22,23]. There are two models to explain these loosely bound filler networks: (i) the filler–filler physical van der Waals interactions [18] and (ii) the attachment through a polymer layer, which is in nanometer-scale, in between two attractive filler surfaces [25]. In the latter, the polymer chains, which are in confinement, are strongly immobilized and these bonds create glassy-like bridges between the filler aggregates and transmit the stresses along the filler network [26].

When an uncured elastomer is blended well with a CB grade for a period, the elastomer chains are bound to the carbon black aggregates through different mechanisms, i.e., chemical/physical bonds, immobilized chains creating glassy-like bridges in-between fillers or the mechanical inter-locking of elastomer chains around/through the filler surfaces. This creates highly immobilized and localized rubber chains forming a rubber shell surrounding the CB aggregates [19]. This highly restricted rubber layer is no longer a part of the elastically active rubber matrix, but a part of the filler network and it increases the effective filler volume [19,24].

In Figure 1, certain models explaining the filler–rubber interaction are summarized. Figure 1a shows the stronger bonding of rubber around the filler aggregates to form a rubber shell on the surface, the so-called “bound rubber”, with increasing stiffness when it is closer to the CB and vice versa. When irregular filler structures exist, the rubber occludes between the inner voids of irregular contours and

forms an outer layer called “occluded rubber” as shown in Figure 1b. It is not strongly bound like the rubber shell, but experiences reduced mobility. As shown in Figure 1c, this bound rubber is strongly attached to the CB closer to the surface; away from the surface, the mobility of rubber is increased. Figure 1d shows a possible cluster mode of fillers, creating filler agglomerates, which trap some rubber excluding from the rest of the matrix. This is called “trapped rubber” and it becomes ‘free’ once the aggregate structure breaks apart during the deformation [17,24]. The bound rubber and the occluded rubber content depend on several factors, i.e., CB loading, CB surface area, structure, temperature, and the dwell time of CB in the rubber before curing [24]. A model to explain the filler–filler bonds to create filler agglomerates is illustrated in Figure 1e, where some rubber molecules remained in-between filler particles and these behave like glassy-like polymer bridges.

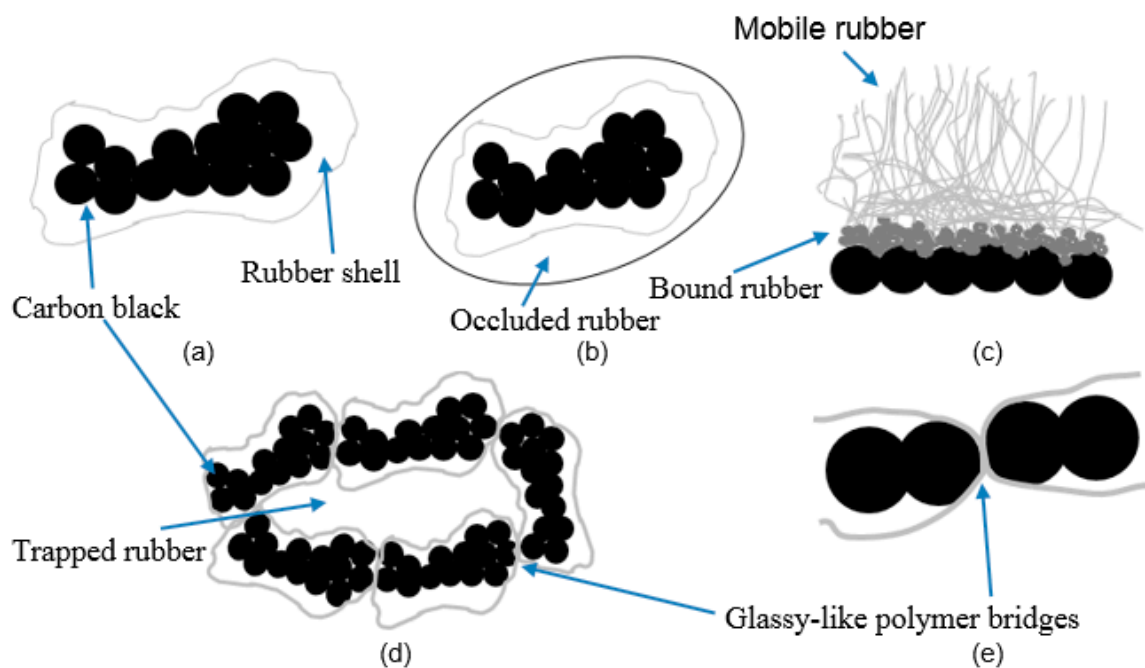


Figure 1. Models of filler–rubber interaction mechanisms and behavior of rubber: (a) strongly bound rubber around the carbon black; (b) occluded rubber around the rubber shell; (c) bound rubber near the carbon black (CB), transition layer, and then the mobile rubber far from the CB surface; (d) CB agglomerate and trapped rubber in between the aggregates; (e) filler aggregates are bound through glassy-like polymer bridges [18,19,24].

The filler aggregates and agglomerates in CB grades are responsible for the unique characteristics of filled elastomers. However, when CB is mixed with a rubber in a mill, the encountered shear forces could damage the aggregates and agglomerates reducing their sizes and structures [26]. In addition, many researchers assumed the well-known elastomeric phenomenon, Mullin’s effect and Payne’s effect, a result of the breakdown and re-aggregation of softer filler agglomerations [17,27,28]. According to these models, the tension and relaxation in a cyclic loading condition lead the dynamic breakdown and the re-aggregation of filler–filler bonds, especially the glassy-like polymer bridges between filler aggregates. The damage to the bonds is structurally reversible, but the re-aggregation of filler particles takes place resulting in hysteretic effects because the re-aggregated polymer bridges do not recover to the same strength as unbroken bridges, leading to a softening of the filler–filler bonds [25]. Furthermore, some researchers discussed the effects of CB in rubber materials; for example, Zhang et al. [29] investigated the effect of the particle size distribution of CB on the mechanical properties, and did microanalysis of the fractured sample of vulcanized NR with high abrasion furnace (HAF). They observed a better particle distribution with increasing emulsifiers in the material and enhanced

mechanical properties with higher filler dispersion in the rubber matrix due to the better interaction of carbon black and rubber matrix [29].

2. Materials and Methods

The influence of CB grades in HNBR on the RGD resistance was tested at component level. The macroscopic and microscopic aspects of the material behavior were observed. The material compositions, the testing methods, and the specific settings are described below in the following section.

2.1. Materials

An HNBR (ACN 36%) grade, peroxide cross-linked, stabilized with anti-oxidants, was selected for the investigations. The manufactured compound was provided as disc plates and cylinders for investigations. In this study, different CB grades, which contained large, middle and small primary particle size CB in different compositions to form 85 phr filled HNBR, as shown in Table 1. The large, middle and small size of CB represent the CB with roughly 50, 100 and 150 mg/g of iodine adsorption number, respectively. The names of exact CB grades are not mentioned here due to confidentiality constraints. The different grades have the similar recipe except the mentioned CB grade difference and they were added to the matrix in an internal mixer. The similar amount of loading of different CBs was selected to ensure a range of particle sizes, surface areas, and structure.

Table 1. The model hydrogenated nitrile butadiene rubber (HNBR) grades and their CB contents.

Grade	Content 1	Content 2
HNBR1	large size (10 phr)	middle size (75 phr)
HNBR2	large size (75 phr)	middle size (10 phr)
HNBR3	large size (40 phr)	middle size (45 phr)
HNBR4	large size (10 phr)	small size (75 phr)

The specimen dimensions and test parameters are summarized below.

2.2. Rapid Gas Decompression Test

The component level-RGD tests, which indicate the bulk deformation behavior of HNBR under highly confined conditions, and study crack initiation and crack growth under high deformation rates, were carried out with a high-pressure autoclave test system (SITEC, Sieber Engineering AG, Zürich, Switzerland). The cylindrical specimens were prepared by machining to obtain the shape of the cross-section of an O-ring, maintaining 8 mm in both diameter and height. The specimens were placed inside the autoclave in a freestanding position (unconstrained). The system was pressurized up to 150 bar with pure CO₂ at 90 °C. After ~22 h, it was depressurized to study the decompression failure with a rate of 100 bar/min. This high decompression rate, compared with the proposed rate in the standard [30], achieves a condition near service level for the elastomeric materials. The sensors continuously measured the pressure and the temperature inside the autoclave. A camera, which was situated outside the autoclave, monitored the in-situ volume expansion of the test specimens through the glass window, and later the volume change was calculated with the assistance of Tracker software (Tracker 4.95, Douglas Brown physlets.org/tracker). This experimental set-up is further explained in the previous research work [6,9,31]. The failure analysis of the tested samples was conducted utilizing a light microscope and scanning electron microscope. Every tested cylindrical specimen was examined at three radial cut sections by light microscope for internal cracks and every material grade test was repeated with three specimens; the crack size and the number of cracks rated the material according to the NORSOK ranking (Table 2).

Table 2. The seal-failure rating criteria according to NORSOK testing standard [30].

Description	Rating
No internal cracks, holes, or blisters of any size.	0
Less than 4 internal cracks, each shorter than 50% of the cross-section, with a total crack length less than the cross-section	1
Less than 6 internal cracks, each shorter than 50% of the cross-section, with a total crack length of fewer than 2.5 times the cross-section.	2
Less than 9 internal cracks of which max. 2 cracks can have a length between 50% and 80% of the cross-section.	3
More than 8 internal cracks, or one or more cracks longer than 80% of the cross-section.	4
Crack(s) going through the entire cross-section or complete separation of the seal into fragments.	5

2.3. Tensile Test

The tension tests on dumbbell-shape specimens (S2) were carried out according to the DIN 53504 standard. The specimens were punched out from the ~2 mm thick plates maintaining a width of 4 mm between the shoulders. All tests were performed with a Zwick universal testing machine (Zwick Roell, Test expert, Ulm, Germany) using a 1 kN load cell, at a constant crosshead speed of 200 mm/min with an initial gauge length of 43 mm. Five specimens of each grade were investigated to ensure the reproducibility.

2.4. Dynamic Mechanical Analysis

The microstructures of differently filled HNBR were investigated using DMA measurements and the experiments were conducted with a DMA 861/40N testing device (Mettler Toledo GmbH, Schwerzenbach, Switzerland). All tests were carried out within the temperature range of -50 °C to 100 °C using liquid nitrogen as a cooling agent with a frequency of 2 Hz and a heating rate of 2 K/min. The parallel parts between the shoulders of the dumbbell specimens (thickness of 2 mm and width of 4 mm) were used as the specimens in tension mode with a clamping distance of 19.5 mm.

2.5. Scanning Electron Microscope (SEM) Analysis

The fracture surfaces of RGD tested samples were observed utilizing an SEM (Tescan VEGA-II, Brno, Czech Republic). The broad and magnified views of surfaces helped to identify the crack initiation and propagation in different material grades and different fracture behaviors based on different CB compositions.

2.6. Transmission Electron Microscope (TEM) Analysis

The TEM micrographs analysis was performed for all four material grades utilizing a Zeiss EM 900 microscope (Carl Zeiss AG, Oberkochen, Germany) with an accelerating voltage of 80 kV. Ultrathin sections (~50 nm thick) were prepared by using a Leica EM FCS cryo-ultramicrotome at -100 °C.

3. Results and Discussion

In the following section, the influence on the RGD behavior of HNBR samples filled with different CB grade compositions is compared. It is vital to understand this complex phenomenon by the influence on macroscopic properties and the micro/nano level observations from different CB grades. Therefore, the CB primary particle/aggregate sizes and their distribution are investigated with TEM micrographs. The monotonic loading tensile properties and dynamic mechanical properties are characterized identifying the macroscopic behavior. The possible microstructural morphologies involved with the RGD damage mechanisms based on the SEM images are discussed as well.

3.1. Morphological Investigations of CB Filled Samples by TEM

Composite structures were observed by TEM micrographs at different magnifications analyzing the CB filler distribution, structure, and network behavior. The representative micrographs for the different material grades are shown in Figure 2, where, a, b, c, and d represent HNBR1, HNBR2, HNBR3, and HNBR4, respectively, with the same magnification. It should be mentioned that at low magnifications, all grades showed relatively homogenous distribution within the elastomer matrix and seemingly, the processing method did not influence the distribution of different CB grades in the conditions tested. Therefore, only the higher magnification micrographs are shown here for comparison purposes. The dark objects represent the CB and the light color areas represent the HNBR matrix material. Pseudo-spherical shaped primary particles could be identified in every sample, while several aggregations of filler particles are formed in the rubber structure, as those sizes are somewhat larger than the primary particle sizes.

As shown in Figure 2a, HNBR1 shows an even distribution of CB aggregates and a well-connected network throughout the matrix. The diameter of the majority of primary particles is in the range of ~30 nm and they are clearly packed creating irregular-shape structures which are connected each other. In Figure 2b, HNBR2 shows a rather disconnected network and more matrix material around and between CB aggregates. In fact, most primary particles in HNBR2 are bigger (~50 nm) than in HNBR1. Therefore, HNBR2 contains rather isometric CB structures, which are a few bigger particles formed together with less random branching, compared with HNBR1. In Figure 2c, small and big primary particles are clearly visible roughly in similar amounts. Further, the CB particle network density is higher compared with the HNBR2, however lower compared with the HNBR1. The number of particles in the structure and the branched nature as well as the matrix material around the aggregates is in moderate range compared with HNBR1 and HNBR2. With reference to the HNBR4 as shown in Figure 2d, the CB primary particles are relatively smaller (~15 nm), the aggregates are bigger and the network is much denser compared with the other tested grades. The aggregates have apparently formed larger agglomerates, which are indicated as dark clouds in three-dimensional form. Therefore, higher filler–filler interactions and relatively less matrix material around the filler particles are observed.

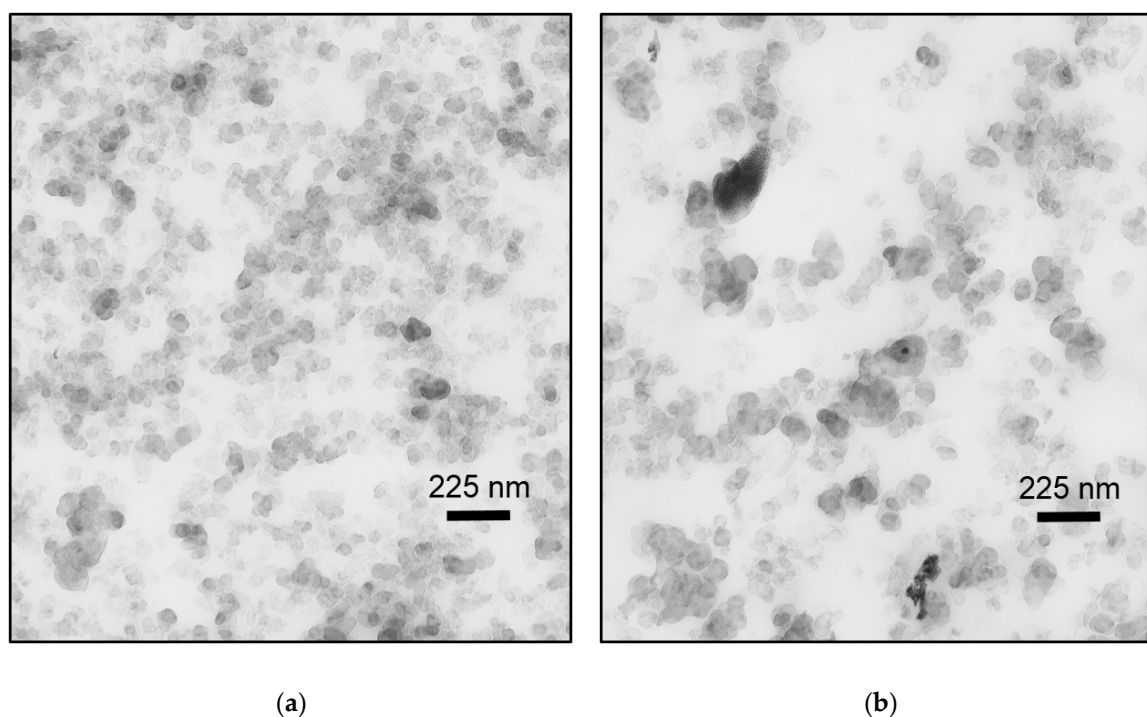


Figure 2. Cont.

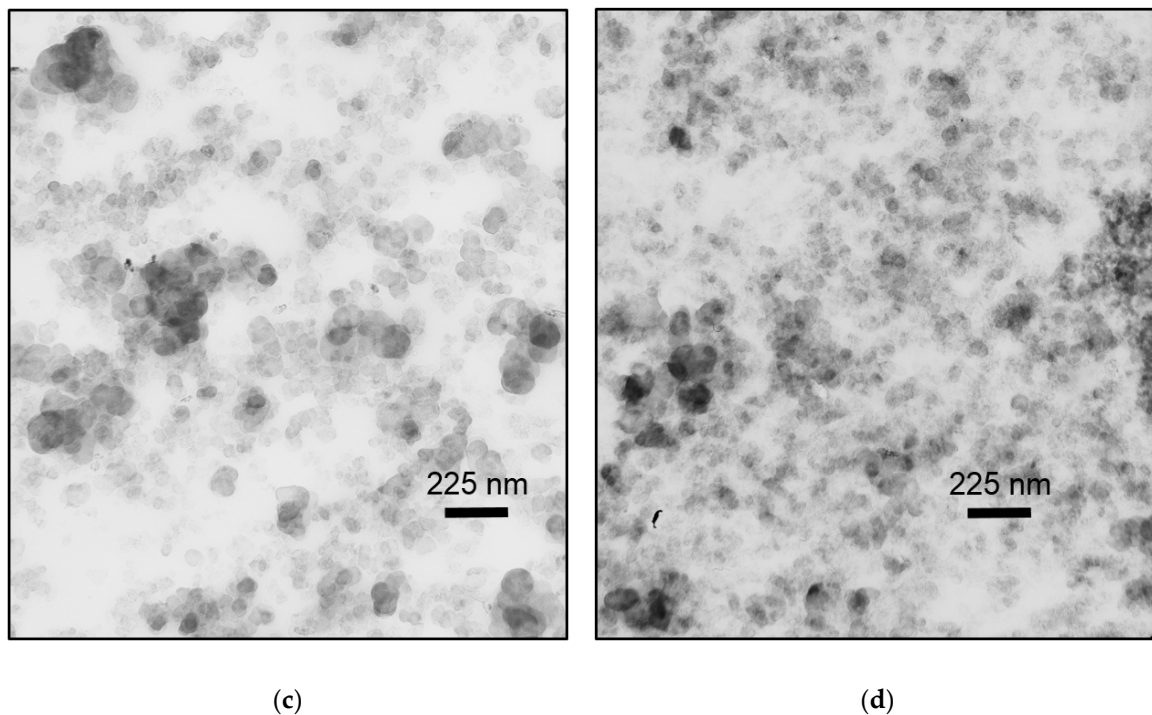


Figure 2. TEM micrographs of HNBR filled with different CB grades: (a) HNBR1; (b) HNBR2; (c) HNBR3; (d) HNBR4.

3.2. CB Grade Influence on Dynamic Mechanical Properties

The influence of the different CB grades on the mechanical properties of rapidly varying stress conditions over a range of temperature ($-50\text{ }^{\circ}\text{C}$ to $50\text{ }^{\circ}\text{C}$) was studied. The CB grade dependence on the loss factor ($\tan \delta$) deviation along the temperature is shown in Figure 3.

As depicted in Figure 3, the peak of the loss factor, which correlates to the glass transition temperature (T_g), and the intensity and width of the loss factor peak, which imply the damping properties [32], are slightly different in every tested grade. The lowest T_g was recorded with HNBR4, while HNBR2, HNBR3, and HNBR1 displayed slightly higher T_g values, respectively. However, a different trend in damping properties was witnessed, for example, the highest damping in HNBR2, and lower damping properties in HNBR3, HNBR4, and HNBR1, respectively. The storage modulus deviation, the glass relaxation onset and the reduced magnitude followed similarly to the loss factor deviation trend. Therefore, it is not shown here.

According to the literature, the higher filler surface and the filler structure offer better filler–rubber interactions as a result of strong bound and occluded rubber layers, where the chain motion is more restricted compared with the rest of the matrix [24]. Consequently, the loss of segmental mobility increases the T_g and damping properties [24,33]. Therefore, the ranking of HNBR2, HNBR3, and HNBR1 for having lower damping properties and higher T_g , respectively, correlate with the relatively higher filler surface area of CB in the composition and their better filler structures. Similarly, the TEM micrographs showed that HNBR1 contained the best filler network, while HNBR3 and HNBR2 contained comparatively less densified filler networks, respectively. However, HNBR4, which accommodates the highest primary particle surface area among the CB grades, does not correlate the trend with other samples. As shown in Figure 2d, HNBR4 contains the highest filler network and larger agglomerates in the material. Therefore, the filler agglomerates in the material reduced the possible filler–rubber interactions and decreased the possible reinforcement and this could be associated with the lowest T_g and moderate damping properties of HNBR4. However, the slightly enhanced damping properties could be associated with the filler–filler interactions. The nominal hardness values for the tested grades showed as 87.3, 85.3, 86 and 86.3 SHA, for HNBR1, HNBR2,

HNBR3, and HNBR4, respectively, and it is also in good agreement with the damping properties revealed in DMA. Theoretically, the rigid rubber shell due to the higher surface and better filler–rubber interactions enhances the hardness of the total composite [19].

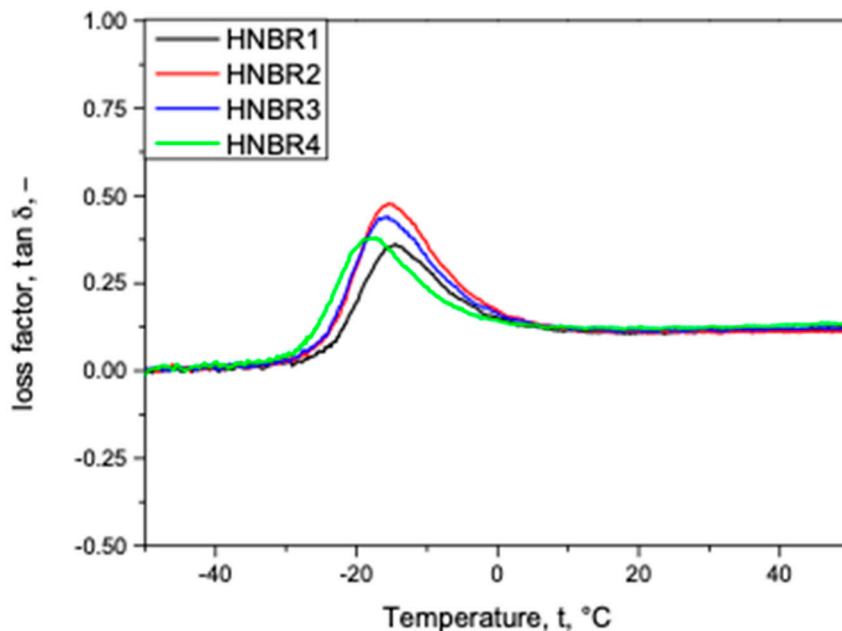


Figure 3. The temperature dependence of different CB grade compositions in HNBR on DMA analysis: the loss factor $\tan \delta$.

3.3. CB Grade Influence on Tensile Properties

The influence of the filled CB grades in HNBR in monotonic loading conditions is compared in Figure 4, where the stress–strain deviation, the tensile strength (σ_R) and the strain at break (ϵ_R), the stress at 10% ($\sigma_{10\%}$) and 50% strain ($\sigma_{50\%}$) deviation in different samples are shown in Figure 4a–c, respectively.

As shown in Figure 4a, a unique stress–strain behavior for the differently filled HNBR was apparent. Especially, HNBR1 shows higher stresses from the beginning of the tests; however, the HNBR2 and HNBR3 deviate with slightly lower values, but in a similar range of properties. HNBR4 behaves differently from the rest, with rather high stresses at the beginning of the test, but showing rather softer material properties thereafter ~10–15% of strain. As depicted in Figure 4b, HNBR1 shows the lowest σ_R , and HNBR2 reveals relatively higher σ_R , while HNBR3 lies in between them. Additionally, the HNBR4 samples demonstrate the highest σ_R values among the tested samples. The trend was similar for the strain at break, ϵ_R . A relatively different behavior for the $\sigma_{10\%}$ and $\sigma_{50\%}$ was observed, as shown in Figure 4c, where, HNBR1 shows the highest stress levels in 10% strain, HNBR2 has the lowest $\sigma_{10\%}$ and HNBR3 remains in-between them, while HNBR4 owns the second best $\sigma_{10\%}$ after HNBR1. However, $\sigma_{50\%}$ reveals a different trend, where HNBR1 has the highest values and HNBR2, HNBR3 and HNBR4 have lower values, respectively.

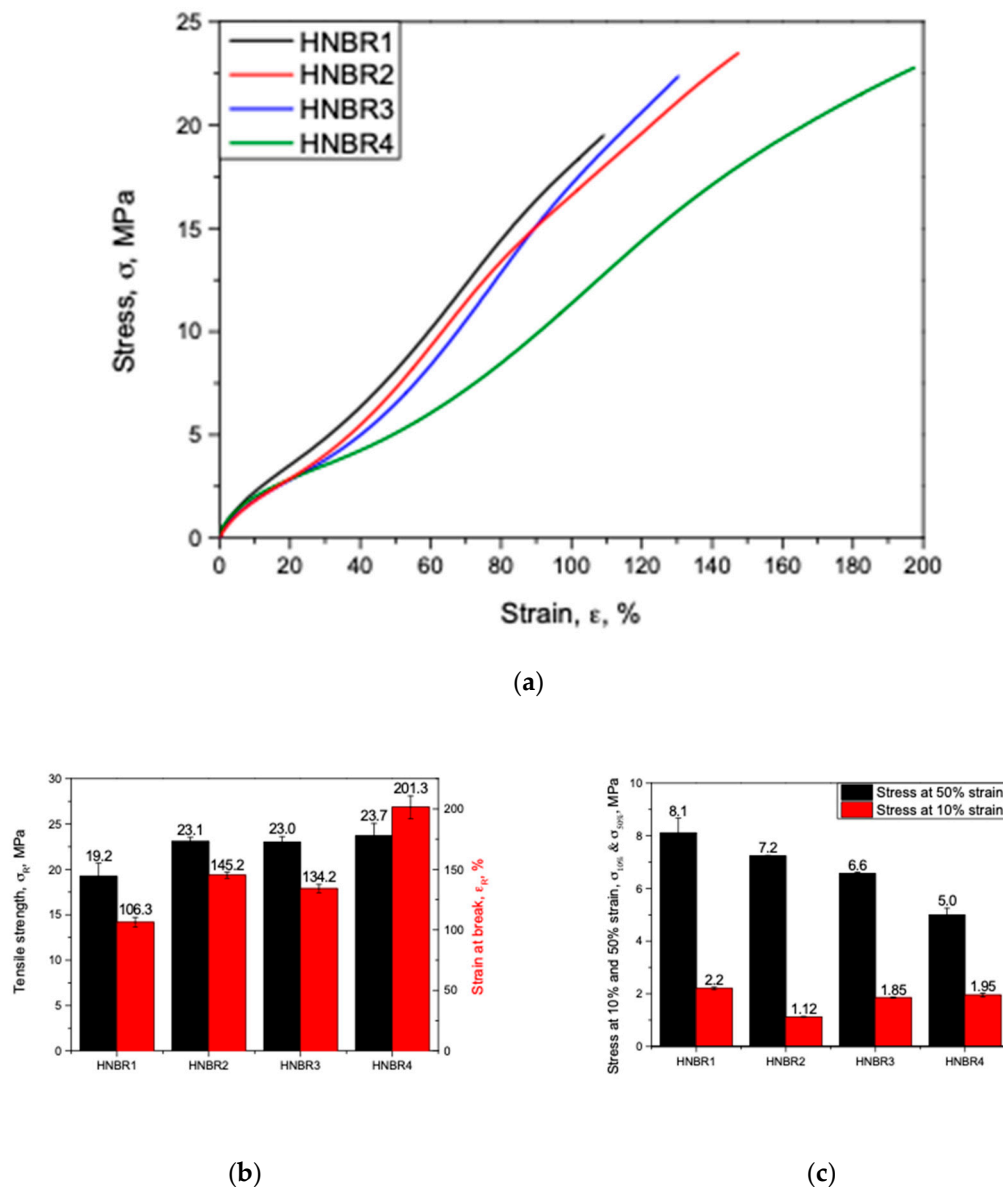


Figure 4. Tensile properties of CB-filled HNBR: (a) typical stress–strain curves; (b) tensile strength; (c) stress at 10% and 50% strain.

Theoretically, the higher surface primary particles tend to form higher structures and subsequently to deliver higher tensile properties [19,23]. However, some researchers experienced different tendencies based on achieving the balance between the CB loading and agglomerates [23]. HNBR1, which has a higher degree of CB with higher surface in the composition, shows a rather brittle nature, with the highest stiffness and lowest strain at break behaviors, compared with HNBR2 and HNBR3. Similarly, the moderate tensile properties of HNBR3, in-between HNBR1 and HNBR2 could be considered as the effect of the amount of CB with higher filler surface in the composition. Additionally, HNBR4, which contains the CB with highest surface area in a higher degree in the composition, shows the highest strength at break, but a softer material behavior compared to other material grades. The TEM micrographs, as shown in Figure 2, perhaps confirm this behavior, as HNBR1 has better-networked, anisometric shaped filler aggregates, while HNBR2 and HNBR3 possess these to the least and moderate degrees. Therefore, the higher primary particle surface area, or structure, has shown an influence to a certain level, even in these highly filled conditions. The irregular shaped structures are expected to increase the possible elastomer–rubber interaction and as a result larger bound and occluded rubber

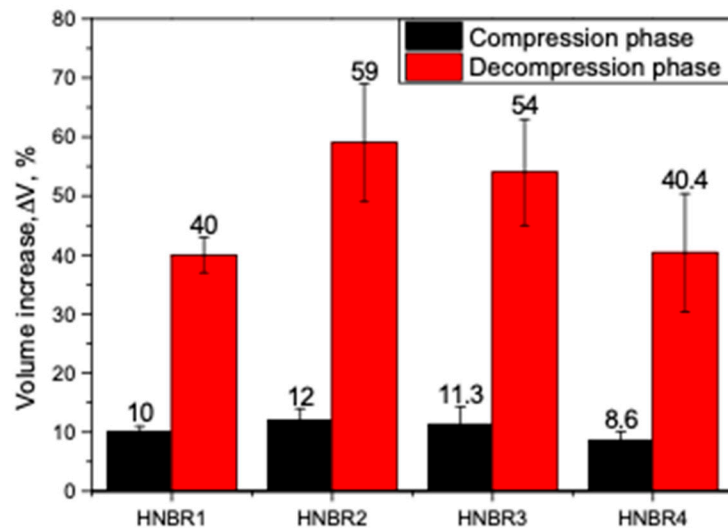
layers around filler. These layers are assumed to be partially restrained from deformation, and this consequently increases the effective filler concentration [18,19,24,33]. Therefore, the whole composite has increased stiffness, owing to the decreased segmental mobility of polymer chains and consequently a reduction of the flexibility of the rubber matrix [18,33]. However, in HNBR4, which contains a higher amount of highest surface area CB, apparently form aggregates and larger agglomerates (as Figure 2d revealed). As shown in Figure 1, these can probably create more filler–filler interactions and decrease the matrix material around the particles. By applied external loading, the weakly bonded filler–filler agglomerates tend to collapse and expose the trapped rubber it may contain. Additionally, at higher stresses, the broken filler agglomerates slightly restrict the free movement of elastomeric chains [18,33]. Therefore, at lower strain levels, relatively higher stress values but at higher strain levels, a softer material behavior and relatively higher strain at break values can be expected in HNBR4.

3.4. CB Effect on Rapid Gas Decompression

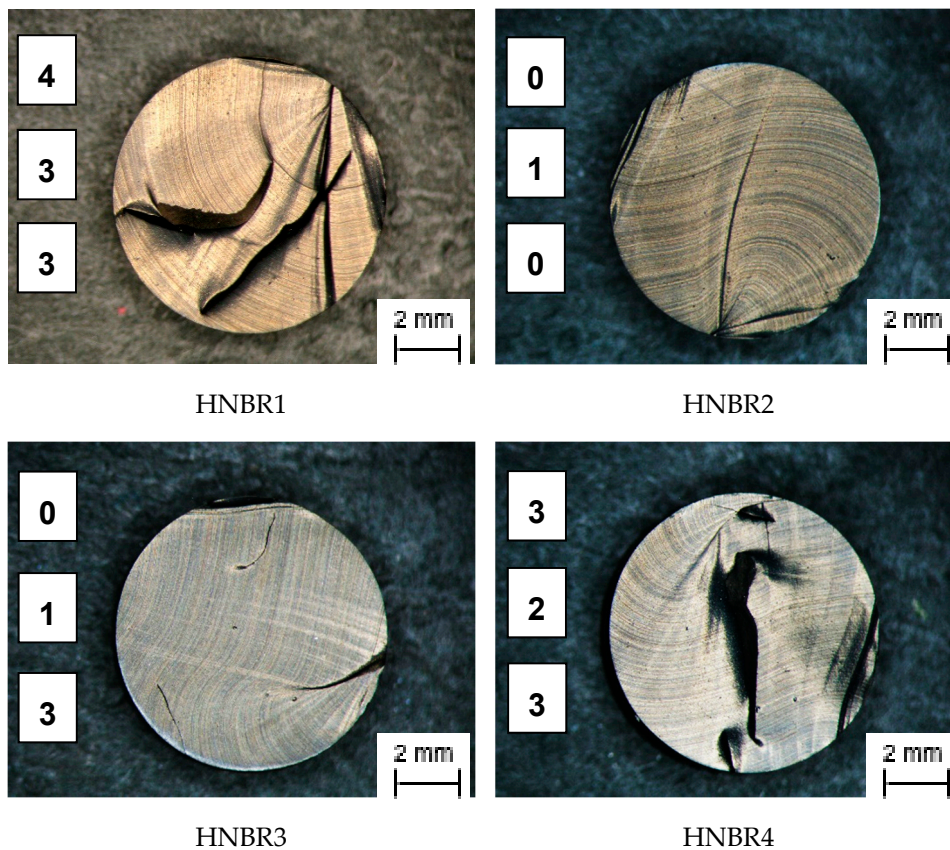
The RGD test data from the autoclave tests were reduced to two specific values; the maximum observed volume change during the compression phase (the difference of volume at saturation phase to initial volume) (ΔVC), and the maximum observed volume change during the decompression phase (volume expansion compared with initial volume) (ΔVD). The behavior of ΔVC and ΔVD for different material grades is as summarized in Figure 5a. The optical microscope pictures for the observed cracks in the cylindrical specimens of the different material grades are shown in Figure 5b. The numbers in the microscope picture indicate the NORSOK rating, measuring the number of cracks and intensity of cracks, of the implemented measurements for every material grade.

As depicted in Figure 5a, tested samples reveal slightly different volume increases to each other during the compression phase; HNBR2 and HNBR4 possess the comparatively highest and lowest volume increase in this small range, respectively. Considering the decompression phase, HNBR1 and HNBR4 demonstrate a lower volume change (~40%), while HNBR2 reveals the highest volume change (~60%), and HNBR3 (~54%) shows a moderate increase. However, it should be mentioned that all tested specimens for HNBR4 fell from view from the observation window of the autoclave after a certain time during the decompression phase with a fast crack growth from the inside to the outside of the specimen. All other specimens remained in their freestanding position with only slight movements. Therefore, ΔVD of HNBR4 samples may not indicate the precise values or hold high scattering. Despite a certain tendency in the ΔVC and ΔVD , the microscope observation and the NORSOK ranking indicate a different behavior. A higher number of cracks were apparent on the cross-sections of HNBR1 and HNBR4; they were considerably more than 80% of the cross-section. Therefore, the lower resistance to RGD was observed with HNBR1 (4, 3, 3) and HNBR4 (3, 2, 3). While HNBR3 (0, 1, 3) and HNBR2 (0, 1, 0) revealed only a few and minor cracks in the cylindrical specimens, respectively, and consequently a better resistance to RGD failure.

As depicted in Figure 5a, the ΔVD follows a trend similar to ΔVC , but in a greater magnitude. The volume increase during the high-pressure CO₂ exposure could be explained as a parameter of solubility of the gas into the material and the dissolved gas in the material as responsible for volume expansion during the decompression phase. In the tested conditions, the CB grades with the different surface area have seemingly influenced the solubility of the gas. For example, in HNBR1, HNBR2, and HNBR3, the ΔVC and ΔVD show a correlation with the CB grade, where a higher degree of middle range primary particles in the composition has caused a comparatively lower volume increase. Similarly, HNBR4 has the lowest volume change during compression among the tested samples, where higher degree of small particles are contained. In general, higher gas solubility and a lower rate of diffusion in elastomers tend to deliver a lower RGD resistance in the material [9,34], however, a clearly improved RGD resistance in HNBR2 and HNBR3 was observed compared with the other two materials, irrespective the higher compression and decompression volume increases.



(a)



(b)

Figure 5. Influence of CB grades composition on rapid gas decompression (RGD) performance of HNBR: (a) volume increase during compression (ΔVC) and decompression (ΔVD); (b) visual observation of cylindrical specimens and the NOROSOK material ranking (every number on the right represents a different measurement).

At high-pressure exposure, gas permeates into the elastomers and dissolves in the matrix material at small imperfections or filler–matrix interfaces, if the filler–matrix interaction is poor, until saturation [4,6,9,31]. In the tested conditions, where the samples contained the same filler loading,

the HNBR with lower surface CB showed a slightly higher volume increase in the compression phase, ΔVC . Briscoe et al. [4], explained the addition of filler into matrix alter the sorption properties based on the quality of the filler–rubber interaction. If the interface is strong, it significantly reduces the gas sorption compared with unfilled and vice versa. This is attributed as the filler–rubber interaction creates strong rubber layers around the filler and it decreases the effective matrix amount, which can possibly dissolve the gas. On the other hand, filler inclusion improves the mechanical properties of the matrix and it reduces the entering gas into the material [4]. Similarly, Jamabe et al. [7] explained, that gas solubility of filled rubber is influenced by surface area of the filler as well as the interface structure of filler–rubber interaction. However, in their experiments with CB filled EPDM in high-pressure (10 MPa) hydrogen atmosphere, they observed that, at lower filler loading levels (25 phr), CB grades with smaller primary particles had a higher solubility, but at higher loading levels (50 phr), they did not find a clear trend [7]. Under the tested conditions, higher surface CB tends to create complex structures (also visible in TEM micrographs in Figure 2); it could deliver better filler–rubber interactions, enhance the effective filler concentration through possible restricted matrix movements (Occluded and bound rubber layers), and consequently, reduce the elastically effective matrix material component. This can be a plausible interpretation for the ΔVC trend. Further, the mechanical properties, especially the trend of $\sigma_{10\%}$ of the quasi-static tensile test results (Figure 4c), have a possible influence on the same trend of ΔVC . The volume increase in compression and decompression phases (ΔVC and ΔVD) deviate in less than 10 percent of strain levels ($<10\%$, ϵ), therefore $\sigma_{10\%}$ is in good agreement with ΔVC and ΔVD . Similarly, the DMA damping properties deviated in a similar order. Therefore, apparently the solubility of gas is slightly decreased due to decreased effective matrix content and increased mechanical properties in higher filler surface conditions.

During the decompression phase, the accumulated gas in the material is subjected to nucleate at expansion-forming micrometer-sized bubbles. Initially, they do not form cracks so long as the material deforms elastically without inhibition [2,4,12]. If no crack was initiated, the dissolved gas becomes extinct desorbing them without any visible traces [8]. However, if the high rate of elastic expansion meets a low strength matrix or hard body inclusions where the stress concentrates, crack initiation and propagation take place in the elastomer bulk as well as in the hard body–matrix interfaces [6,35]. In the tested conditions, the volume increase during the decompression, ΔVD , (Figure 5a) seemed to follow the same trend of ΔVC and it is probably correlated to the stiffness of the different grades and the degree of dissolved gas in the saturated state. Additionally, ΔVD could be reduced by possible cracks propagated during the decompression phase. It is generally accepted that the resistance to RGD of elastomers is increased if the gas sorption into the material is lower and the physical properties (stiffness, tensile strength, tear resistance, etc.) of the material are higher [6–9,31,35]. However, NORSOK ranking of tested samples revealed otherwise: where HNBR1 and HNBR4 have the lowest RGD resistance, while HNBR3 and HNBR2 reveal a significantly better resistance to RGD. The RGD phenomenon of elastomers is a rather complex process with a combination of many factors. However, in this test series, the samples are highly filled, consequently an enhanced filler network and agglomerates as well as reduced matrix component are expected. As revealed in TEM micrographs (Figure 2), the networks of CB in all four material grades are clearly influenced by the higher particle surface. The higher CB structures, which were formed due to higher surface area, tend to form thick rubber layers around them, which enhance the effective filler amount and decrease the active matrix component. However, HNBR4, which contains CB with the highest surface area, apparently creates larger filler agglomerates and less matrix material around fillers. In these highly filled conditions, the higher surface area CB is adversely effective in RGD resistance; HNBR2, which has the lowest structure and CB network density, reveals the best RGD resistance, while HNBR3 and HNBR1 disclose relatively lower RGD resistance. HNBR3 and HNBR1 contain comparatively higher CB structures and networks in the materials, respectively. Therefore, it could be assumed that if there were a sufficient amount of elastically active matrix material in the material, the bubbles nucleation and growth during the decompression phase would be assisted. However,

when the filler network is densified or effective CB volume increased due to the rigid matrix around the CB, subsequently the active matrix composition is decreased and the possible bubble growth in matrix hinders during decompression phase. This concentrates stresses around the rigid inclusions and tends to initiate cracks.

HNBR4 at lower strain levels maintains relatively higher stress values due to filler–filler interactions. However, above a certain strain level, the agglomerates tend to break and steer to a softer material behavior. Therefore, the lower ΔVC values were observed and at the same time, a lower RGD resistance was experienced. This material grade even fell from sight from the observation window during the autoclave test: the sample, which was in a freestanding position on the ground displaced, as a result of faster crack growths in the material. The stress concentrations during the decompression volume expansion probably tend to break the CB agglomerates and once the crack initiates, it grows faster through the rather soft material.

CB loading and CB surface area improve the mechanical properties in elastomeric composite, which are essential for RGD resistance. However, apparently, after a certain level of CB loading, it is better to have lower CB surface/bigger primary particles in the material in terms of RGD resistance.

3.5. SEM Based Fractography

In the following section, the fracture surfaces of RGD tested cylindrical specimens, which were examined using SEM, are displayed for understanding the crack initiation, the modes of crack propagations and the morphology of rubber/CB of differently filled samples. Figure 6 shows the SEM images of a fracture surface of HNBR1 on a more global scale (a) and the magnified view of the crack initiation (b). The point where many small tearing lines converge, as highlighted in Figure 6a by arrows, can identify the crack origin. The crack growth lines seem to create a microscopically rough surface. Therefore, the fracture surface texture of the HNBR1 suggests that it contains pits/cavities as a result of reinforcing CB agglomerates coming out of the matrix surface. As shown in Figure 6b, no real pre-existing cracks or defects were apparent in the vicinity of the initiation point, but only a rough surface as a result of loosened agglomerate detachment. The literature suggests that the loosened agglomerates, due to the inhomogeneous cross-link density, can act as stress raisers and offer a path for the tear to follow [7,12]. However, this seems like a stable crack growth as the fracture surface has a similarly rough texture along the crack growth.

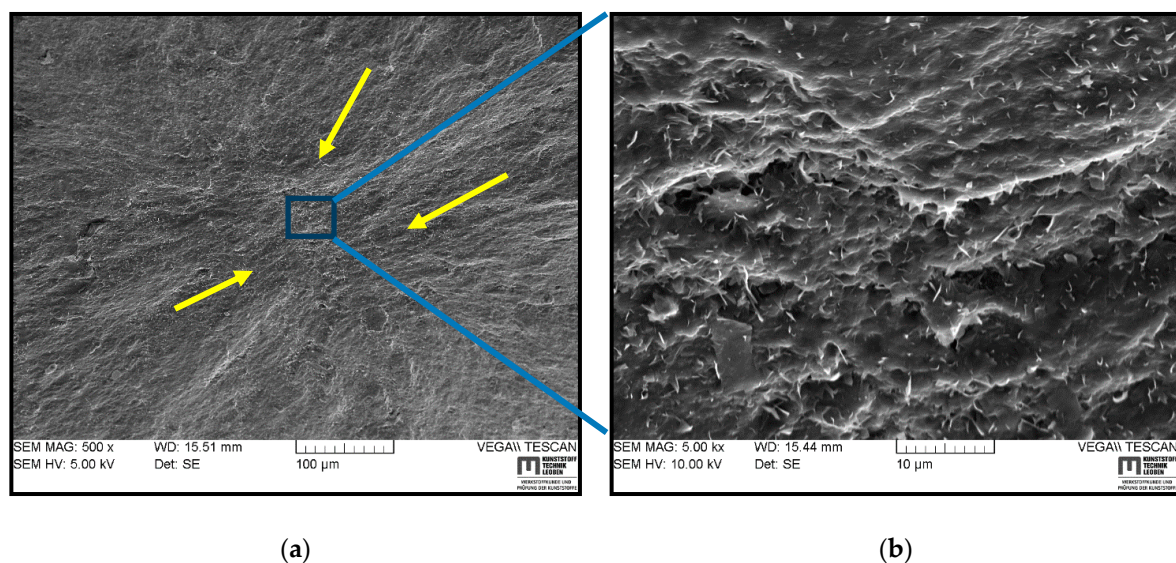


Figure 6. SEM images of a typical fracture surface of HNBR1 in different magnifications: (a) fracture initiation and propagation; (b) magnified view of fracture initiation.

Figure 7 shows a fracture surface of HNBR2 in different magnifications. A crack initiation and propagation sight are indicated in Figure 7a, while Figure 7b focuses on the initiation point. Similar to Figure 6, the crack initiation is clearly visible in Figure 7a, where many small tear lines spread out from one place. As visible in the magnified view in Figure 7b, the crack initiated from a rather flat surface of $\sim 15 \mu\text{m}$, which is not an extrinsic defect, but seemingly a low strength matrix area. This could have been introduced to the material by poor CB networks as confirmed by TEM micrographs (Figure 3b). However, a rough fracture surface is visible indicating a slow crack growth throughout the crack propagation.

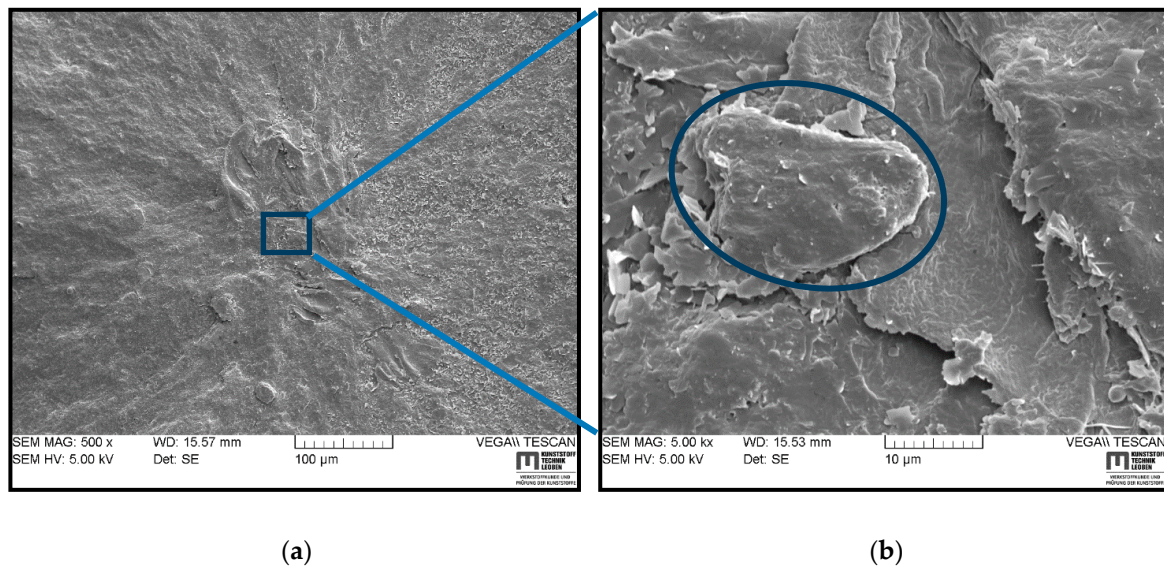


Figure 7. SEM images of a typical fracture surface of HNBR2 in different magnifications: (a) fracture initiation and propagation; (b) magnified view of fracture initiation from a low strength site.

SEM images of a fracture surface for HNBR3 are shown in Figure 8, where the crack initiated from a large cluster and as a result of the fracture (Figure 8a). The cluster was exfoliated from the surface creating a large pit on the surface and it could be a large CB agglomerate covered by the matrix or formed by other additives in the compound with a defect size $\sim 150 \mu\text{m}$. The Figure 8b magnifies the edge of the pit and the vicinity of the initiation point. Inside the pit, it seems that the matrix has failed around the large cluster, which was loosely bound. The vicinity of the initiation point was a rough and lamellar structure, which apparently indicates a stable crack growth. Therefore, it could be assumed that the gas is accumulated near the rigid inclusion during gas compression and upon decompression, the expansion of gas volume encounters the crack initiation and propagation through low-strength sites. The large inclusions behave as if they were smaller voids causing gas to accumulate, which helps a crack to grow and inflate under depressurization [34].

Figures 9 and 10 show two fracture surfaces of HNBR4 in different magnifications, which contain different crack initiation and propagation morphologies. Figure 9a displays an initiated crack inside the cylinder propagating to the outer surface, while Figure 9b magnifies the origin of the crack. As indicated by the arrows, the cracks were pronounced in the material in the fracture initiation region. This could be an indication that the fracture propagated from cavities, which were initiated as a result of inherent voids in the material. It can be assumed that the small voids in the material nucleated the gas during the pressurization, while during depressurization, they rupture, creating cavities in the material. These open cavities could act as stress raisers and offer an easy path to propagate flaws with cracks perpendicular to the cavities to a fatal fracture as many were observed in this material grade.

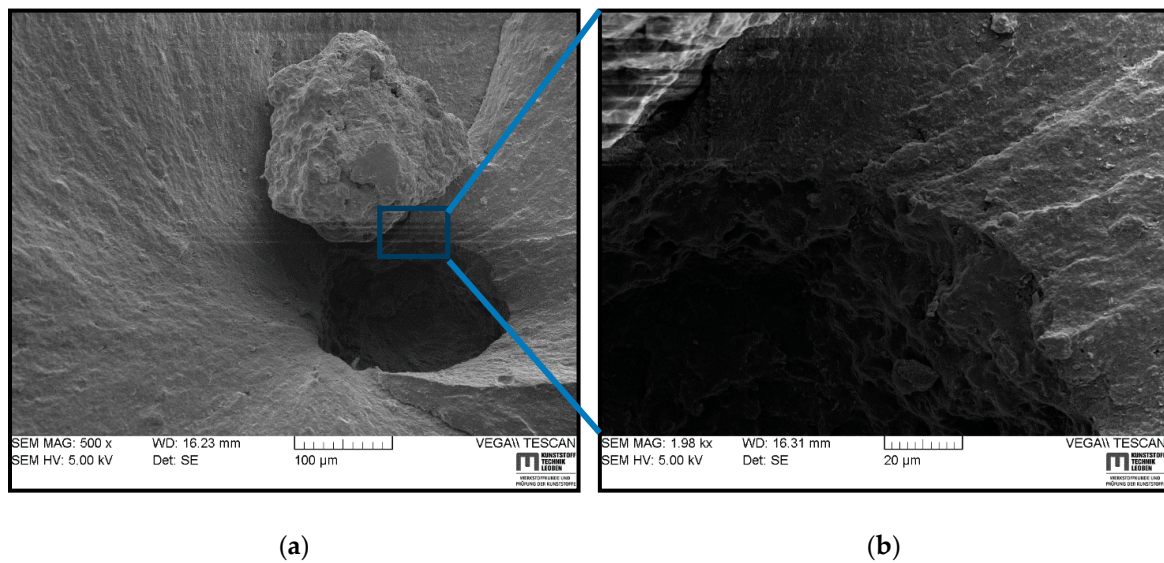


Figure 8. SEM images of a fracture surface of HNBR3 in different magnifications: (a) fracture initiation from a rigid body; (b) magnified view of fracture initiation and propagation.

As shown in Figure 10, the initiation point (square highlighted) did not occur at a rigid inclusion or a cavity, but a flat surface, seemingly a low strength matrix surface. The crack propagation is different from other observed morphologies of the previous SEM images. As indicated in Figure 10a by arrows, there are hackle lines, which are formed by converging the small tearing lines to create a large crack. After the hackle lines, the crack propagation mode seemingly transitions from slow crack propagation to a stable fast crack. Therefore, a fast crack growth region is apparent with a rather flat, smooth surface compared with the slow crack propagation region. During the autoclave test, every HNBR4 specimen fell from the standing position and disappeared from the observation window due to this high-speed crack growth similar to a bursting behavior. The cracks were even visible to the naked eye on the outer surface of the tested cylindrical specimen.

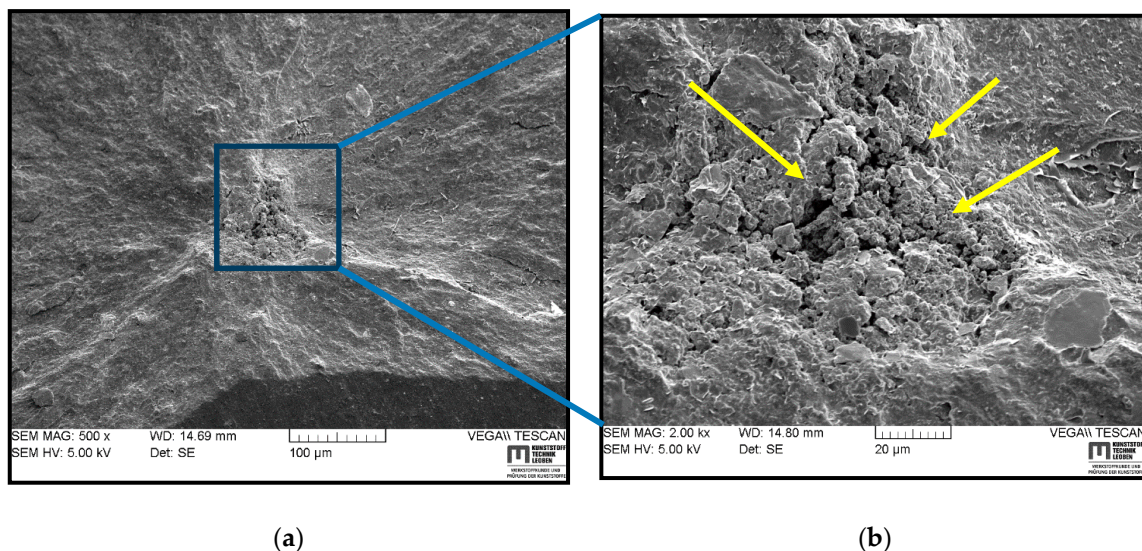


Figure 9. SEM images of a fracture surface starting from inherent voids of HNBR4 in different magnifications: (a) fracture initiation and propagation; (b) magnified view of fracture initiation and cracks into the material.

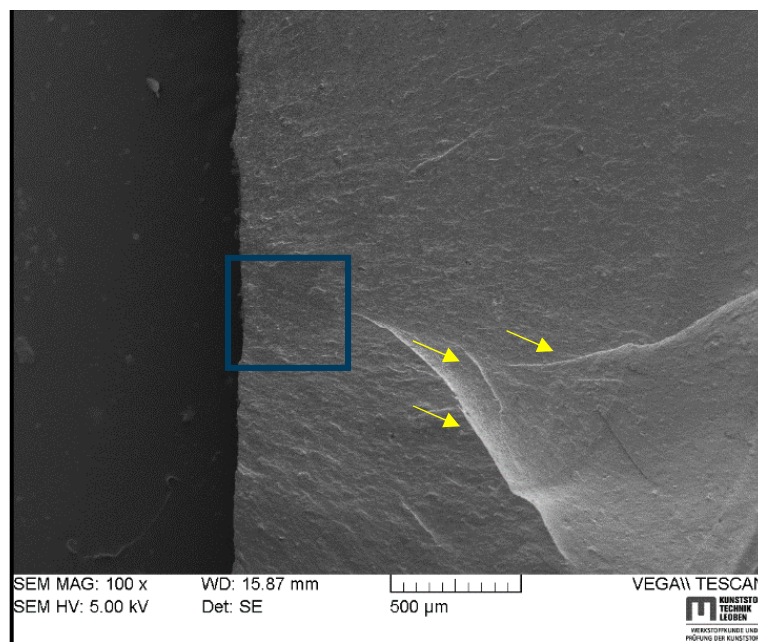


Figure 10. SEM image of a fracture surface starting from low-strength matrix site and a propagation in slow and subsequently fast stable crack growth for HNBR4.

The SEM analyses of the fracture surfaces of RGD tested samples revealed that the cracks initiated in the center region of the cylinder and propagated towards the circumference. The cracks were apparently initiated at the existing voids, hard body inclusions (particle agglomerate), or a low strength matrix site. Similar observations were reported in the literature for the RGD fracture initiation [3,6,7,12]. The small voids or hard inclusions are hard to avoid during processing [34], the low strength matrix sites are a result of lower filler distribution, uneven cross-link density or trapped rubber between large CB agglomerates which becomes ‘free’ once the aggregate structure breaks apart [7,12,24]. It was challenging to correlate the SEM fractography observations to the CB grade or size of the primary particles or agglomerates in different materials. However, HNBR1, HNBR2, and HNBR3 showed coarse surfaces, which contained small pits on the fracture surface, and it can be assumed to be traces of reinforcing agglomerates detached from the matrix. In HNBR4, a slow crack growth was transformed into rapid crack propagation to a catastrophic failure after the initial cracks converged into a critical size crack (hackle).

4. Summary and Conclusions

This work focused on the influence on rapid gas decompression failure of different grades of CB, which had different surface areas, filled in HNBR. Regarding the RGD test results, the trend of the volume increase of cylindrical specimens during the compression phase, which is a measurement of gas solubility into the material, evidently followed the component of CB with a lower surface area in the material. In general, filler loading reduces the elastically effective matrix component, increases mechanical properties of matrix, and decreases the gas sorption into elastomers. However, a poor filler–rubber interaction can trap the gas and increase sorption. In these highly filled conditions, the CB surface area has slightly influenced the solubility (assumed by compression phase volume increase) by reducing the effective matrix component and the increased mechanical properties. The tensile and DMA results proved the slight improvements in the mechanical properties based on higher CB surface area. However, HNBR4, which contained a greater amount of relatively higher surface area CB, revealed a rather different behavior compared with the other three grades. In addition, from the TEM micrographs, it can be assumed that HNBR4 contained bigger CB agglomerates and filler–filler networks. Therefore, a relatively higher stiffness at lower strain levels and softer material behavior at

higher strain levels could be associated with the breakage of loosely bonded CB agglomerates and consequently, a rather free movement of molecules at higher strains. The volume increase in the decompression phase followed the same trend in compression phase in RGD tests, as a consequence of mechanical properties and the amount of saturated gas in the material, but NORSOK ranking showed a different rating. The initiated cracks can also possibly be responsible for some extent of lower volume increase during decompression phase. The TEM micrographs disclosed higher anisometric structures and better networks in samples with higher surface CB and relatively lower matrix components around them. HNBR2 showed the best RGD resistance next to HNBR3, where they retained lower CB structures as well as relatively greater matrix components around the CB structures. HNBR4 and HNBR1 disclosed relatively larger and higher number of cracks on the cross-sections after RGD. The greater filler structure discourages movement of rubber molecules around them from forming bound rubber and occluded rubber and it decreases effective matrix components. Therefore, HNBR1 lacks matrix material around the hard inclusions, which can elastically deform and assist the possible bubble nucleation and growth during the decompression phase. However, HNBR4, which contains a greater amount of CB agglomerates, eases crack growth after loosely bonded filler–filler bond rupture. Apparently, a minimum amount of matrix component around the CB grades is necessary to maintain the RGD resistance, along with other highly relevant parameters, as discussed above, for example, higher stiffness, tear, and tensile strength, lower gas solubility, etc. Therefore, in highly filled conditions, the size of the CB primary particles influences the properties in harsh environment utilization. The smaller CB particles tend to create denser filler networks and greater amount of agglomerates, which reduce the effective matrix component in the composite. Apparently, this is adversely effective in RGD resistance. SEM-based fractography did not influence the crack initiation based on different CB grades. However, it revealed that the cracks initiated from possible low strength matrix areas, hard inclusions or existing voids propagated to the outer surface.

Author Contributions: W.B. conducted the tests and L.C. obtained the TEM micrographs; W.B. and B.S. analyzed the data and discussed the results; T.S. contributed the materials; G.P. and T.S. consulted on the research work and held scientific discussions; W.B. conducted the literature research and wrote the paper.

Funding: This research was funded under one of the projects (grant number: 854178) by the Austrian Research Promotion Agency (FFG).

Acknowledgments: The research work was performed at the Polymer Competence Center Leoben GmbH (PCCL, Austria) within the framework of the COMET-program of the Austrian Federal Ministry for Transport, Innovation and Technology (BMVIT), the Austrian Federal Ministry of Digital and Economic Affairs (BMDW) with contributions from the material science and testing of polymers of the Montanuniversität Leoben and SKF Sealing Solutions Austria GmbH. The PCCL is funded by the Austrian Government and the State Governments of Styria, Lower Austria and Upper Austria.

Conflicts of Interest: The authors declare no conflict of interest.

References

1. Hofmann, W. *Rubber Technology Handbook*, 2nd ed.; Hanser Publishers: Munich, Germany; Vienna, Austria; New York, NY, USA, 1989.
2. Briscoe, B.J.; Zakaria, S. Gas-induced damage in elastomeric composites. *J. Mater. Sci.* **1990**, *25*, 3017–3023. [[CrossRef](#)]
3. Major, Z.; Lang, R.W. Characterization of the fracture behavior of NBR and FKM grade elastomers for oilfield applications. *Eng. Fail. Anal.* **2010**, *17*, 701–711. [[CrossRef](#)]
4. Briscoe, B.J.; Savvas, T.; Kelly, C.T. “Explosive Decompression Failure” of Rubbers: A Review of the Origins of Pneumatic Stress Induced Rupture in Elastomers. *Rubber Chem. Technol.* **1994**, *67*, 384–416. [[CrossRef](#)]
5. Ho, E. Elastomeric Seals for Rapid Gas Decompression Applications in High-Pressure Services. In *BHR Group Limited Research Report 485 for the Health*; BHR Group Limited for the Health and Safety Executive: Sudbury, UK, 2006.

6. Major, Z.; Lederer, K.; Moitzi, M.; Mitterhuber, M.; Schwarz, T.; Lang, R.W. Development of a Test and Failure Analysis Methodology for Elastomeric Seals Exposed to Explosive Decompression. *Eng. Struct. Integr. Res. Dev. Appl.* **2006**, *2*, 754–757.
7. Yamabe, J.; Nishimura, S. Influence of carbon black on decompression failure and hydrogen permeation properties of filled ethylene-propylene-diene-methylene rubbers exposed to high-pressure hydrogen gas. *J. Appl. Polym. Sci.* **2011**, *122*, 3172–3187. [[CrossRef](#)]
8. Yamabe, J.; Nishimura, S. Influence of fillers on hydrogen penetration properties and blister fracture of rubber composites for O-ring exposed to high-pressure hydrogen gas. *Int. J. Hydrogen Energy* **2009**, *34*, 1977–1989. [[CrossRef](#)]
9. Schrittester, B.; Pinter, G.; Schwarz, T.; Kadar, Z.; Nagy, T. Rapid gas decompression performance of elastomers—A study of influencing testing parameters. *Procedia Struct. Integr.* **2016**, *2*, 1746–1754. [[CrossRef](#)]
10. Embury, P. High-pressure gas testing of elastomer seals and a practical approach to designing for explosive decompression service. *Seal. Technol.* **2004**, *2004*, 6–11. [[CrossRef](#)]
11. Schrittester, B.; Pinter, G.; Schwarz, T.; Nagy, T.; Urbán, M. Fracture and Fatigue Behavior of Elastomers Used in the Oil and Gas Industry. In Proceedings of the High Performance for Oil and Gas, Oil and Gas Polymer Engineering Texas Conference, Houston, TX, USA, 10–12 April 2013.
12. Mbwadzawo, T.; Hodzic, A. Scanning Electron Microscopy Analysis of Elastomeric O-Rings and Spring Seals Fractured during Rapid Gas Decompression. In Proceedings of the 16th European Conference on Composite Materials (ECCM16), Seville, Spain, 22–26 June 2014.
13. Vorotnikov, D.A. Dissipative solutions for equations of viscoelastic diffusion in polymers. *J. Math. Anal. Appl.* **2008**, *339*, 876–888. [[CrossRef](#)]
14. Comyn, J. *Polymer Permeability*; Springer: Dordrecht, The Netherlands, 1985.
15. Hertz, D.L. Elastomers in CO₂. In Proceedings of the High Performance Elastomers & Polymers for Oil & Gas 2012 International Conference, Aberdeen, UK, 20–21 April 2012.
16. Daou, F.; de Miranda, C.R.; de Oliveira, J.L.; Engelke, B.; Borman, C.; Le Roy-Delage, S.; Lungwitz, B. Swelling of Elastomers in CO₂ Environment: Testing Methodology and Experimental Data. In Proceedings of the SPE International SPE Latin America and Caribbean Petroleum Engineering Conference, Maracaibo, Venezuela, 21 May 2014.
17. Heinrich, G.; Klüppel, M.; Vilgis, T.A. Reinforcement of elastomers. *Curr. Opin. Solid State Mater. Sci.* **2002**, *6*, 195–203. [[CrossRef](#)]
18. Fröhlich, J.; Niedermeier, W.; Luginsland, H.-D. The effect of filler–filler and filler–elastomer interaction on rubber reinforcement. *Compos. Part A Appl. Sci. Manuf.* **2005**, *36*, 449–460. [[CrossRef](#)]
19. Li, Z.H.; Zhang, J.; Chen, S.J. Effects of carbon blacks with various structures on vulcanization and reinforcement of filled ethylene-propylene-diene rubber. *Express Polym. Lett.* **2008**, *2*, 695–704. [[CrossRef](#)]
20. Orion Engineered Carbons GmbH. *What Is Carbon Black?* Luxembourg, Germany, 2015; Available online: <https://www.thecarycompany.com/media/pdf/specs/orion-what-is-carbon-black.pdf> (accessed on 28 February 2018).
21. Carbon Black. Available online: <https://monographs.iarc.fr/ENG/Monographs/vol93/mono93-6.pdf> (accessed on 12 March 2018).
22. Leblanc, J. Rubber–filler interactions and rheological properties in filled compounds. *Prog. Polym. Sci.* **2002**, *27*, 627–687. [[CrossRef](#)]
23. Savetlana, S.; Zuhendri; Sukmana, I.; Saputra, F.A. The effect of carbon black loading and structure on tensile property of natural rubber composite. *IOP Conf. Ser. Mater. Sci. Eng.* **2017**, *223*, 12009. [[CrossRef](#)]
24. Kohls, D.J.; Beaucage, G. Rational design of reinforced rubber. *Curr. Opin. Solid State Mater. Sci.* **2002**, *6*, 183–194. [[CrossRef](#)]
25. Stübler, N.; Fritzsche, J.; Klüppel, M. Mechanical and electrical analysis of carbon black networking in elastomers under strain. *Polym. Eng. Sci.* **2011**, *51*, 1206–1217. [[CrossRef](#)]
26. Jha, V. Carbon Black Filler Reinforcement of Elastomers. Ph.D. Thesis, University of London, Queen Mary, UK, October 2008.
27. Gent, A.N.; Lindley, P.B. Internal Rupture of Bonded Rubber Cylinders in Tension. *Proc. R. Soc. A Math. Phys. Eng. Sci.* **1959**, *249*, 195–205. [[CrossRef](#)]
28. Harwood, J.A.C.; Mullins, L.; Payne, A.R. Stress Softening in Natural Rubber Vulcanizates. Part II. Stress Softening Effects in Pure Gum and Filler Loaded Rubbers. *Rubber Chem. Technol.* **1966**, *39*, 814–822. [[CrossRef](#)]

29. Zhang, A.; Wang, L.; Lin, Y.; Mi, X. Carbon black filled powdered natural rubber: Preparation, particle size distribution, mechanical properties, and structures. *J. Appl. Polym. Sci.* **2006**, *101*, 1763–1774. [[CrossRef](#)]
30. Norsok. *Qualification of Non-Metallic Sealing Materials and Manufacturers*, 1st ed.; (NORSOK M-710); Norwegian Technology Center: Trondheim, Norway, 1994; Available online: <http://www.standard.no/pagefiles/1152/m-cr-710r1.pdf> (accessed on 22 March 2018).
31. Balasooriya, W.; Schritteser, B.; Pinter, G.; Schwarz, T. Induced material degradation of elastomers in harsh environments. *Polym. Test.* **2018**, *69*, 107–115. [[CrossRef](#)]
32. Balasooriya, W.; Schritteser, B.; Karunakaran, S.; Schlögl, S.; Pinter, G.; Schwarz, T.; Kadar, Z. Influence of Thermo-Oxidative Ageing of HNBR in Oil Field Applications. *Macromol. Symp.* **2017**, *373*, 1600093. [[CrossRef](#)]
33. Bokobza, L. Multiwall carbon nanotube elastomeric composites: A review. *Polymer* **2007**, *48*, 4907–4920. [[CrossRef](#)]
34. Monaghan, K.J.; Newlands, C.; Ho, E. Specification of Elastomeric Materials for Rapid Gas Decompression Applications. In Proceedings of the Oilfield Engineering with Polymers Conference: 5th International MERL Conference, London, UK, 29–30 March 2006.
35. Achten, D. Next Generation HNBR Grades—New Materials for Oilfield Application. In Proceedings of the Oilfield Engineering with Polymers Conference: 5th International MERL Conference, London, UK, 29–30 March 2006.



© 2019 by the authors. Licensee MDPI, Basel, Switzerland. This article is an open access article distributed under the terms and conditions of the Creative Commons Attribution (CC BY) license (<http://creativecommons.org/licenses/by/4.0/>).